ADAPTIVE MULTIVARIATE SOLUTION SCHEMES FOR INVERSE
ELECTROCARDIOGRAPHY PROBLEM

A THESIS SUBMITTED TO
THE GRADUATE SCHOOL OF APPLIED MATHEMATICS
OF
MIDDLE EAST TECHNICAL UNIVERSITY

BY

ÖNDER NAZIM ONAK

IN PARTIAL FULFILLMENT OF THE REQUIREMENTS
FOR
THE DEGREE OF DOCTOR OF PHILOSOPHY
IN
SCIENTIFIC COMPUTING

SEPTEMBER 2018

Approval of the thesis:

ADAPTIVE MULTIVARIATE SOLUTION SCHEMES FOR INVERSE ELECTROCARDIOGRAPHY PROBLEM

submitted by **ÖNDER NAZIM ONAK** in partial fulfillment of the requirements for the degree of **Doctor of Philosophy in Scientific Computing Department, Middle East Technical University** by,

Prof. Dr. Ömür Uğur
Director, Graduate School of **Applied Mathematics** _____

Assist. Prof. Dr. Hamdullah Yücel
Head of Department, **Scientific Computing** _____

Assoc. Prof. Dr. Yeşim Serinağaoğlu Doğrusöz
Supervisor, **Electrical and Electronics Engineering, METU** _____

Prof. Dr. Gerhard Wilhelm Weber
Co-supervisor, **Faculty of Engineering Management, PUT** _____

Examining Committee Members:

Assist. Prof. Dr. Hamdullah Yücel
Institute of Applied Mathematics, METU _____

Assoc. Prof. Dr. Yeşim Serinağaoğlu Doğrusöz
Electrical and Electronics Engineering, METU _____

Prof. Dr. İlkay Ulusoy
Electrical and Electronics Engineering, METU _____

Assist. Prof. Dr. Osman Serdar Gedik
Computer Engineering, AYBU _____

Assist. Prof. Dr. Evren Değirmenci
Electrical and Electronics Engineering, MeU _____

Date: _____

I hereby declare that all information in this document has been obtained and presented in accordance with academic rules and ethical conduct. I also declare that, as required by these rules and conduct, I have fully cited and referenced all material and results that are not original to this work.

Name, Last Name: ÖNDER NAZIM ONAK

Signature   :

ABSTRACT

ADAPTIVE MULTIVARIATE SOLUTION SCHEMES FOR INVERSE ELECTROCARDIOGRAPHY PROBLEM

Onak, Önder Nazım

Ph.D., Department of Scientific Computing

Supervisor : Assoc. Prof. Dr. Yeşim Serinağaoğlu Doğrusöz

Co-Supervisor : Prof. Dr. Gerhard Wilhelm Weber

September 2018, 111 pages

Electrocardiographic Imaging (ECGI) is an emerging medical imaging modality to visualize the heart's electrical activity. It has a promising potential for diagnosing cardiac abnormalities and facilitate the planning and execution of necessary treatments. Visualizing heart's electrical activity requires solving the ill-posed inverse electrocardiography (ECG) problem. Despite the considerable efforts and improvements in this field, there exist some limitations and challenges that hinder its application to daily clinical practice. Hence, the inverse ECG problem still attracts the attention of researchers.

Since the inverse ECG problem has a ill-posed characteristic, it is necessary to regularize the problem by imposing constraints based on prior information about the solution. Although, several regularization methods have been applied to solve the inverse ECG problem, none of the them has been accepted as an optimal technique. Because, each method has limitations and there exist some cases where they have pros and cons in terms of accuracy, computational complexity and required prior information about the solution.

This study focuses on developing adaptive methods that do not claim strong assumptions about the functional form of the unknown epicardial potential distribution and requires less or relatively easily obtainable prior information compared to traditional

inverse problem solution techniques. In order to reach these goals the inverse ECG problem is handled both from statistical and deterministic solution techniques perspectives. Firstly, minimum relative entropy method is adopted as an alternative statistical solution technique for inverse ECG problem and effects of method parameters are comprehensively assessed. From deterministic solution technique perspective, we have proposed multivariate adaptive spline-based method in order to decrease the number of unknown in the problem while increasing the estimation accuracy by taking advantage of local support property of spline-based approaches.

Keywords: inverse problem, inverse electrocardiography, minimum relative entropy, multivariate adaptive regression splines, regularization

ÖZ

TERS ELEKTROKARDİOGRAFİ PROBLEMİNİN ÇÖZÜMÜNDE ÇOKDEĞİŞKENLİ UYARLANABİLİR YÖNTEMLER

Onak, Önder Nazım

Doktora, Bilimsel Hesaplama Bölümü

Tez Yöneticisi   : Doç. Dr. Yeşim Serinağaoğlu Doğrusöz

Ortak Tez Yöneticisi   : Prof. Dr. Gerhard Wilhelm Weber

Eylül 2018 , 111 sayfa

Elektrokardiyografik görüntüleme (ECGI) kalp elektriksel aktivitesini daha detaylı görselleştirmek için üzerinde çalışılan bir tıbbi görüntüleme yöntemidir. Kardiyak anormalliklerin teşhisi ve gerekli tedavilerin planlanmasını ve uygulanmasını kolaylaştırıcı potansiyele sahiptir. Kalp elektrik aktivitesinin görüntülenmesi, kötü konumlandırılmış ters elektrokardiyografi (EKG) problemini çözmeyi gerektirmektedir. Çeşitli çözüm yöntemleri geliştirilmesine ve uygulanmasına rağmen, günlük klinik uygulamalarda kullanımını engelleyen bazı sınırlamalar ve zorluklar bulunmaktadır. Bu nedenle, ters EKG problemi hala araştırmacıların ilgisini çekmektedir.

Ters EKG problemini çözmek için çeşitli düzenlileştirme yöntemi uygulanmış olsa da bunların hiçbiri optimum yöntem olarak kabul edilmemektedir. Çünkü, bu yöntemlerin hassasiyet, hesaplama karmaşıklığı ve çözümle ilgili gerekli önsel bilgilerin elde edilmesi bakımından birbirlerine göre artıları ve eksileri bulunmaktadır.

Çalışmamızda, bilinmeyen epikardiyal potansiyel dağılımının fonksiyonel yapısı hakkında güçlü varsayımlarda bulunmayan esnek yöntemler geliştirmeyi amaçladık. Bununla beraber mevcut ters problem çözüm teknikleri ile karşılaştırıldığında, uygulayacağımız yöntemin göreceli daha az veya elde edilmesi kolay önsel bilgi içermesini hedefledik. Bu amaçlara ulaşmak için, ters EKG problemi istatistiksel ve deterministik çözüm teknikleri açısından ele alınmıştır. Öncelikle, ters EKG problemi için

alternatif istatistiksel çözüm yöntemi olarak minimum bağıl entropi yöntemi benimsenmiş ve yöntem parametrelerinin etkileri detaylı incelenmiştir. Deterministik çözüm tekniği olarak, çok değişkenli parametrik olmayan bağlayıcı fonksiyon temelli çözüm yöntemi önerilmiş, tahmin doğruluğunu arttırırken problemin bilinmeyen sayısını azaltılmıştır.

Anahtar Kelimeler: Ters problemler, ters EKG, minimum bağıl entropi, çok değişkenli uyarlanabilir regresyon eğrileri, düzenlileştirme.

To my family.

ACKNOWLEDGMENTS

I am heartily thankful to my supervisor, Assoc. Prof. Yeşim Serinağaoğlu Doğrusöz, whose encouragement and support from the initial to the final level of the study enabled me to develop a deep understanding of the scientific development process. Her willingness to give her time and valuable advices during development and preparation of this dissertation has brightened my path. I also express my gratitudes to my co-supervisor, Prof. Dr. Gerhard-Wilhelm Weber for the numerous contributions, encouragements and enormous support. It is honor for me to study with them.

I also would like to thank my family, their value cannot be expressed in words.

TABLE OF CONTENTS

LIST OF TABLES

LIST OF FIGURES

FIGURES

LIST OF ALGORITHMS

ALGORITHMS

LIST OF ABBREVIATIONS

AF	Atrial Fibrillation
AV	Antrioventricular Valve
ATP	Adenosine Triphosphate
AP	Action Potential
BEM	Boundary Element Method
BF	Basis Function
BSP	Body Surface Potentials
BSPM	Body Surface Potential Measurements
CC	Correlation Coefficient
CEI	Consortium of Electrocardiographic Imaging
CT	Computed Tomography
ECG	Electrocardiogram
ECGI	Electrocardiographic Imaging
EDL	Equivalent double layer
GCV	Generalized Cross-Validation
GES	Generalised Eigensystem
LE	Localization Error
MARS	Multivariate Adaptive Regression Splines
MR	Magnetic Resonance
MRE	Minimum Relative Entropy
PRSS	Penalized Residual Sum of Squares
PVC	Premature Ventricular Contraction
pdf	Probability Density Function
RE	Relative Error
SNR	Signal to Noise Ratio
SI	Spline Inverse
TTLS	Truncated Total Least Squares
TMV	Transmembrane Voltages

VCM	Volume Conductor Model
$\mathbb{R}$	Set of Real Numbers

CHAPTER 1

INTRODUCTION

Heart is an electro-mechanical organ that pumps the blood through the whole body via contracting and expanding its muscles. The contraction of the cardiac muscles is triggered and accompanied by the electrical current, which causes potential fields through the heart tissue. Spread of these potential fields over the heart surface activates the resting tissues for contraction. It also propagates throughout the body tissues encircling the heart and on the thorax.

Heart diseases are the foremost cause of death worldwide. According the World Health Organization (WHO), heart diseases represented 31% of all global deaths in 2015, which is higher than all form of cancer combined [110]. Since the heart failure can occur rather unexpectedly or happen gradually over months, anyone who are at cardiovascular risk need early detection and inspection via counseling, guidance and medication as deemed appropriate.

Medical imaging modalities have been important tools to visualize tissues, organs and chemical or electrical activities of the human body in order to diagnose the patients clinical problems. In the field of *Cardiac Electrophysiology*, 12-lead electrocardiography (ECG) has become the broadly used non-invasive tool for visualizing the time-varying electrical activity of the heart. The information provided by ECG might be crucial to diagnose heart diseases. Since, any deviation from the regular behavior of the electrical activity may be the indicator of cardiovascular disorders and, it can help diagnose a disease while it is still in its early stages. However, ECG suffers from a low-resolution information due to the sparse body surface measurement locations, attenuated and smoothed signal measurements, which significantly restraint its bene-

fits. Since the activity of the heart arise as a result of complex electrical and biological phenomenons, low-resolution information prevents determination of clear-cut separation between normal and abnormal ECG signal [65]. For this reason, researchers have been working on the imaging technology, known as Electrocardiographic Imaging (ECGI), and developed computational methods to obtain more extensive information of cardiac electro-physiology to tackle with difficulties confronted in clinical diagnosis arising from limited data.

Imaging heart's electrical activity by ECGI systems requires solving the inverse problem of electrocardiography. Solution of this inverse problem can be defined as estimating the parameters of the cardiac source model using the forward model relating the source to body surface potential measurements (BSPM). It could be an alternative imaging modality by filling the gap between 12-lead ECG and invasive cardiac electrical activity monitoring methods if it is supported by a sufficient patient statistical evaluation [20, 62]. The establishment of the forward model relies on the geometry and electrical conductivities of inhomogeneities inside the torso. Due to the dispersing effect of the torso on the heart signals and the discretization process, inverse problem is ill-posed [16]. Thus, small variations in the model or measurements can give rise to large errors in the solution.

Solving an ill-posed inverse ECG problem to reconstruct a physiologically meaningful electrical activity of the heart is a challenging task. On the other hand, it is possible to increase the solution stability against the perturbations by means of regularization methods by incorporating prior knowledge about the desired solution. Although several methods have been proposed, this task still receives a lot of attention from researchers, who are trying to develop a solution technique that is optimal both in terms of accuracy and computational complexity [23, 31, 116].

1.1   Motivation and Goals of the Study

Because of advancements in applied mathematics and supported by emerging computer technology, solution techniques (quadratic, non-quadratic, statistical, etc.) have been developed to solve inverse problems in various fields of science and engineer-

ing. Many of these algorithms have been adopted to solve the inverse ECG problem by considering the properties of underlying cardiac electrical process. On the other hand, all methods have their pros and cons compared to each other in terms of accuracy, computational complexity and required prior information about the solution. For example, while quadratic methods assumes that the epicardial potential distribution is smoothly changing over the heart surface, on the contrary l_1-norm regularization implicitly seek a sparse solution [37, 114]. However, hearts electrical activity starts from a few focal sites but then propagates throughout heart surface. As a result, the structure of epicardial potential distribution has complex spatio-temporal behavior during the cardiac cycle [84]. Assuming that we have no a priori information about the current form of epicardial potential distribution, the question remains as which particular norm solution should be employed. Alternatively, inverse problem can be solved by statistical methods. Given an estimate of the multivariate probability distribution function (pdf), one can obtain estimation of the unknown variables. Although the studies on Bayesian estimation of epicardial potentials [91, 104] assumed that prior pdf is multivariate Gaussian distribution. This definition is based on empirical study of the epicardial potential distributions, and it is not proven that Gaussian prior is the best way to represent the epicardial potentials.

The main goal of this thesis is to develop adaptive methods that do not claim strong assumptions about the functional form of the unknown epicardial potential distribution, and that need less or relatively easily obtainable prior information compared to other inverse problem solution techniques. To reach these goals, inverse ECG problem is handled both from statistical and deterministic solution perspectives. For each perspective, the goals and contribution of this research can be summarized as follows:

- *Adopting a statistical solution method for the solution of the inverse ECG problem which requires prior information about the unknown epicardial potential distribution that can be obtained more easily, compared to other statistical methods. Reducing the dependency of this information could facilitate and improve the quality of the solution.*

  The success of statistical methods relies on good prior information such as prior expected value and variance, which are not always easy to obtain. Even with

a simple Gaussian distribution, prior expected value (mean) vector and covariance matrix are necessary to fully represent the epicardial potentials. On the other hand, the form of the probability density function (pdf) may not be known or be highly suspected and some important statistical parameters, such as the mean or the variance may not be well-known or difficult to estimate [111, 114].

- *Constructing an adaptive method that represents the epicardial potential distribution such that the number of unknown variables are less than the original problem but overcome the shortage of l_2-norm approaches when the epicardial potential distribution is sparse.*

Spline-based methods are alternative approach to solve ill-posed inverse problems. The main advantage of them is the parametrization of the problem in terms of a small number of unknowns. In addition, the local support of the splines allows changing the approximation in local regions without affecting remote portions of the curve to increase accuracy of the approximation [10, 18]. Despite these advantages, there are very few studies in literature that solve the inverse ECG problem using splines [28, 118, 119]. These studies use parametric methods, i.e., assumptions on functional relationship between dependent and independent variables must be specified in advance. However, determination of the optimal number of basis functions and the knot locations requires preliminary works on the data to obtain an accurate approximation. Typical approach to choose these parameters is quite arbitrary by using trial-and-error [45]. A possible way to remedy this issue is to use non-parametric regression methods.

1.1.1 Contributions of the Thesis

This dissertation achieves the following major contributions.

- Minimum Relative Entropy (MRE) method is successfully adopted to reconstruct epicardial potential distribution, and effects of its parameters to the solution have been systematically investigated. Starting from simple box car distribution, first of all prior pdf is constructed with the help of body surface mea-

4

surements. This step eliminates the strong assumption about prior pdf definition for statistical inversion. Instead, it is shown for inverse ECG problem that prior pdf can be constructed starting from any simple probability distribution. Next, posterior pdf is computed and than impacts of parameters lower-upper bounds, mean and expected uncertainty to the solution have been investigated. It is also revealed that, the most important parameter is the expected mean value unless the other parameters are under-estimated. Compared to Bayesian estimation, information about the MRE parameters can be obtained more easily.

This work has resulted in the following publications and presentations:

- Onak, O. N., Serinagaoglu Dogrusoz, Y., G.-W. Weber, *Effects of a priori parameter selection in minimum relative entropy method on inverse electrocardiography problem.* Inverse Problems in Science and Engineering, 26(6), 877–897, 2018. (SCI)

- Onak, O. N., Serinagaoglu Dogrusoz, Y., G.-W. Weber, *Minimum relative entropy method for inverse electrocardiography problem*, Problems of Non-linear Analysis in Engineering Systems No.1(41), vol. 20, 64-70, 2014.

- Multivariate adaptive non-parametric reduced-order model for ill-posed linear inverse ECG problem is proposed. Its strong features and properties that need to be improved have been investigated using a large dataset under several simulation scenarios. Proposed method adaptively constructs functional representation of the unknown epicardial potential distribution using a small number of basis functions, which significantly reduces problem dimension while increasing the estimation accuracy in earlier times of the stimulation. Our approach differs from the other spline based methods such that the underlying functional relationship between dependent and independent variables do not need to be determined in advance.

As a result of this study, it is shown that non-parametric regression methods provide a flexible way of modeling epicardial potential distribution function for the inverse ECG problem. Hence, necessity of preliminary work to determine the functional representation of the unknown epicardial potential distribution is alleviated by means of non-parametric regression technique. Additionally,

it is also demonstrated that, local support of the spline based modeling can facilitate the shortage of l_2-norm solutions in some extend when the epicardial potential distribution is sparse (i.e., close to stimulation time). The success in estimating the sparse epicardial potential leads to determination of pacing site more accurately.

This work has resulted in the following publications and presentations:

- Onak, O. N., Serinagaoglu Dogrusoz, Y., and Weber G.-W., *Evaluation of multivariate adaptive non-parametric reduced-order model for solving the inverse electrocardiography problem: A simulation study*. In review: Medical and Biological Eng and Computing. (SCI)

- Onak, O. N., Serinagaoglu Dogrusoz, Y, and Weber G.-W., *Robustness of Reduced Order Non-Parametric Model for Inverse ECG Solution Against Modelling and Measurement Noise*, Computing in Cardiology, Maastricht, Netherlands, Sep. 23-26, 2018.

- Onak, O. N., Serinagaoglu Dogrusoz, Y., and Weber G.-W., *Effects of Measurement Noise in MARS-based Inverse ECG Solution Approach*, 26th IEEE Signal Processing and Communications Applications Conference, Çesme, Izmir, 2-5 May. 2018.

- Onak, O. N., Serinagaoglu Dogrusoz, Y., and Weber G.-W., *Effect of the Geometric Inaccuracy in MARS-based Inverse ECG Solution Approach*, Computing in Cardiology, Rennes, France, Sep. 24-27, 2017.

- Onak, O. N., Serinagaoglu Dogrusoz, Y., and Weber G.-W., *Application of Multivariate Adaptive Regression Splines for Inverse ECG Problem*, 20th National Biomedical Engineering Meeting, Seferihisar, Izmir, 3-5 Nov. 2016.

Consequently, both MRE and proposed non-parametric spline-based method in this dissertation construct models for representation of unknown epicardial potential distribution step by step using available measurements. They are less restrictive, and demand less prior information compared to other parametric regularization techniques. They can also be used to confirm the correctness of the parametric model for the inverse ECG problem under consideration.

1.2 Scope of the Thesis

This dissertation is composed of 4 main chapters excluding the introduction and appendices:

- The second chapter provides background information about cardiac anatomy and electrophysiology. After that, foundation of the forward and inverse ECG problems, along with a comprehensive literature survey including the inverse problem solution techniques are presented. This chapter also includes the explanation of datasets that we used for solving the inverse ECG problem and quantitative accuracy measurement metrics for comparison purposes.

- Chapter 3 starts with the detailed description of the MRE method and its application to linear inverse ECG problem. After that, second part of the chapter presents the estimation results and assessments on the effects of MRE parameters.

- Chapter 4 presents the definition of Multivariate Adaptive Regression Splines (MARS) algorithm, and a reformulation of the linear inverse ECG problem based on MARS method. The rest of the chapter includes estimation results obtained under perturbations such as modeling error and measurement noise.

- Chapter 5 includes concluding remarks and an outlook to future studies.

CHAPTER 2

BACKGROUND

2.1 Anatomy of the Heart

The heart is a cone shaped, fibromuscular organ. It lies in the middle mediastinum of the thoracic cavity between the right and left pleural sacs, which is called pericardium [61]. A small amount of fluid is present within the sac, called as the pericardial fluid, which lubricates the surface of the heart and allows it to move freely during contraction and relaxation functions [61, 68, 109]. The heart continuously operates as a pump to deliver blood to whole body. It is at the a centre of the circulatory system. The average human heart beats at 72 beats per minute and pumps approximately 4.7-5.7 liters of blood per minute. It weighs approximately 250 to 300 grams in females and 300 to 350 grams in males [106].

The wall of the heart is composed of three layers as shown in Fig. 2.1:

- The epicardium is the outer lining of the cardiac chambers and is formed by the visceral layer of the serous pericardium [47]. It is the interior pericardium layer and also called visceral pericardium.

- The myocardium is the middle layer of the cardiac wall and is composed of three discernable layers of muscles that are seen predominantly in the left ventricle and inter-ventricular septum alone. It includes a subepicardial layer, a middle concentric layer and a subendocardial layer [92]. The myocardium also contains important structures such as excitable nodal tissue and the conducting system.

- The endocardium is the innermost layer of the heart. It is formed of the endothelium and subendothelial connective tissue [92, 101].
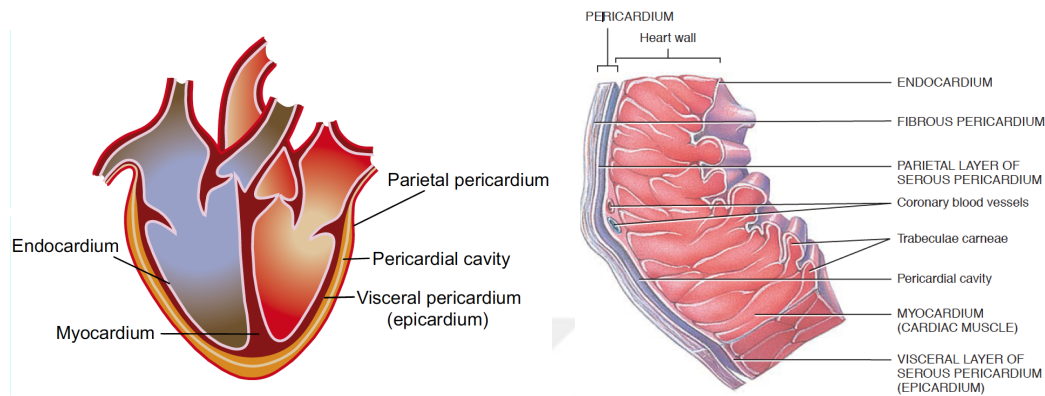
Figure 2.1: Layers of the heart [92, 101].

The heart is separated into four distinct chambers as shown in Fig. 2.2. The two superior receiving chambers are the left and right atria, which are thin-walled, located just above the thick-walled inferior pumping chambers called as left and right ventricles, respectively. The atria receive blood from the venous system and lungs and then contract and eject the blood into the ventricles. The right ventricle pumps blood through the pulmonary circulatory system, and the left ventricle pumps blood through the longer systemic circulatory system [26, 92, 101].

The heart contains four valves located between each atrium and ventricle and in the two arteries that empty blood from the ventricle (Fig. 2.2). These valves are primarily composed of fibrous connective tissues that originate and extend from the heart walls.

Tricuspid valve manages blood flow from the right atrium to the right ventricle. The bicuspid (mitral) valve controls blood flow from the left atrium to the left ventricle. The pulmonary valve blocks the blood pumped to left pulmonary arteries from flowing back to the right ventricle. The aortic valve restricts blood flow direction only towards the aorta [26].
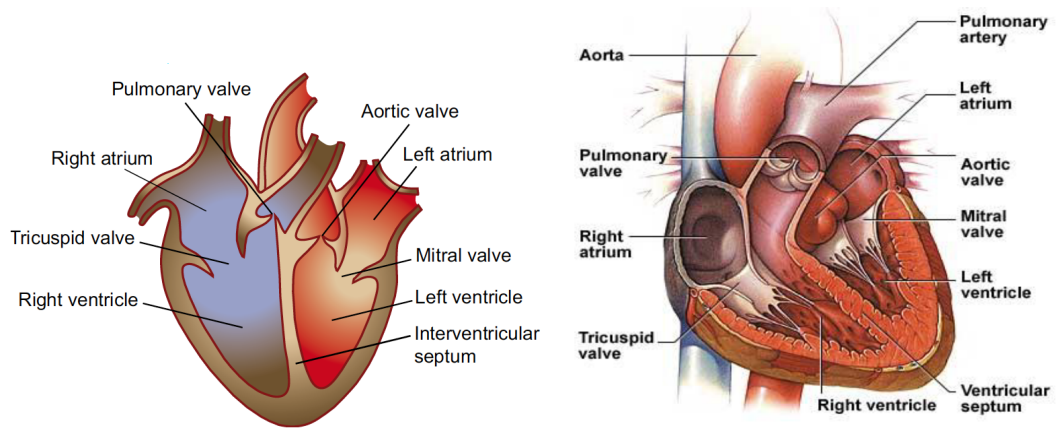
Figure 2.2: The Chambers and valves of the heart [26, 92].

2.2 Cardiac Electrophysiology

Cardiac muscle cells also known as cardiac myocytes are packed with mitochondria to maintain the steady supply of ATP required for contraction [78]. The contraction of the cardiac muscles is a complex process and can be divided into neural, hormonal and intrinsic components. Under normal conditions, the contraction of heart muscles is initiated by an electrical impulse in the sinotrial node located at the right atrium and spread through the atria and antrioventricular node. The stimulation of one cardiac cell initiates stimulation of adjacent cells. The difference between excited and resting tissue voltages leads to electrical current which causes excitation of the resting tissues in a wave-like manner [65]. Concurrently with electrical stimulation and contraction of atrium, blood is pumped to the ventricles. Afterwards, excitation wave-front activates ventricular conduction system, Fig. 2.3, and advances throughout the ventricular muscle and triggers contraction of ventricular myocardium, resulting in blood being pumped to the body. The conduction system provides an automatic rhythmic beat in order to pulmonary and systemic circulation operate in synchrony.

The electrical impulse that travels through the heart is formed by ion movements across the membranes of heart cells that result in a potential difference across cellular membranes. This imbalance, which is called the Action Potential (AP), reflects the complex intracellular and extracellular concentration variation of sodium (Na^+), potassium (K^+) and calcium $(Ca2^+)$ ions. The shape of AP differs depending on lo-
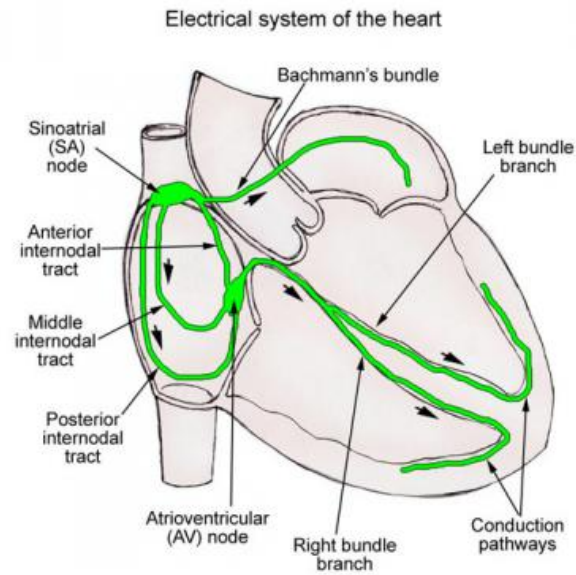
Figure 2.3: Schematic illustration of the cardiac conduction system [26].

cation of the cell in the heart, due to different ion channels and anatomy of myocytes muscle cells. Notwithstanding differences, APs have strong similarities and their shape can be divided into five phases. The shape of AP as shown in Fig. 2.4, represents different phases of opening and closing of different ion-channel types, which results in ion currents and also membrane potentials as follows [58]:
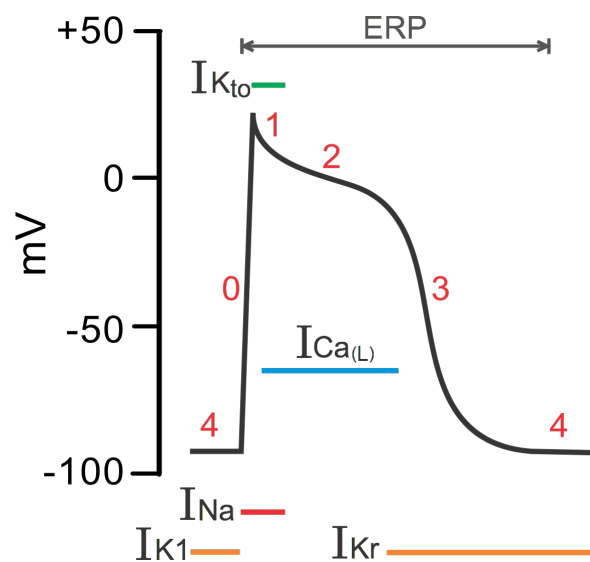
Figure 2.4: Phases of a cardiac action potential (myocardium) [58].

- **Resting phase (4):** It is the natural state, and a cell will remain in the resting

12

state until an electrical stimulation arrives.

- **Depolarization phase (0):** The sharp increase in AP is caused by the transient influx of Na^+ ions.

- **Early re-polarization phase (1):** Corresponds to the Na^+ channel inactivation and the polarizing efflux of K^+ ions.

- **Plateau phase (2):** The distinctive plateau is associated with the opening of voltage-sensitive Ca^{2+} channels.

- **Re-polarization phase (3):** Outward K^+ channels remain open, but the Ca^{2+} channels close.

Electrically discharging frequency of sinotrial node determines the rate of heart beats. Any premature discharges due to electrical irregularities of the heart muscles disrupt the heart rhythm. If premature contraction occurs in the lower chambers of the heart, it is called Premature Ventricular Contraction (PVC). During PVC, the ventricle generates an action potential too soon without waiting for a stimulation initiated by a normal conduction mechanism of the heart, causing an irregular heart beat. The source and pattern of PVC can be identified via electrocardiogram (ECG). Treatment procedure depends on the severity of the symptoms. In case of ablation therapy, determination of exact source location of premature contraction is important for the success of the procedure. However, classical ECG techniques offer limited information about the spatial properties of cardiac abnormalities [22]. It is the goal of noninvasive ECGI techniques to provide high resolution information for clinicians in order to increase the success of treatment. For example, priory localization of PVC via ECGI would facilitate the planning and execution of radio frequency catheter ablation [103].

2.3 Electrocardiographic Imaging

Electrocardiographic imaging (ECGI) is a noninvasive technique for cardiac electrophysiology to provide high resolution information from body surface potential measurements (BSPM) with the use of patient-specific cardiac MR and CT images. All these measurements and images are used to reconstruct cardiac electrical activity such

as potential and activation patterns of the heart tissues. The idea of developing high resolution electrocardiographic method derives from the aspiration to obtain a high resolution image of cardiac electrical activity beyond the capabilities of the classical 12-lead ECG [49, 86, 88]. It has been gaining attention of the researchers both from academia and industry. Because of the strong interest in this field Consortium of Electrocardiographic Imaging (CEI) [23] and EDGAR data repository [4] has been formed for interaction and collaboration of researchers and data exchange through the workgroups. The basic ECGI methodology involves solving the electrocardiographic forward and inverse problems. While the forward problem of ECG aims to predict body surface potential distributions from the known cardiac source model, the inverse problem of ECG reconstructs electrical activity of the heart from body surface measurements and previously constructed forward model. In this chapter, we provide a brief description and mathematical structure of both problems, then summarize the important solution techniques that have been proposed to solve the ill-posed inverse problem of ECG.

2.4 ECG Forward Problem

The term *forward problem* refers to modeling some physical fields, processes, or phenomena. Mainly, forward problem includes: domain and equations of process, the initial conditions if applicable (i.e., process is non-stationary) and boundary conditions of the domain [55]. The forward problem of ECG aims at computation of the body surface potential distribution resulting from cardiac electrical activity. Calculation of the electric field in the torso is mainly dependent on size, location and properties of the internal structures between the heart and torso surface [73]. Skeletal muscles, lungs, fats, bones and blood are some of the major internal structures that can be taken into account in the solution of the forward problem. On the other hand, considering all the inhomogeneities increases the computational complexity of the forward problem. For this reason, it is required to find a balance between the accuracy of the solution and the computational complexity of the problem.

Besides structure of the torso, the cardiac source model also needs to be specified to complete the model of the forward ECG problem. The equivalent double layer

14

(EDL) and the surface potential representation (endocardial and epicardial) are two major cardiac source models that have been used to solve inverse and forward problems [105]. After selecting torso and cardiac source models, potential distribution on the body surface can be computed either by boundary element method (BEM) or by volume conductor model (VCM) [41, 42, 73, 81].
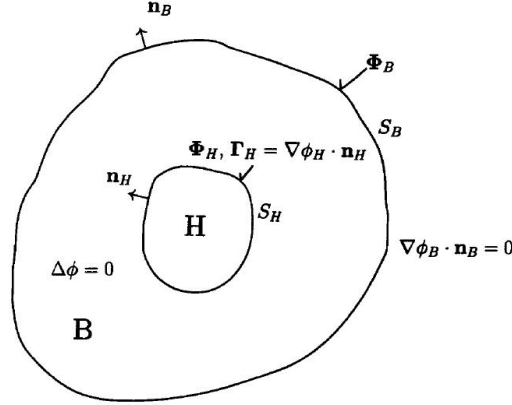
Figure 2.5: A model of homogeneous torso-volume conductor. The human thorax is bordered by a surface, S_B, and surrounded by a non-conductive air; all cardiac bio-electric sources are planted in the closed region covered by epicardial layer, S_H [71].

The system depicted in Figure 2.5 represents the thorax and epicardium forming two nested non-intersecting surfaces. This system is described by a quasi-static approximation of Maxwell's equations with the assumption of no active bioelectric sources existing between these two surfaces. In terms of the epicardial potentials, the ECG forward problem can be formulated as Laplace's equation with boundary condition defined in Eqn. (2.1) [71].

$$\nabla \cdot \sigma \nabla \phi(\mathbf{p}) = 0 \qquad (\mathbf{p} \in B), \qquad \nabla \phi(\mathbf{p}) \cdot \mathbf{n_b} = 0 \qquad (\mathbf{p} \in S_B), \qquad (2.1)$$

where $\mathbf{B}$ is an isotropic volume conductor (the human torso) in which is contained the region of bioelectric sources, $\mathbf{H}$, σ is the scalar conductivity of $\mathbf{B}$, $\phi(\mathbf{p})$ is the electric potential at a field point $\mathbf{p} = (x, y, z)$, and S_H and S_B are smooth surfaces with unit normals $\mathbf{n}_H$ and $\mathbf{n}_B$ that are oriented outward with respect to the region $\mathbf{H}$.

The outcome of the forward solution can be represented in vector-matrix notation as

15

follows:

$$\mathbf{y} = \mathbf{A}\mathbf{x}. \tag{2.2}$$

Here, $\mathbf{A} \in \mathbb{R}^{m \times n}$ is a forward operator, $\mathbf{y} \in \mathbb{R}^m$ stands for the measurement vector and $\mathbf{x} \in \mathbb{R}^n$ denotes the source (epicardial potential) vector.

It is important to ensure a rigorous identification of the forward transfer operator in ECGI, which characterizes the relationship between measurements and source. However, as we stated previously, taking into account all inhomogeneities within the torso increases computational complexity of the forward problem. For this reason, it is required to find a balance between accuracy of the solution and computational complexity of the problem. Nevertheless, which inhomogeneous electric properties of internal structures need to be accounted for is not clear enough [11]. Several studies have been done by researchers to find out how much detail needs to be considered for the forward/inverse ECG problems. In [85], Ramanathan et al. attempted to characterize and understand the effects of conductor properties within the torso using a detailed realistic torso model that includes all the major inhomogeneities and epicardial potentials as a cardiac source model. Results of this study showed that, if there were no pathology causing variations in volume conductor properties, potential patterns on body surface were minimally affected by the torso inhomogeneities. Klepfer et al. [59] concluded that including inhomogeneities have minor influence on the of body surface potential pattens but they alters the magnitude of potentials. The results of Klepfer's study suggest that subcutaneous fat, anisotropic skeletal muscle and lungs should be included in simulating the torso potentials. Keller et al. [57] discussed different organs have varying influences on the different ECG segments; While lungs are more important for atrial signals, ventricular signals are more effected by the heart conductivities. But, blood and anisotropic skeletal muscle have greater impact on both atrial and ventricular signals. In recent study by Bear et al. [11], the inhomogeneous torso models produced potential amplitudes closer to the true potentials compared to those obtained by the homogeneous model. Common conclusion in these studies was, despite the amplitude differences between simulated and measured body surface potentials their potential maps were quite similar. On the other hand, Cluitmans et al. [20] argued that to decide the complexity of the forward

16

model, more in-vivo studies need to be conducted.

2.5 ECG Inverse Problem

Inverse problem is a field in mathematics and the applied sciences, which refers to approximating underlying function or estimating model parameters of a physical phenomena from indirect measurements [25, 97]. In this sense, inverse problem of ECG can be described as inferring cardiac electrical activity from the given BSPM and mathematical model that characterizes the relationship between measurements and sources. Here, the mathematical model is constructed by solving the forward ECG problem. Depending on the selected cardiac source model, the parameters to be estimated vary. On the other hand, the generic form of the problem is similar [105]. If the cardiac source is taken as an epicardial potential distribution, then the problem can be represented as follows:

$$\mathbf{y}_k = \mathbf{A}\mathbf{x}_k + \mathbf{n}_k \quad (k = 1, 2, \dots T), \tag{2.3}$$

where, $\mathbf{A} \in \mathbb{R}^{m \times n}$ and k are the forward transfer matrix and the time index, respectively: $\mathbf{y}_k \in \mathbb{R}^m$ stands for the body surface potentials at all observation points, and $\mathbf{x}_k \in \mathbb{R}^n$ denotes the unknown epicardial potentials to be estimated. In our study, these parameters are the potentials on the epicardial surface. The last term $\mathbf{n}_k \in \mathbb{R}^m$ represents the measurement noise.

The difficulty of the inverse ECG problem arises from their ill-posed nature. This ill-posedness originates from the discretization process in the forward solution and attenuation of the signal inside the torso. Amount of attenuation also changes depending on the measurement location, because of the distance to the source and the inhomogeneities through propagation direction. Although there is no formal definition of an ill-posed problem, it should involve all the problems that have no solutions or have many solutions in the desired class, or the solutions are unstable. But in common use, the term *ill-posed* is related to unstable problems [55]. From the perspective of inverse ECG problem, instability means that relatively small changes in the body surface measurements are abundantly amplified in the solution. In addition to mea-

surement noise, inaccuracies in the heart-torso geometric model and errors in the conductivities of the organs, which are used to calculate forward operator, also affect the solution. Furthermore, if the number of the measurement locations is less than the number of the parameters to be estimated (i.e., the forward transfer matrix $\mathbf{A}$ in Eqn. (2.3) is under-determined) there can be no unique solution [82]. Consequently, problem need to be appropriately constrained by introducing prior information about the solution in order to obtain physiologically meaningful outcome.

2.5.1 Solution Methods

Inverse problems have gained lots of attention due to their important applications in different fields of science. Several algorithms have been developed to solve linear and non-linear inverse problems. These algorithms solve the inverse ECG problem by considering the properties of underlying cardiac electrical process. These solution techniques can be divided into two categories: deterministic and statistical frameworks [82]. In this part of the thesis we will review the most commonly used methods solving the inverse ECG problem.

2.5.1.1 Deterministic Methods

The solution techniques in deterministic framework usually called as regularization methods, in which an objective function to be minimized or a constraint function to be satisfied is composed of a combination of the norm of the residual error and some norm of a constraint functions [82]. In this part, we will summarize notable deterministic methods which are proposed for solving inverse ECG problem.

Tikhonov Regularization:
It is well-known standard technique to eliminate the instability in the inverse solution [5, 17, 38]. It has been applied in several areas including electrocardiography. The form of the Tikhonov regularization for the linear inverse problem takes the form given in Eqn. (2.4). In this equation, since the problem is solved at each time instant

18

separately, the time index k is omitted.

$$\arg \min_{\mathbf{x} \in \mathbb{R}^n} \{ \|\mathbf{y} - \mathbf{A}\mathbf{x}\|_2^2 + \lambda \|\mathbf{R}\mathbf{x}\|_2^2 \}, \tag{2.4}$$

where $\lambda \geq 0$ is a regularization parameter. It controls the trade-off between fidelity to the measurements and the defined constraint. Although several methods have been proposed to determine the optimal value for λ, the L-curve method [43] is commonly utilized for the inverse ECG problems. The L-curve is a plot on log-log scale with λ is a parameter on this curve and the optimal regularization parameter is assumed to be the value of λ which minimizes both $\|\mathbf{y} - \mathbf{A}\mathbf{x}\|_2^2$ and $\|\mathbf{R}\mathbf{x}\|_2^2$ in some sense [8]. Regularization matrix $\mathbf{R}$ is used to incorporate the priori information about the solution. It can be the identity matrix or the first or second order derivative operator depending on the desired smoothness of the solution. If $\mathbf{R} = \mathbf{I}$, then the Tikhonov estimation can be calculated using singular value decomposition (SVD) as follows:

Singular value decomposition of matrix $\mathbf{A}$ is represented as:

$$\mathbf{A} = \mathbf{U}\mathbf{\Sigma}\mathbf{V}, \tag{2.5}$$

where

$$\mathbf{U} = [\mathbf{u_1} \ldots \mathbf{u_n}], \quad \mathbf{V} = [\mathbf{v_1} \ldots \mathbf{v_n}], \tag{2.6}$$

$$\mathbf{\Sigma} = diag(\sigma_\mathbf{1}, \ldots, \sigma_\mathbf{n}), \quad (\sigma_1 \geq \sigma_2 \geq \ldots \geq \sigma_n). \tag{2.7}$$

The Tikhonov estimation is given by

$$\hat{\mathbf{x}}_\mathbf{Tikh} = \sum_{i=1}^{n} \frac{\sigma_i^2}{\sigma_i^2 + \lambda} \frac{\mathbf{u_i}^T y}{\sigma_i} \mathbf{v_i}. \tag{2.8}$$

The idea of Tikhonov method is to suppress the contribution of small singular values into solution, i.e., high frequency components are filtered out. Tikhonov regularizations of zero-first and second order were applied to inverse ECG problem and its estimation accuracy reported in [21, 70, 71]. According the results of these studies, although the major features of epicardial potential distribution pattern could be detected, the solutions were smooth and had lower amplitudes then the true epicardial potentials.

Truncated Singular Value Decomposition (TSVD):

TSVD method uses first $k < n$ singular values and corresponding right and left eigen-vectors to solve the problem, which is called truncation.

$$\hat{\mathbf{x}}_{Tsvd} = \sum_{i=1}^{k} \frac{\mathbf{u_i}^T y}{\sigma_i} \mathbf{v_i}. \tag{2.9}$$

The truncation parameter k is used to prevent the perturbation error from blowing up, at the cost of introducing bias in the regularized solution. But the determination of optimal k is another issue to be solved.

Generalised Eigensystem:

Generalised eigensystem (GES) proposed by Throne et al. [99] employs finite element technique to define a truncated eigenvector expansion. The BSPM are approximated in terms of the eigenvectors, and a least squares fit is used to estimate the expansion coefficients. The resultant expansion can be used to calculate the heart surface potentials as follows:

$$\begin{bmatrix} \mathbf{x}_H \\ \mathbf{x}_V \\ \mathbf{y} \end{bmatrix} = \sum_{i=1}^{N_\alpha} \alpha_i \begin{bmatrix} \boldsymbol{\nu}_H^i \\ \boldsymbol{\nu}_V^i \\ \boldsymbol{\nu}_y^i \end{bmatrix}, \tag{2.10}$$

where the α_i and N_α are expansion coefficients and number of eigenvector considered in the solution respectively and: $\mathbf{x}_H$, $\mathbf{x}_V$ and $\mathbf{y}$ are heart surface, volume and body surface potentials respectively. On the other hand, $\boldsymbol{\nu}_H^i$, $\boldsymbol{\nu}_V^i$ and $\boldsymbol{\nu}_y^i$ correspond to the ith eigenvectors. The increase in the surface mesh structure resolution and the optimally selected N_α value produces better estimations as expected.

GES, TSVD methods and Tikhonov regularization were employed for solving the problem of inverse ECG using inhomogeneous eccentric sphere model in [100] to examine the effects of geometry and conductivity errors. Although the outcomes of GES had lower RMS values for almost all range of tested modeling error cases, studies on more realistic geometries are required in order to comprehensively its success.

Truncated Total Least Squares

Shou et al. [95] tested Truncated Total Least Squares (TTLS) method using a realistic

heart–lung–torso model with inhomogeneous conductivities.

$$\underset{\tilde{\mathbf{A}},\tilde{\mathbf{y}}}{\text{minimize}} \|(\mathbf{A}, \mathbf{y}) - (\tilde{\mathbf{A}}, \tilde{\mathbf{y}})\|_F \quad \text{subject to} \quad \tilde{\mathbf{y}} = \tilde{\mathbf{A}}\mathbf{x}. \tag{2.11}$$

Here, $\tilde{\mathbf{A}}$, $\tilde{\mathbf{y}}$ are the erroneous version of $\mathbf{A}$ and $\mathbf{y}$. This study concludes that TTLS results are very close to Tikhonov and TSVD estimations if there is only measurement noise, but performed better in case of geometric errors imposed into the model.

However these standard regularized solutions produce smeared output and lead to decrease in accuracy when locating minimum and maximum potential values [16]. In order to improve the smooth solution of Tikhonov regularization, several approaches have been proposed. Some of the important methods are explained subsequently.

Genetic Algorithm with Tikhonov and TSVD:

In [51], heuristic optimization technique genetic algorithm (GA) was used to improve the estimations of Tikhonov and TSVD regularizations. The idea is to start from the initial population, which is actually constructed by using Tikhonov or TSVD estimations, and find the best epicardial potential vector by solving the following minimization problem:

$$\underset{\mathbf{x}}{\text{minimize}} \|\mathbf{y} - \mathbf{A}\mathbf{x}\|_2^2. \tag{2.12}$$

According to the simulation results in [51] that were performed under different measurement noise levels, estimation accuracies significantly improved. On the other hand the success of this approach strongly depends on the number of generations in the GA algorithm and must be properly determined to improve the estimation.

Binary quadratic optimization:

Potyagaylo et al. [79] developed an approach to determine the ischemic areas and ectopic foci based on transmembrane voltages (TMV). Using the fact that faster depolarization process compared to re-polarization and plateau phase after depolarization, the TMV is assumed to have a constant value in the depolarization phase. Under these assumptions the problem was reformulated as an unconstrained binary quadratic optimization problem.

$$\arg \underset{\mathbf{x} \in [l,u]^n}{\min} \{\|\mathbf{y} - \mathbf{A}\mathbf{x}\|_2^2 + \lambda \|\mathbf{R}\mathbf{x}\|_2^2\}. \tag{2.13}$$

Here, l and u stand for binary values corresponding to the upper and lower bounds that every solution component may take. The problem in Eqn. (2.13) has finite but very large possible solutions. For this reason the authors implemented heuristic search and difference of convex functions algorithms in order to reduce the dimension of the problem to locate ischemic region and ectopic foci.

Multiple Constraint Regularization:

Imposing multiple spatial constraints into the problem was proposed to improve the Tikhonov-based estimations. In [1], incorporation of both spatial energy and Laplacian of the solution constraints were employed.

$$\arg\min_{\mathbf{x}\in\mathbb{R}^n}\{\|\mathbf{y} - \mathbf{A}\mathbf{x}\|_2^2 + \lambda_1\|\mathbf{x}\|_2^2 + \lambda_2\|\mathbf{L}\mathbf{x}\|_2^2\}. \tag{2.14}$$

Here, $\lambda_1 \geq 0$ and $\lambda_2 \geq 0$ are regularization parameters and $\mathbf{L}$ is the Laplacian operator. On the other hand, these methods ignore the time-evolution dynamics of the potential distribution and solve the problem at each time frame separately. Therefore, successively more progressive method was attempted in [16] to account for both spatial and temporal information in the solution by using an augmented model addressed by Eqn. (2.15).

$$\arg\min_{\bar{\mathbf{x}}\in\mathbb{R}^n}\{\|\bar{\mathbf{y}} - \bar{\mathbf{A}}\bar{\mathbf{x}}\|_2^2 + \lambda_1\|\bar{\mathbf{R}}\bar{\mathbf{x}}\|_2^2 + \lambda_2\|\bar{\mathbf{T}}\bar{\mathbf{x}}\|_2^2\}. \tag{2.15}$$

The elements of augmented model are defined as follows: There is the measurement vector $\bar{\mathbf{y}} = [\mathbf{y}_1^T, \ldots, \mathbf{y}_k^T]^T$, where k is the number of time samples. The unknown vector $\bar{\mathbf{x}}$ is defined in a similar way as $\bar{\mathbf{y}}$. The augmented forward operator is constructed as $\bar{\mathbf{A}} = \mathbf{I}_k \otimes \mathbf{A}$. Here, $\otimes$ represents the Kronecker product, and $\mathbf{I}_k$ is $k \times k$ identity matrix. The matrices $\bar{\mathbf{R}}, \bar{\mathbf{T}}$ are operators for spatial and temporal constraints.

It was shown that the conjecture of using spatial and temporal constraints increased the temporal behavior of estimations compared to spatial constraint alone. However, the drawback of this approach is the need for determination more than one regularization parameter. The original study suggested L-surface method to find these parameters. Later on, a genetic algorithm based approach was also proposed in to find these parameters [34].

22

Greensite Spatio-Temporal Approach:

Greensite [40] included temporal correlation of potentials in the problem by concurrently regularizing the equations associated with all time instants. Greensite's method relies on the use of principal components of measurement matrix $\mathbf{Y} = [\mathbf{y}_1, \ldots, \mathbf{y}_T]$ to compute unknown matrix $\mathbf{X} = [\mathbf{x}_1, \ldots, \mathbf{x}_T]$.

If we compute the SVD of the measurement matrix, we obtain:

$$\mathbf{Y} = \mathbf{PST}^T, \tag{2.16}$$

where $\mathbf{P}$, $\mathbf{T}$ are eigenvector matrices related to spatial and time domains of BSPM, respectively. $\mathbf{S}$ is the diagonal matrix containing singular values of $\mathbf{Y}$. Then Eqn. (2.3) can be modified as follows:

$$\mathbf{Y} = \mathbf{AX}, \tag{2.17}$$

$$\mathbf{PST}^T = \mathbf{AX}. \tag{2.18}$$

If we multiply both sides by $\mathbf{T}$ from the right side, we receive:

$$\mathbf{AXT} = \mathbf{PS}, \tag{2.19}$$

$$\mathbf{A\check{X}} = \mathbf{PS}. \tag{2.20}$$

Here, $\mathbf{\check{X}} = \mathbf{XT}$ is the new unknown matrix and Tikhonov regularization can be used to estimate it. After that the solution of $\mathbf{X}$ can be obtained by multiplying $\mathbf{\check{X}}$ by $\mathbf{T}^T$. It was shown that behind in [40] Greensite method produced more accurate solution by increasing the temporal stability of the estimation.

Greensite's idea can be summarized as follows; First the time series of the signals decorrelated prior to applying spatial regularization. After decorrelation is achieved, the resulting set of equations is solved by the standard Tikhonov regularization and finally, the decorrelation is reversed to restore the temporal correlation.

Twomey Technique:

The modification of Tikhonov method was proposed by Twomey [102] in order to avoid unwanted oscillations by including a priori information on the solution.

$$\arg \min_{\mathbf{x} \in \mathbb{R}^n} \{ \|\mathbf{y} - \mathbf{A}\mathbf{x}\|_2^2 + \lambda \|\mathbf{x} - \mathbf{x_p}\|_2^2 \}, \tag{2.21}$$

where $\mathbf{x_p}$ is a prior estimate of $\mathbf{x}$. It is intended to minimize the difference between the solution and an a priori knowledge. Twomey regularization was employed to solve the inverse ECG problem in [36, 77].

Non-Quadratic Methods:

Besides the quadratic regularization methods, non-quadratic approaches have also been proposed for cardiac source reconstruction and locating arrhythmic substrates on the heart. Since l_2-norm penalty functions lead to smooth solutions, they do not produce accurate solution for sparse source imaging, such as locating diseased regions or pacing sites.

The l_1-norm regularization scheme, also known as total-variation regularization, has been applied with considerable success especially, when restoring high-frequency spatial features of inverse ECG problem [37, 115]. This method can be formulated as follows:

$$\arg \min_{\mathbf{x} \in \mathbb{R}^n} \{ \|\mathbf{y} - \mathbf{A}\mathbf{x}\|_2^2 + \lambda \|\mathbf{D}\mathbf{x}\|_1 \}, \tag{2.22}$$

where $\mathbf{D} = \dfrac{\partial \mathbf{x}}{\partial \mathbf{n}}$ is the normal derivative of the potential on the heart surface. It was concluded in [37] that, l_1-norm method has a better capability when detecting and localizing the areas of early activated regions than l_2-norm regularization. Despite its success in reconstructing sparse signals, l_1-norm regularization has high computational complexity due to its nondifferentiable structure. For this reason, smoothed l_0-norm regularization [108] has been proposed to estimate epicardial potential distribution.

Besides the l_0- and l_1- norm based regularization for reconstructing sparse signals, Rahimi et al. [84] utilized l_p-norm regularization to bridge the gap between overly smeared and overly focal solutions. In their subsequent study, a multi-model adaptive

24

estimation approach in which the weighted combination of l_0, l_1 and l_p solution was employed to determine the final estimation [83].

Reduced Order Models:

In order to reduce complexity and increase the estimation accuracy in the inverse ECG problem, reduced-order models were also considered. Use of Proper Orthogonal Decomposition (POD) was attempted to identify ionic parameters and infarction locations [15]. Spline-based methods were applied to the ill-posed inverse ECG problems in order to take the advantages of spline-based regression. Their main advantage is the parametrization of the problem in terms of a small number of unknowns, and their local support that allows for changing the approximation in local regions without affecting remote portions of the function to be estimated. Recently published works of Zettinig [118, 119] and Erem et al. [28] modeled the problem based on cubic polynomials in order to benefit from splines. We call the method in [28] as *Spline Inverse* (SI) in the rest of thesis.

The method proposed in [28] can be summarized as a low-order parametrization of an individual beat using temporal splines. First, the spline fitting procedure for body surface potentials is realized by employing the spline curves that are defined in terms of pseudo-time parameters. After that, the fitting procedure is completed by mapping the outcome from pseudo-time to actual time. For this method, the relationship between the epicardial potentials and the noise-free body surface potentials, which is part of the relationship given in Eqn. (2.2), is rewritten in matrix form as:

$$\mathbf{Y} = \mathbf{AX}, \tag{2.23}$$

where

$$\mathbf{Y} = \left[\mathbf{y}_1, \mathbf{y}_2, \ldots, \mathbf{y}_T \right], \tag{2.24}$$

and

$$\mathbf{X} = \left[\mathbf{x}_1, \mathbf{x}_2, \ldots, \mathbf{x}_T \right]. \tag{2.25}$$

The spline approximation of the body surface potentials ($\mathbf{Y}$) is then defined as follows:

$$\mathbf{Y} \approx \mathbf{K_Y P_1 P_2}, \tag{2.26}$$

where $\mathbf{K_Y}$ is a coefficient matrix for the knot points, $\mathbf{P_1}$ and $\mathbf{P_2}$ are the operators for the spline interpolation in the pseudo-time parameter, and for mapping the pseudo-

time parameter to actual time, respectively. Similarly, heart surface potentials can be represented as follows:

$$\mathbf{X} \approx \mathbf{K_X P_1 P_2}. \tag{2.27}$$

Using Eqns. (2.26) and (2.27), Eqn. (2.23) can be written as:

$$\mathbf{Y} \approx \mathbf{K_Y P_1 P_2} = \mathbf{A K_X P_1 P_2}. \tag{2.28}$$

Then, the inverse problem reduces to solving the following equation for the coefficient matrix $\mathbf{K_X}$:

$$\mathbf{K_Y} = \mathbf{A K_X}. \tag{2.29}$$

In order to solve the unknown matrix $\mathbf{K_X}$ given in Eqn. (2.29) Tikhonov regularization is applied for each column separately. In this study, we employed zero-order Tikhonov regularization, in which the regularization matrix is chosen as the identity matrix.

However, a common issue of such parametric approaches is the determination of the optimal number of spline functions to avoid model over-fitting and obtaining an accurate approximation. A typical approach to choose these parameters is quite arbitrary by using trial-and-error [45].

Other Methods:

In addition to all these regularization methods, other notable approaches can be listed as follows:

- Vectorcardiographic optimization combined with patient specific information [19].

- Partial differential equation (PDE)-constrained optimization [107], in which the whole PDE model is used as a constraint in both equality and inequality forms rather than only the source constraints.

- Combination of the Support Vector Regression (SVR) with Self-Organizing Feature Map (SOFM) techniques [52].

- Iterative numerical methods generalized minimal residual (GMRes) [86], and Lanczos-bidiagonalization method combined along with TTLS [35].

26

2.5.1.2   Statistical Methods

All physical measurements include uncertainties because of the noise and the nature of physical phenomena which we wish to observe. Therefore, all these measurements are not simply observed values but they provide an information about the states of some observable parameters [97]. In classic inversion techniques, the noise is assumed to be deterministic and bounded. On the other hand, some applications cannot be modeled properly in this way. Consequently, statistical models have been proposed, in which the noise is assumed to be a random variable [12]. The interpretation of statistical modeling is that the information about values of these variables is incomplete but, based on our prior knowledge they can be expressed by their probability distributions [56]. Here, by a priory information we mean that the theoretical assumption about the probability density function, which is independent of the measurements. In that sense, probabilistic inverse problem solution techniques differs from the classical estimation methods such that they treats the unknown parameters as a random variables rather than unknown constants. These random variables are characterized in terms of a multivariate pdf which is deduced from prior knowledge about the problem under consideration.

Bayesian estimation and Kalman Filter are the most commonly utilized statistical methods for solving inverse ECG problems.

Bayesian Estimation:
In Bayesian Maximum a Posteriori (MAP) estimation, prior information about the epicardial potentials is used to construct a conditional a posteriori probability density function and then the solution is the potential distribution which maximizes the posterior pdf, given BSPM [91, 104]. Later on it was advanced by including spatial and temporal correlations of the epicardial potentials simultaneously [39, 76].

From a Bayesian inversion theory point of view, the model parameters $\mathbf{y}$, $\mathbf{x}$, $\mathbf{n}$ in Eqn. (2.3) are random variables. Let us assume that the parameter $\mathbf{x}$ is the only unknown. But, on the other hand, the form of prior density function $p(\mathbf{x})$ and a conditional probability density function $p(\mathbf{y}|\mathbf{x})$ are assumed to be known. The idea

consist in computing the posterior density function $p(\mathbf{x}|\mathbf{y})$ as follows:

$$p(\mathbf{x}|\mathbf{y}) = \frac{p(\mathbf{y}|\mathbf{x})p(\mathbf{x})}{\int_{\mathbb{R}^N} p(\mathbf{y}|\mathbf{x})p(\mathbf{x})d\mathbf{x}}. \tag{2.30}$$

After computation of the Bayesian solution, i.e., the posterior probability density, if we would like to accept the most probable value of $\mathbf{x}$ in the distribution as a solution. It is defined as follows:

$$\hat{\mathbf{x}}_{MAP} = \arg\max_{\mathbf{x}} p(\mathbf{x}|\mathbf{y}). \tag{2.31}$$

The term of $\hat{\mathbf{x}}_{MAP}$ is the *Maximum A Posteriori* (MAP) estimation of the unknown variable.

Similarly, *Conditional Mean* (CM) estimate can be defined as in Eqn. (2.32):

$$\hat{\mathbf{x}}_{CM} = \int_{\mathbb{R}^N} \mathbf{x}p(\mathbf{x}|\mathbf{y})d\mathbf{x}. \tag{2.32}$$

Kalman Filter:

Kalman filter was applied to inverse electrocardiography to incorporate the spatio-temporal behavior of electrocardiographic signals [6, 13, 24, 54]. In Kalman filter approach, the unknown potentials are the states to be estimated and the state transition matrix represents our knowledge or assumptions about the temporal behaviour of the unknown potentials at two consecutive time instants. Kalman filter includes two major steps: prediction and correction. Assuming that the unknown potential vector $\mathbf{x}_k$ defined in Eqn. (2.3) within the process of the subsequent form;

$$\mathbf{x}_k = \mathbf{G}\mathbf{x}_{k-1} + \mathbf{w}_k, \tag{2.33}$$

where $\mathbf{G}$, $\mathbf{w}_k$ are the state transition matrix and process noise vector, respectively.

Prediction step:

$$\mathbf{x}_k^- = \mathbf{G}\mathbf{x}_{k-1}^+, \tag{2.34}$$

$$\mathbf{P}_k^- = \mathbf{G}\mathbf{P}_{k-1}^+\mathbf{G}^T + \mathbf{V}_k, \tag{2.35}$$

28

Correction step:

$$\mathbf{K}_k = \mathbf{P}_k^- \mathbf{A}^T (\mathbf{A} \mathbf{P}_k^- \mathbf{A}^T)^{-1} + \mathbf{W}_k, \tag{2.36}$$

$$\mathbf{x}_k^+ = \mathbf{x}_k^- + \mathbf{K}_k(\mathbf{x}_k - \mathbf{A}\mathbf{x}_k^-), \tag{2.37}$$

$$\mathbf{P}_k^+ = (\mathbf{I} - \mathbf{K}_k \mathbf{A})\mathbf{P}_k^-. \tag{2.38}$$

Here, $\mathbf{K}_k$ is the Kalman gain matrix, and $\mathbf{V}_k$, $\mathbf{W}_k$ correspond to the covariance matrices for $\mathbf{n}_k$ and $\mathbf{w}_k$, respectively. The superscripts $(-)$, $(+)$ indicate the pre- and post-estimation values.

The estimation accuracy of the statistical methods depends on the quality of available prior information. Performance of the Bayesian MAP estimation method depends on a good a priori pdf, which is not usually available. Similarly, Kalman filter approach requires well-formed state transition rule in order to obtain robust and accurate estimation. Forming an appropriate state transition matrix is still an issue to be solved.

2.5.2 Trends in the Inverse ECG Field

Trends in the inverse problems of ECGI can not be thought independent from the researches in the field of forward ECG problem. Hence, similar to the forward problem discussed in Chapter 2.4, effects of torso inhomogeneities on the inverse ECG problem have not been fully revealed yet. The conclusion of prior study of Ramanathan et al. [85] was: homogeneous approximation does not cause significant deterioration in the accuracy of inverse solutions. However, the study of van Oosterom [105] showed that inverse solutions improved if the effects of lungs were taken into account. But, this study mainly focuses on comparing the performances of two major source types rather than investigating the effects of torso inhomogeneities. In addition, the recent study of Zemzemi et al. [117] has shown that for small noise values in the BSPM, the effect of torso heterogeneities is clear. But their influence decreases when the noise level in the measurements was increasing. In light of current state of the forward ECG problem studies, Rudy in [87] concluded that, although including inhomogeneities into model has some advantages, clinical ECGI applications show

that homogeneous approximation would be adequate. Cluitmans et al. [20] argued that extensive validation by in vivo studies should be applied for interpretation and validation of the results.

The images obtained by solving inverse problem of ECG contain valuable diagnostic and therapeutic information. It was initially applied for localizing focal ventricular arrhythmias, such as ventricular premature beats [50]. However, inverse ECG problems were usually modeled and solved with the assumption of static torso-heart geometries and the geometric error due to the cardiac motion and contraction are not included into the problem. Jiang et al. in [53] concluded that, although the inverse solutions obtained from both the static and the dynamic models approximately produced the similar results during QRS complex period, for the ST-T segment, static inverse problem approaches generated large errors in the estimates. In [24], electrical and mechanical measurements were combined in order to obtain more precise estimation of the electrical state of the ventricles throughout the heart beat. These studies suggest that the inclusion of cardiac motion into the model leads to more accurate solutions.

The inverse problem of electrocardiography has not been fully studied for fibrillating rhythms [31, 50, 89], but mostly analyzed and validated during stationary rhythms. ECG Imaging for Atrial Fibrillation (AF) is a challenging problems because the signal at the level of torso is weak compared with that from the ventricles [50] and during AF, besides the epicardial potentials additional parameters such as, dominant frequency, phase maps and singularity points should be considered that might be clinically more relevant than the raw potentials [31].

Hearts electrical activity starts from a few focal sites but then propagates throughout heart surface. Classical l_1- and l_2-norm regularization methods tend to produce focal and smooth solutions, respectively. However, epicardial potential distribution shows both sparse and smooth characteristic behavior while propagating over the heart surface during the cardiac cycle. Consequently, these classical methods have some shortages to represent the complete behavior of the epicardial potential distribution. Similarly, in order to obtain good estimates by using statistical methods it is required to have a good a priory information such as, form of the multivariate the probability dis-

tribution function, mean and covariance informations about the unknown epicardial potentials. Assuming that we have not enough a priori information about the current form of epicardial potential distribution, the question still remains as which particular norm solution or probability distribution function should be employed.

2.6 Test Data and Evaluation Methods

In this section, we give information about the datasets and quantitative metrics that are used to measure success of the proposed methods from various perspectives.

2.6.1 Data

Two different data collections, which were prepared in University of Utah and Karlsruhe Institute of Technology (KIT), have been used to evaluate the performance of algorithms. Both of the collections consist of unipolar body surface potentials. Although we have used only Utah data collection in our research related to Minimum Relative Entropy method (Chapter 3), later on both data collections have been utilized to examine the performance of the proposed solution technique in Chapter 4.

UTAH COLLECTION: Epicardial potentials employed in this study were measured at University of Utah by Robert S. MacLeod and his co-workers [67]. They were taken from dog hearts, which were perfused from another dog's circulatory system and suspended in an electrolytic filled (500 Ω) adolescence human thorax-shaped fibreglass tank. To measure the epicardial potentials, a nylon sock electrode with silver wires was slipped over the ventricles. The epicardial measurements were recorded from 490 points with a sampling rate of 1000 samples per second. In order to achieve maximum diversity from data-set standpoint, we utilized 23 recordings with 23 different stimulation sites on the epicardial surface, coming from 5 different experiments. Body surface potential measurements corresponding to these epicardial potential measurements were not available to us, therefore we used BSPs simulated from the measured epicardial potentials. Then, BSPs were simulated at these electrode locations by solving the forward ECG problem using the boundary element method (BEM) [42], and by adding independent and identically distributed Gaussian noise to noise-free BSPs.

In these BSP simulations, lungs were included in the geometric torso model, since they have been considered to be among the most influential inhomogeneities in the forward computations [59]. On the other hand, a homogeneous torso model was assumed in the BEM solution of the forward matrix $\mathbf{A}$ that was used for solving the inverse problem.

The original dataset includes 771 lead-set configuration on the body surface. In our MRE study (Section 3) we used the original dataset but later on in the studies presented in Section 4 the number of lead sets on the torso surface reduced to 192 as by employing the method proposed by Lux et al. [63].

KIT COLLECTION: This data collection is provided by Karlsruhe Institute of Technology (KIT), and can be obtained from the ECGI Consortium EDGAR Time Signal Catalog database [27]. It includes extracellular potentials on the pericardium for 8 ventricular beats with different pacing locations: epicardium, endocardium and septum. BSPs were simulated using the finite element method, and the bi-domain model on an inhomogeneous human patient model, but forward transfer matrix was computed using the boundary element method for a simplified homogeneous model.

2.6.2 Evaluation Metrics

In order to evaluate performances of the inverse ECG solution algorithms used in this study, we employ quantitative metrics and qualitative comparisons. In addition to comparing estimated epicardial potentials with the true epicardial potentials, we have also obtained and compared the activation time distributions. Activation times are calculated from the epicardial potentials using the spatio-temporal approach proposed by Erem et al. [28], and evaluated by Cluitmans et al. [21]. This algorithm involves a two step procedure:

- Step 1: Temporal derivative of the time series at each node on the epicardial surface is computed. Then, from this derivative waveform, temporal activation time is defined for each node as the time instant that has the most negative derivative value. These temporal activation times are collected in a vector $\boldsymbol{\tau}$.

- Step 2: The propagation pattern represented by the temporal activation times

on the surface of the heart are smoothed by solving the following optimization problem:

$$\arg \min_{\boldsymbol{\tau}_D \in \mathbb{R}^N} \{ \|\boldsymbol{\tau} - \boldsymbol{\tau_D}\|_2^2 + \gamma \|\mathbf{L}\boldsymbol{\tau_D}\|_2^2 \}, \tag{2.39}$$

where $\mathbf{L}$ represents the surface Laplacian operator and γ controls the smoothness of potential propagation pattern on the heart surface. The solution of Eqn. (2.39) is called the spatio-temporal activation time estimate.

The minimum value of the estimated spatio-temporal activation time vector was then calculated as the earliest activation time, and the corresponding node on the heart surface was accepted as the estimated pacing site.

For quantitative evaluation of the epicardial potential and activation time estimates, correlation coefficient (CC), relative error (RE) and pacing site localization error (LE) are computed. For CC and RE calculations, $\mathbf{z} \in \mathbb{R}^N$ is assumed to be the true parameter vector (epicardial potentials at a single time instant, or activation times), and $\hat{\mathbf{z}}$ is its estimate, with the corresponding mean vectors, $\bar{\mathbf{z}}$ and $\bar{\hat{\mathbf{z}}}$, respectively:

$$CC = \frac{\sum_{i=1}^N (z_i - \bar{z}_i)(\hat{z}_i - \bar{\hat{z}}_i)}{\sqrt{\sum_{i=1}^N (z_i - \bar{z}_i)^2 \sum_{i=1}^N (\hat{z}_i - \bar{\hat{z}}_i)^2}}, \tag{2.40}$$

$$RE = \frac{\|\mathbf{z} - \hat{\mathbf{z}}\|_2}{\|\hat{\mathbf{z}}\|_2}. \tag{2.41}$$

Here, subscript i stands for the ith element of the corresponding vector. In this study, CC and RE are calculated at each time instant for the epicardial potentials, and then mean and standard deviation values of these CC and RE are obtained over time for comparison of results. Activation time vectors yield single CC and RE values. LE between the estimated and the actual pacing sites is calculated by computing the Euclidean distance between the estimated and the true pacing sites. Besides quantitative comparisons, qualitative assessments are made by visual inspection to efficaciously capture the local variations between the real and the estimated epicardial potential maps and activation time maps using the Map3d software [66], which was developed by researchers at University of Utah as a part of the Scientific Computing and Imaging software.

33

CHAPTER 3

INVERSION VIA MINIMUM RELATIVE ENTROPY

Minimum Relative Entropy (MRE) principle (also known as minimum cross entropy) describes a statistical method to infer a posterior probability density function (pdf) that avoid bias, from prior estimate of pdf and new obtained data as a constraints on expected values [93, 94, 112]. It was introduced by Kullback [60] and called minimum directed divergence. Since its derivation, MRE principle has been applied in a wide variety of areas in science and engineering including: pharmacokinetic parameter estimation [2], detecting the origin of pollutant in drinking water structures and reformation of groundwater contaminant diffusion history [75, 80, 114], locating and detecting CO_2 leakage [96], identification of the source term of gas emission in atmosphere [64], estimation problem for quantum systems to reconstruct the behavior of a quantum channel or in retrieving information at the receiver of a communication system [120]. In contrast to the Bayes estimation, the idea behind the application of MRE to inverse problem is that: the form of the prior pdf is highly suspected or may not be available. In addition to this, statistical parameters such as variance or moments are difficult to estimate. Instead, MRE defines a way of pdf approximation by considering that the measured data are expected values of some unknown pdf and put them into a suitable form of constraints.

3.1 Motivation

In statistical inverse problem solving approaches such as Maximum A Posteriori (MAP) estimation, the form of prior probability distribution is assumed to be known.

In most of the applications, it is common to use Gaussian prior pdf that also requires reliable prior information about mean and covariance matrices in order to an obtain accurate estimation. However, in some cases, prior pdf itself may be unknown or it may not be possible to obtain good information about full covariance matrix. At this point, the MRE-based inversion procedure proposed in [112] defines a more flexible way, based on limited information.

In this part of the thesis, we have explored the impacts of changes in parameter values of the MRE estimation and assessed its limitations. These parameters are the lower, upper bounds and the expected value of the solution, and the expected uncertainty in the model. By employing these parameters, initially a priori pdf is constructed, after that this pdf is used to estimate an a posteriori pdf. This a posteriori pdf is utilized to determine a estimation. MRE method is more flexible when we compare to the Bayesian MAP estimation. Since, Bayesian MAP method requires a full covariance matrix in addition to a expected value vector, even if the simplified Gaussian assumption has been made. Besides these issues, we have also explored different approaches in order to define prior expected value, which become the most important parameter.

This chapter is organized as follows: Chapters 3.2 and 3.3 describe the mathematical background of estimating multivariate pdf via MRE method and its application to linear inverse ECG problem, respectively. The further sections include the experimental results and concluding remarks.

3.2 Minimum Relative Entropy

The application of MRE method for estimating unknown parameters of the inverse problem explained in this part is rely on the principles developed by Shore [94]. It follows coherent inference axioms of uniqueness, invariance, system independence. In other words, if a problem can be solved in different ways, each path must lead to the same answer [111]. It was adapted by Woodbury et al. [112] to solve hydrogeological inverse problem.

Suppose that $\mathbf{q}^{\dagger}(\mathbf{x})$ is a unknown multivariate density function of the random vector $\mathbf{x}$, having an initial estimate $\mathbf{p}(\mathbf{x})$. In addition, additional constraints exist to restrict

the $\mathbf{q}^\dagger(\mathbf{x})$. Typical constraint information consists of:

$$\mathbf{q}^\dagger(\mathbf{x}) \geq 0, \tag{3.1}$$

$$\int_{\mathbb{R}^\mathbb{N}} \mathbf{q}^\dagger(\mathbf{x})d\mathbf{x} = 1. \tag{3.2}$$

The constraints in Eqn. (3.1) and normalizing constraint Eqn. (3.2) are necessary to construct a valid pdf $\mathbf{q}^\dagger(\mathbf{x})$.

$$\int_{\mathbb{R}^\mathbb{N}} \mathbf{q}^\dagger(\mathbf{x})f_j(\mathbf{x})d\mathbf{x} = \hat{f}_j \qquad (j = 1, 2, \ldots, M). \tag{3.3}$$

Here, in the Eqn. (3.3), functions $f_j(\mathbf{x}) \quad (j = 1, 2, \ldots, M)$ are assumed to be known and new information exist in expected value constraints form $\hat{f}_j$. The task at hand is determining pdf $\mathbf{q}(\mathbf{x})$, which is the estimation of $\mathbf{q}^\dagger(\mathbf{x})$, consistent with provided new information. The relative entropy principle states that the solution $\mathbf{q}^\dagger(\mathbf{x})$ is to minimize Eqn. (3.4) subject to constraints given in Eqns. (3.1)–(3.3).

$$H(\mathbf{q}, \mathbf{p}) = \min_{\mathbf{q}^\dagger} H(\mathbf{q}^\dagger, \mathbf{p}). \tag{3.4}$$

Here $H(\mathbf{q}, \mathbf{p})$ is the *Kullback-Leibler* divergence that defines the relative entropy of $\mathbf{q}(\mathbf{x})$ with respect to $\mathbf{p}(\mathbf{x})$ and defined as:

$$H(\mathbf{q}, \mathbf{p}) = \int_{\mathbb{R}^\mathbb{N}} \mathbf{q}(\mathbf{x}) \ln \frac{\mathbf{q}(\mathbf{x})}{\mathbf{p}(\mathbf{x})} d\mathbf{x}. \tag{3.5}$$

The Kullback-Leibler divergence measures the non-symmetric difference between two probability distributions over the same variable $\mathbf{x}$. One of the alternative methods for solving the optimization problem in Eqn. (3.4) is introducing Lagrange multipliers μ and γ_i, $i = (1, 2, \ldots, M)$ corresponding to the constraints. After introducing the Lagrange multipliers, optimization problem can be stated as:

$$\mathbf{q}(\mathbf{x}) = \operatorname*{argmin}_{\mathbf{q}^\dagger} \left(\begin{array}{c} \int_{\mathbb{R}^\mathbb{N}} \mathbf{q}^\dagger(\mathbf{x}) \ln \frac{\mathbf{q}^\dagger(\mathbf{x})}{\mathbf{p}(\mathbf{x})} d\mathbf{x} + \mu \left[\int_{\mathbb{R}^\mathbb{N}} \mathbf{q}^\dagger(\mathbf{x})d\mathbf{x} - 1 \right] + \\ \sum_{j=1}^M \gamma_j \left(\int_{\mathbb{R}^\mathbb{N}} \mathbf{q}^\dagger(\mathbf{x})f_j(\mathbf{x})d\mathbf{x} - \hat{f}_j \right) \end{array} \right). \tag{3.6}$$

We should note that the constraint given in Eqn. (3.1) is indirectly included in Eqn. (3.6). Since $\mathbf{q}^\dagger(\mathbf{x})$ is placed in the logarithmic term, $\mathbf{q}^\dagger(\mathbf{x})$ has to be greater or equal to zero. Otherwise, Eqn. (3.6) becomes an invalid mathematical term.

By taking derivative of Eqn. (3.6) with respect to $\mathbf{q}^{\dagger}(\mathbf{x})$ solution can be obtained. Therefore, $\mathbf{q}(\mathbf{x})$ satisfies:

$$\mathbf{q}(\mathbf{x}) = \mathbf{p}(\mathbf{x}) \exp\left(-1 - \mu - \sum_{j=1}^{M} \gamma_j f_j(\mathbf{x})\right). \tag{3.7}$$

Furthermore, the constraint in Eqn. (3.3) can be modified in order to deal with uncertainty in the $\hat{f}_j$ to find the solution within a specified tolerance:

$$\sum_{j=1}^{M} \left(\int_{\mathbb{R}^{\mathbb{N}}} \mathbf{q}^{\dagger}(\mathbf{x}) f_j(\mathbf{x}) d\mathbf{x} - \hat{f}_j\right)^2 \leq \epsilon^2. \tag{3.8}$$

Then, Eqn. (3.6) can be stated as:

$$\mathbf{q}(\mathbf{x}) = \underset{\mathbf{q}^{\dagger}}{\operatorname{argmin}} \left(\begin{array}{c} \int_{\mathbb{R}^{\mathbb{N}}} \mathbf{q}^{\dagger}(\mathbf{x}) \ln \dfrac{\mathbf{q}^{\dagger}(\mathbf{x})}{\mathbf{p}(\mathbf{x})} d\mathbf{x} + \mu \left[\int_{\mathbb{R}^{\mathbb{N}}} \mathbf{q}^{\dagger}(\mathbf{x}) d\mathbf{x} - 1\right] + \\ \gamma \left[\sum_{j=1}^{M} \left(\int_{\mathbb{R}^{\mathbb{N}}} \mathbf{q}^{\dagger}(\mathbf{x}) f_j(\mathbf{x}) d\mathbf{x} - \hat{f}_j\right)^2 - \epsilon^2\right] \end{array}\right), \tag{3.9}$$

where μ and γ are Lagrange multipliers.

The constant term $\hat{f}_j$ can be carried into the integral equation. Let us define a function $g_j(\mathbf{x})$ such that

$$g_j(\mathbf{x}) = f_j(\mathbf{x}) - \hat{f}_j, \tag{3.10}$$

the last integral term of Eqn. (3.9) can be stated as:

$$\int_{\mathbb{R}^{\mathbb{N}}} \mathbf{q}^{\dagger}(\mathbf{x}) f_j(\mathbf{x}) d\mathbf{x} - \hat{f}_j = \int_{\mathbb{R}^{\mathbb{N}}} \mathbf{q}^{\dagger}(\mathbf{x}) \left(f_j(\mathbf{x}) - \hat{f}_j\right) d\mathbf{x} = \int_{\mathbb{R}^{\mathbb{N}}} \mathbf{q}^{\dagger}(\mathbf{x}) g_j(\mathbf{x}) d\mathbf{x}. \tag{3.11}$$

Then we can obtain the solution of Eqn. (3.9) by computing its variation relative to $\mathbf{q}^{\dagger}(\mathbf{x})$. Therefore, $\mathbf{q}(\mathbf{x})$ satisfies:

$$\mathbf{q}(\mathbf{x}) = \mathbf{p}(\mathbf{x}) \exp\left(-1 - \mu - \sum_{j=1}^{M} \lambda_j g_j(\mathbf{x})\right), \tag{3.12}$$

where

$$\lambda_j = 2\gamma \int_{\mathbb{R}^{\mathbb{N}}} \mathbf{q}^{\dagger}(\mathbf{x}) g_j(\mathbf{x}) d\mathbf{x} \qquad (j = 1, 2, \ldots, M). \tag{3.13}$$

Defining a prior pdf, $\mathbf{p}(\mathbf{x})$, is the fundamental part of the MRE method. In many estimation problems, it is possible to gather adequate information about upper and lower bound for the unknowns. Then, pdf of the unknown random vector $\mathbf{x}$ can be defined by a multivariate uniform distribution using these basic information:

$$
\mathbf{b}(\mathbf{x}) = \begin{cases} \prod_{i=1}^{N} \frac{1}{U_i - L_i}, & \text{if} \quad L_i \leq x_i \leq U_i, \\ 0, & \text{otherwise,} \end{cases}
\tag{3.14}
$$

where U_i and L_i are the upper and lower bounds of x_i (i^{th} element of $\mathbf{x}$), respectively. An estimate of the prior pdf (we will call this estimate $\hat{\mathbf{p}}(\mathbf{x})$) can be obtained by minimizing entropy of $\mathbf{p}(\mathbf{x})$ relative to the boxcar pdf $\mathbf{b}(\mathbf{x})$, subject to the expected value constraint:

$$
\bar{x}_j = \int_{\mathbb{R}^N} x_j \mathbf{p}(\mathbf{x}) d\mathbf{x} \qquad (j = 1, 2, \ldots, N),
\tag{3.15}
$$

where $\bar{\mathbf{x}} = [\bar{x}_1, \ \bar{x}_2, \ \ldots, \ \bar{x}_N]^T$ is the prior mean vector, and $\bar{x}_i$ is the mean value of x_i. The optimization problem is similar to Eqn. (3.6), and estimate of $\mathbf{p}(\mathbf{x})$ is given as:

$$
\hat{\mathbf{p}}(\mathbf{x}) = \underset{\mathbf{p}}{\text{argmin}} \left(\begin{array}{c} \displaystyle\int_{\mathbb{R}^N} \mathbf{p}(\mathbf{x}) \ln \frac{\mathbf{p}(\mathbf{x})}{\mathbf{b}(\mathbf{x})} d\mathbf{x} + \eta \left[\int_{\mathbb{R}^N} \mathbf{p}(\mathbf{x}) d\mathbf{x} - 1 \right] + \\ \displaystyle\sum_{i=1}^{N} \beta_i \left(\int_{\mathbb{R}^N} x_i \mathbf{p}(\mathbf{x}) d\mathbf{x} - \bar{x}_i \right) \end{array} \right).
\tag{3.16}
$$

Solving the minimization problem yields:

$$
\mathbf{p}(\mathbf{x}) = \mathbf{b}(\mathbf{x}) \exp \left(-1 - \eta - \sum_{i=1}^{N} \beta_i x_i \right),
\tag{3.17}
$$

where η and β_i are the Lagrange multipliers, where each β_i is determined by the definition from Eqn. (3.15) and η by the normalization requirement:

$$
\int_{\mathbb{R}^N} \mathbf{p}(\mathbf{x}) d\mathbf{x} = 1.
\tag{3.18}
$$

3.3 Application to Discrete Linear Inverse Problem

This section describes the application of MRE method to the ill-posed linear inverse ECG problem defined in Eqn. (3.19) at a single time instant separately:

$$
\mathbf{y} = \mathbf{A}\mathbf{x} + \mathbf{n}.
\tag{3.19}
$$

In this problem the goal is to estimate $\mathbf{x}$. The known function $f_j(\mathbf{x})$ and its mean value in discrete linear case can be defined as:

$$f_j(\mathbf{x}) = \sum_{i=1}^{N} A_{ji} x_i, \tag{3.20}$$

$$\hat{f}_j = \int_{\mathbb{R}^{\mathbb{N}}} q(\mathbf{x}) \left[\sum_{i=1}^{N} A_{ji} x_i \right] d\mathbf{x}, \tag{3.21}$$

where A_{ji} is the element located at j^{th} row and i^{th} column of matrix $\mathbf{A}$. From linear inverse ECG point of view, body surface measurement f_j corresponds the expected value $\hat{f}_j$. Let us assume that the upper and lower bound of $\mathbf{x}$ given in Eqn. (3.14) can take a value in the range of $(0, U)$, then we can define the pdf $q(\mathbf{x})$ as:

$$q(\mathbf{x}) = \prod_{i=1}^{N} \frac{-a_i}{\exp(-a_i U) - 1} \exp(-a_i x_i), \tag{3.22}$$

where

$$a_i = \beta_i + \sum_{j=1}^{M} \lambda_j A_{ji}. \tag{3.23}$$

The estimate $\hat{\mathbf{x}}$ is then the expected value of Eqn. (3.22). The ith element of this estimate is:

$$\hat{x}_i = \frac{\exp(-a_i U) a_i U + \exp(-a_i U) - 1}{a_i [\exp(-a_i U) - 1]}. \tag{3.24}$$

For non-zero lower bounds, the problem can be re-scaled by defining $\hat{\mathbf{x}} = \hat{\mathbf{x}}_0 + \mathbf{L}$, where $\hat{\mathbf{x}}$ is the true solution, $\hat{\mathbf{x}}_0$ is the corresponding model solution for zero lower bound, and $\mathbf{L}$ is the vector of lower bounds. Zero lower bound solution $\hat{\mathbf{x}}_0$ can be calculated using modified data $\mathbf{y}_m = \mathbf{y} - \mathbf{AL}$. The upper bounds and expected values must be replaced by $U_i - L_i$ and $\bar{x}_i - L_i$, respectively. After $\hat{\mathbf{x}}_0$ is computed with the MRE method, the true solution calculated as $\hat{\mathbf{x}} = \hat{\mathbf{x}}_0 + \mathbf{L}$.

3.4   Results

The MRE implementations given in [74, 75] have been adapted to linear inverse ECG problem. To achieve this, information about the three parameters of the MRE method: upper and lower bounds, prior mean of the unknown variable $\mathbf{x}$, and the expected uncertainty value ϵ^2, is required. In this part, the impacts of these parameters are

investigated by altering only one of them at a time and by keeping unchanged the other parameters at their true values. True values of these parameters are defined as follows:

- *Prior mean vector:* The true prior mean vector at the kth time instant is equal to the true epicardial potential vector at that time instant, i.e., $\bar{\mathbf{x}}_k = \mathbf{x}_k$.

- *Upper and lower bounds:* We use upper and lower bounds that are fixed with respect to time, but different for each lead. In order to find the true upper and lower bound vectors at time instant k, we first obtain an epicardial potential matrix $\mathbf{X} \in \mathbb{R}^{N \times T}$, whose k^{th} column consists of the true epicardial potential vector at the kth time instant ($k = 1, \ldots, T$):

$$\mathbf{X} = \begin{bmatrix} \mathbf{x}_1 & \mathbf{x}_2 & \ldots & \mathbf{x}_k & \ldots & \mathbf{x}_T \end{bmatrix}. \tag{3.25}$$

After that, the maximum and minimum values of the epicardial potentials at lead j ($j = 1, \ldots, N$) over all time instants are computed as follows:

$$x_{max}(j) = \max(\mathbf{X}(j, :)), \tag{3.26}$$

$$x_{min}(j) = \min(\mathbf{X}(j, :)). \tag{3.27}$$

Then, for all time instants k, the same true upper and lower value vectors are used:

$$\mathbf{u}_k = \begin{bmatrix} x_{max}(1) & x_{max}(2) & \ldots & x_{max}(N) \end{bmatrix}^T, \tag{3.28}$$

$$\mathbf{l}_k = \begin{bmatrix} x_{min}(1) & x_{min}(2) & \ldots & x_{min}(N) \end{bmatrix}^T. \tag{3.29}$$

This means that the true values of the upper and lower bounds for the jth lead at the kth time instant are equal to $\mathbf{u}_k(j)$ and $\mathbf{l}_k(j)$, respectively.

- *Expected uncertainty:* The true value of expected uncertainty ϵ^2 is equal to the variance of measurement noise, i.e. $\sigma^2(n)$.

41

3.4.1 Effects of upper and lower bounds

In this part, the impacts of over and underestimated lower and upper bound values are examined by fixing the expected uncertainty to its true value. On the other hand, use of the true mean vector is not realistic, because it is not possible to obtain; hence, besides the true mean vector, noisy mean vectors have also been utilized. The upper and lower bound vectors are modified in Eqns. (3.28) and (3.29) by multiplying them by a scalar, α as:

$$\hat{\mathbf{u}}_k = \alpha \, \mathbf{u}_k, \quad \hat{\mathbf{l}}_k = \alpha \, \mathbf{l}_k, \tag{3.30}$$

and then, by varying α in the range 0.4 to 2.0.
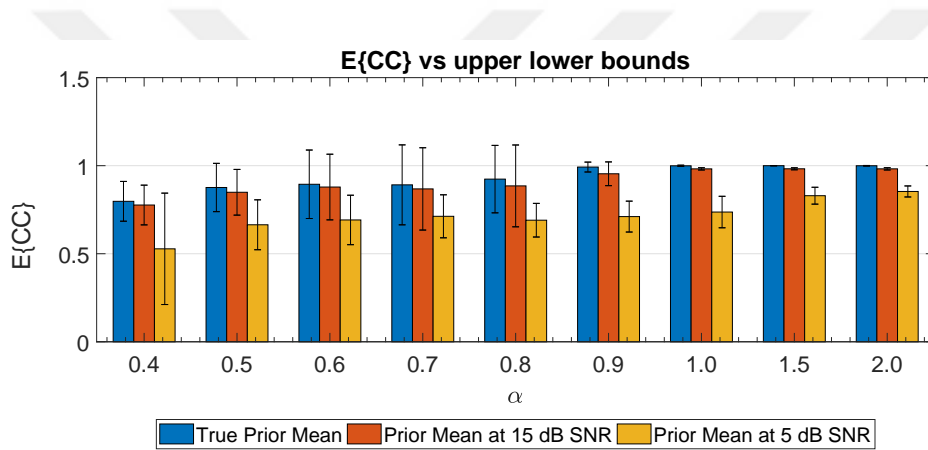
Figure 3.1: Obtained $E\{CC\} \pm \sigma\{CC\}$ values for different upper and lower bounds.

The results are presented in Fig. 3.1 as mean and standard deviation values of CC over time. Estimation results shows that it is better to chose prior upper and lower bounds large enough such that the extreme values of true epicardial potentials can lie between these bounds to obtain high CC values. Otherwise, estimation accuracy start to degrade even in the noise free case, especially if $\alpha < 0.9$. Moreover, use of large upper and lower bound values compensates the performance drops caused by noise in the prior mean values to some degree. For example; prior mean at 5 dB SNR, CC value increase as α rises from 1 to 2. All this observations suggests that it is much better to overestimate the upper and lower bound values rather then using the true values or underestimating them.

3.4.2 Effects of prior mean

In this test, the aim is to observe impacts of the prior mean value. In order to conduct this, upper and lower bounds of epicardial potentials are fixed a large value as given by Eqn. (3.30) with $\alpha = 2$ and the true value of the expected uncertainty is used to eliminate the possible effects of these parameters on the estimation results. In order to change the prior mean vector, Gaussian white noise at different SNR levels (1, 5, 10 and 20 dBs) is added to true mean value vector. CC values of all estimations at all time instants have been calculated to compare the accuracy of outcomes. The mean and standard deviation of these CC values over time are displayed at Fig. 3.2.
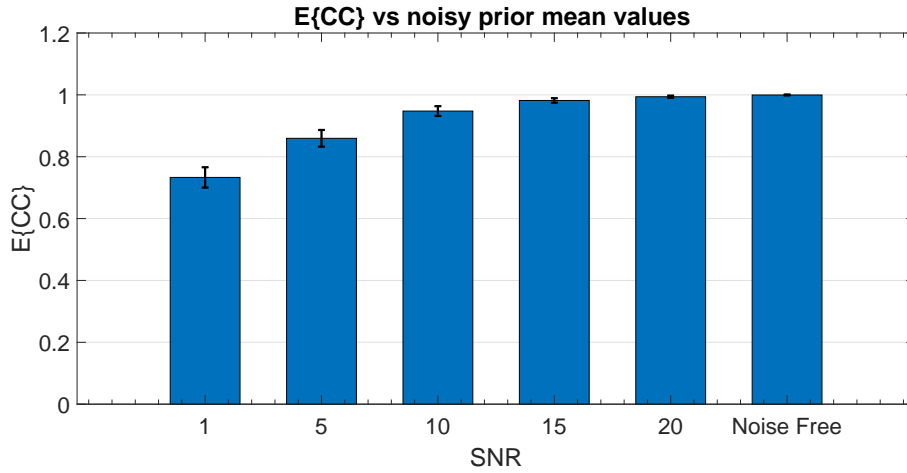
Figure 3.2: Obtained $E\{CC\} \pm \sigma\{CC\}$ values for various prior mean vectors.

Results show that deviation from the true mean causes degradation in estimation accuracy of MRE method. Although it is tolerable for down to 10 dB SNR, *i.e.* the average CC values are still above 90%, the accuracy of estimation severely degrades for lower values of SNR in terms of CC metric.

3.4.3 Effects of expected uncertainty

In this part of the study, the impacts of expected uncertainty are explored if its value is over- and under-estimated. The expected uncertainty is modified by multiplying its true value by a scalar, β in the range 0.4 to 1.6. The upper and lower bound values are fixed as given by Eqn. (3.30) with $\alpha = 2$. Similar to other test cases, besides the true

43

mean value results for noisy mean values at 5 and 15 dB SNR have also presented.

The results are given in In Fig 3.3 in terms of mean and standard deviation values of CC. If $\beta > 1$ (over-estimated expected uncertainty case), even with the noisy mean values, high CC values can be achieved ($CC > 0.8$). On the other hand, if β decreases (under-estimated expected uncertainty case), even with the true mean values, CC values decrease significantly.
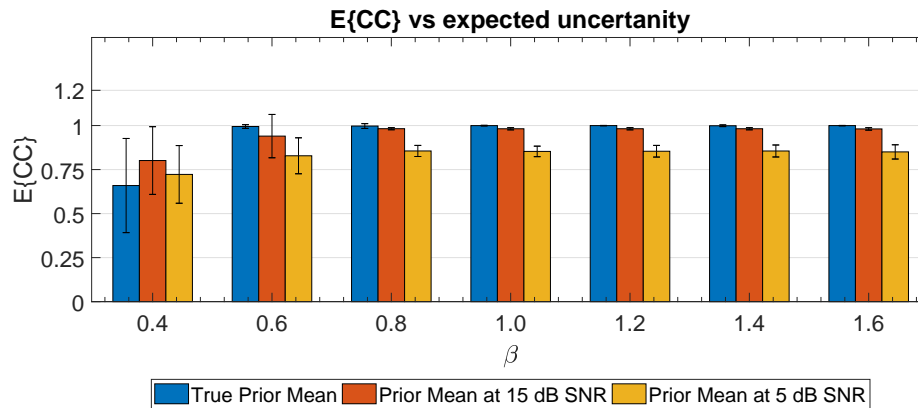
Figure 3.3: Obtained $E\{CC\} \pm \sigma\{CC\}$ values for various expected uncertainty values.

3.5 Determination of MRE parameters

In the previous section the effects of three parameters of MRE methods have been examined on the estimation accuracy. The results show that the most important parameter of MRE method is the prior mean value. However, it is not easy to define prior mean vector and requires more attention. The other parameters can be more easily determined compared to prior mean vector. The upper and lower bounds might be deducted from available training data obtained from in-vivo studies or mathematical simulations. The expected uncertainty can be deduced based on measurement system sensitivity information and possible noise sources. Hence, from this point of view we have presented and tested two simple method to define a prior mean value. We should note that, upper and lower bounds of epicardial potentials are defined as in Eqns. (3.28) and (3.29) with $\alpha = 2$, and the true expected uncertainty value has been
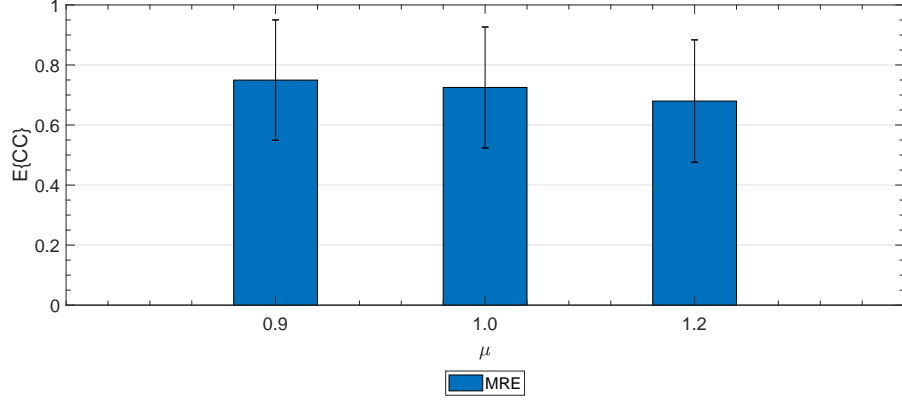
Figure 3.4: Obtained $E\{CC\} \pm \sigma\{CC\}$ values for method 1.

used.

Method 1: In order to calculate the prior mean value, the estimated potential vector obtained for the preceding time frame ($\hat{\mathbf{x}}_{k-1}$) is altered by multiplying a scalar value (μ), Eqn.(3.31):

$$\bar{\mathbf{x}}_k = \mu \hat{\mathbf{x}}_{k-1}. \tag{3.31}$$

This simple assumption relates the epicardial potentials at a certain lead with only the epicardial potential at the same lead in the previous time frame. It is called *Random Walk* model that used to characterize transitions of states in the Kalman filtering literature [3]. We should note that, the prior mean at $k = 0$ is equal to a zero vector ($\bar{\mathbf{x}}_0$).

Three distinct scalar coefficient values are, $\mu = 0.9, 1.0, 1.1$. In Fig. 3.4 estimation accuracies are presented in terms of average and standard deviation values of CC. The highest estimation accuracy is obtained for $\mu = 0.9$.

Method 2: This approach use the same constant value as a prior mean value for all leads. Three different cases have been tested:

- **Case 1:** Time varying (TV) prior mean value:

$$\bar{x}_k = \frac{1}{N} \sum_{j=1}^{N} x_k(j), \tag{3.32}$$

45

$$\bar{\mathbf{x}}_k = \bar{x}_k \mathbf{1}, \tag{3.33}$$

where $\mathbf{1} = [1, 1, \ldots, 1]^T$, and $x_k(j)$ is the jth lead potential value on the epicardial surface at k^{th} time frame. $\bar{x}_k$ is calculated using true epicardial potentials.

- **Case 2:** Constant prior mean value for all leads and time instants, where the averaging is over all times and leads:

$$\bar{x} = \frac{1}{NT} \sum_{k=1}^{T} \sum_{j=1}^{N} x_k(j), \tag{3.34}$$

$$\bar{\mathbf{x}}_k = \bar{x}\mathbf{1}. \tag{3.35}$$

Similar to Case 1, true epicardial potentials have been used to obtain $\bar{x}$ in this solution.

- **Case 3:** This case is very similar to Case 2; an average $\bar{x}$ value is used to obtain the mean vector at all time instants. However, different then Case 2, Case 3 utilize training set to define $\bar{x}$, and upper, lower bounds. The training set includes 22 different ectopic beats, which were recorded during the QRS interval, when the initial stimulation site is on the ventricles. Each recording was initiated from a different part of the heart surface. For each of these 22 recordings, an upper bound, a lower bound and a mean value have been calculated as explained in Case 2. Then mean values of these parameters have been used in the MRE solution.

Table 3.1: Calculated $E\{CC\} \pm \sigma\{CC\}$ values for different prior mean value determination approaches.

	Tikhonov	MRE $\mu = 0.9$ from prev. sol.	MRE Case 1	MRE Case 2	MRE Case 3
$E\{CC\}$	0.7695	0.7496	0.7584	0.7581	0.7713
$\sigma\{CC\}$	0.1826	0.2005	0.2168	0.2077	0.1659

The estimation performances of the MRE method, in which the prior mean values determined by using these three cases, presented in Table 3.1 in terms of CC metric. Tikhonov regularization results are also included in order to construct a comparison

basis. According to these results, there is no considerable difference, in term of average CC metrics, between any of these three cases. On the other hand, mean CC metrics provide us general idea about the estimation performances. It is required to examine the outcomes in more detailed especially if CC values are close to each other. For this reason, the original and estimated isochronous maps for different time frames are presented in Figure 3.5.
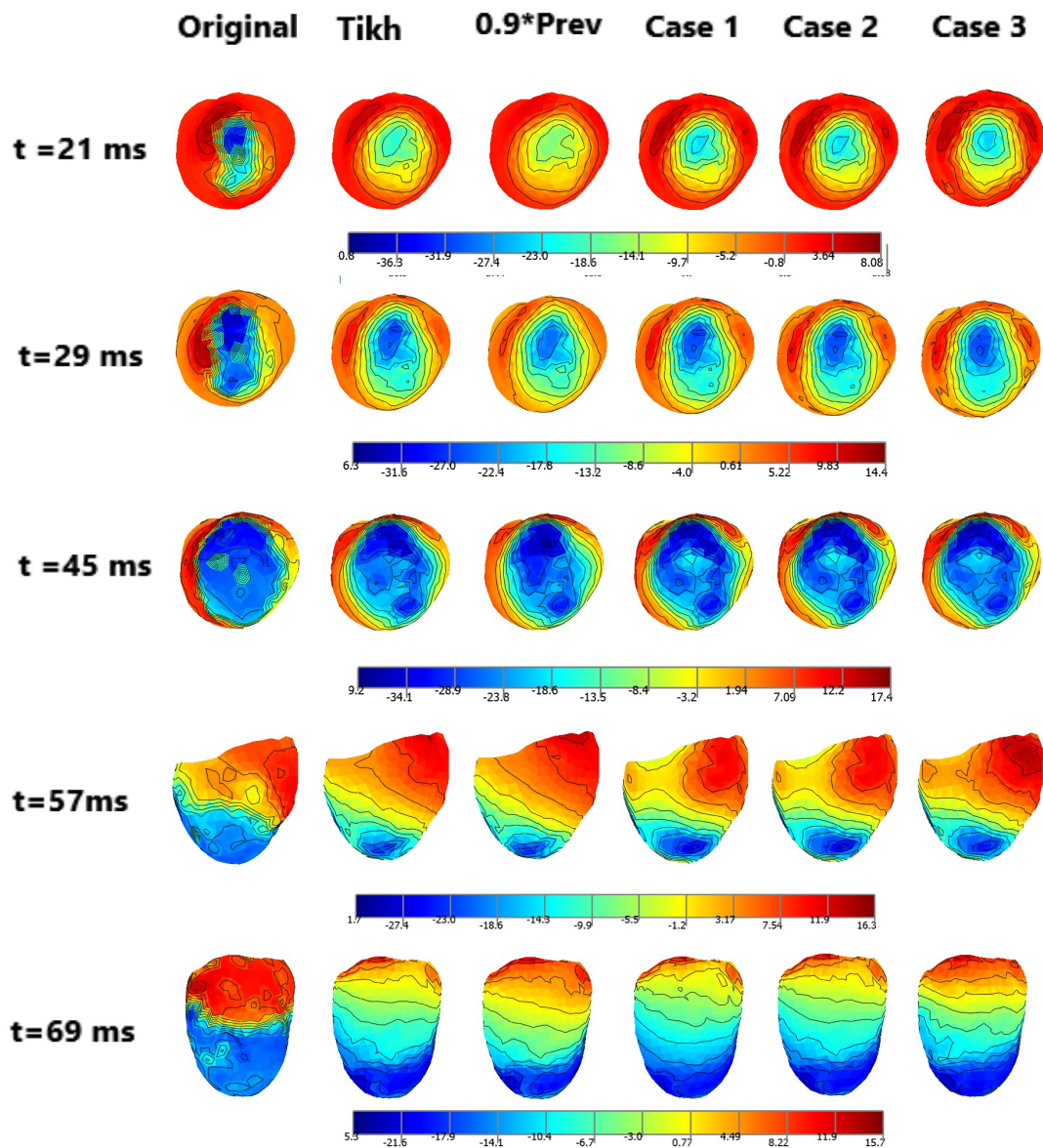
Figure 3.5: True and estimated isochronous maps in the QRS duration.

When we examine these maps, we observe that at most of the time instants, there is no clear advantage of using the MRE approach over the traditional Tikhonov regulariza-

47

tion method with our simple prior mean definitions. On the other hand, at $t = 57$ ms, wave-front reconstructions of the MRE method (in all three cases) show better fidelity to the original map. In these maps, the contour lines are more tightly packed compared to Tikhonov regularization and random-walk approach (with $\mu = 0.9$) solutions. Sharp turns in the original wave-front around the 10 o'clock direction cannot be observed with the latter two approaches, but visible in Case 1, Case 2 and Case 3 results. Another observation is that, there is considerable advantage between time varying and constant mean values on the estimation accuracies. We haven't observed any significant difference on estimations when prior means deduced from training sets and from true epicardial potential distribution are employed. But this is not unexpected result, because we have used constant prior mean value for all time instants and leads, which is calculated from all available training dataset. Under different stimulation scenarios, propagation patterns over the heart surface and epicardial waveform shapes with respect to time may vary significantly, but the average values more or less stays constant.

3.6 Discussion and Conclusion

In this part of the thesis, the appropriateness of the MRE approach to solve the ill-posed linear inverse ECG problem is examined. We especially focused on the impacts of MRE parameters on the estimation results. In order to reach these goals, we have implemented different numerical simulations by modifying only one parameter at a time and kept all the others unchanged. Based on our observation we concluded that:

- If the prior mean is close to its true value, upper and lower bounds do not have a significant effect on the estimation accuracies unless they are underestimated. On the contrary, overestimated upper and lower bound helps to deal with the performance degradation originated from the deviations in the prior mean value.

- The expected uncertainty value should be chosen greater or equal to the true uncertainty, otherwise estimation accuracy decreases.

- The prior mean value is the crucial parameter for MRE method. its deviation

from the true mean significantly reduces estimation performance.

Except the expected mean value, other parameters (upper, lower bounds and uncertainty) can be deducted from experimental data, mathematical models, simulations and specification of the measurement devices. Nonetheless, in order to obtain better estimations of the unknown epicardial potential, one needs a good prior estimate for the expected mean. We have proposed and tested two simple approaches to obtain the expected mean; random-walk and constant mean. Random-walk produced similar results with the Tikhonov regularization. On the other hand, even with the simple approach using a constant mean for all leads and all times, wave-front reconstructions at some time instants are improved compared to Tikhonov regularization. Although the MRE method seems to yield similar results with the conventional regularization methods, the results given in Section 3.4 suggest that with a more careful definition of the MRE parameters, this approach has promise for real data applications. When we compare the results of Sections 3.4 and 3.5, we can conclude that there is room for improving the MRE method to solve the inverse ECG problem more accurately then the traditional regularization methods. However more studies are required to obtain a good prior expected mean.

There are several studies that exist in the literature to define an appropriate prior pdf for the epicardial potentials and other types of electrical activity of the heart. Previous works on Bayesian estimation of epicardial potentials [91, 104] assumed that prior pdf is multivariate Gaussian distribution. This definition is based on empirical study of the epicardial potential distributions, and it is not proven that Gaussian prior is the best way to represent the epicardial potentials. Moreover, even though the potentials are assumed to have a Gaussian distribution, depending on the initial stimulation site or in general the pathology of the heart that produces the corresponding epicardial potentials, it was still a challenge to define an appropriate mean and covariance matrix that best represent the data. In previous studies, the prior pdf model parameters were either obtained from training sets of previously recorded potentials [91] or from simulated potentials that result from mathematical modeling of cardiac electrical activity [30]. More recently, Rahimi et al. applied hierarchical Bayesian estimation to estimate the 3D distribution of trans-membrane potentials in the heart [83], and they observed that depending on the current time within the cardiac cycle, l_1-norm prior

(Laplacian), l_2-norm prior (Gaussian) or l_p-norm prior ($1 < p < 2$) should be chosen, and value of p should be one of the estimated parameters as well. In light of these studies, it is obvious that the prior probability distribution should be chosen carefully. In this study, we wanted to keep the simple uniform (box-car) pdf definition for the epicardial potentials, however we did not want to use it directly as the prior pdf in the Bayesian estimation procedure. Hence, we have preferred to employ two step procedure in order to define the prior probability distribution of epicardial potentials; At first, the uniform pdf is defined by using upper and lower bounds only, after that this simple pdf is utilized to estimate the prior pdf that will be used with the Bayesian estimation.

3.6.1 Limitations of the Study, and Future Work

In this part of the thesis, we have followed original studies on MRE based ill-posed linear inverse problem solution approaches [75, 113]. We have constructed the prior pdf to be an exponential distribution starting from the uniform pdf. It is of course possible to define the Gaussian prior pdf as similar to in [91], or as an l_p-norm prior as in [83], and starting from the box-car pdf, estimate the parameters of these representations. It is even possible to skip the box-car pdf step and directly specify the prior pdf and use it in the Bayesian estimation of epicardial potentials. This is our first effort in applying the MRE method to inverse ECG problem, thus we have followed the same steps of MRE implementation presented in most of the studies in the literature.

CHAPTER 4

MULTIVARIATE ADAPTIVE NON-PARAMETRIC MODEL

Spline-based methods have been applied to ill-posed inverse problems in various fields of science, engineering. Baussard et al. in [9, 10] and Miller et al. in [72] proposed the B-spline based approximations to solve inverse scattering problem in order to detect and characterize buried object. In Impedance Tomography [7] spline-based method was used to determine the general shape of the inhomogeneities in the torso. There are very few studies in literature that solve the inverse ECG problem using splines; recently published works of Zettinig [118, 119] and Erem [28] modeled the problem based on cubic polynomials in order to take advantage of splines. The main advantages of the spline-based methods are the parametrization of the problem in terms of a small number of unknowns and changing the approximation in local regions without affecting remote portions of the curve or the surface that we wish to approximate. These properties improve the robustness of the inversion and increase the accuracy of the reconstruction [9]. In this context, the constructed model for the unknown parameter of the inverse problem is the projection of data onto the space spanned by the selected spline basis in the model.

4.1 Motivation

The aforementioned applications of splines in the inverse ECG problem use parametric methods. However, common issue in these parametric approaches is how to determine the optimal number of spline functions and the knot locations to avoid over-fitting of the model and to obtain an accurate approximation. Typical approach

to choose these parameters is quite arbitrary by using trial-and-error [46]. In other words, assumptions on functional relationship between dependent and independent variables must be specified in advance.

Parametric techniques assume that the underlying function can be described by a pre-selected number of parameters. These approach can be preferable if reliable information are available about the underlying model. On the other hand, if the number of independent variables in the model need to be increased and interaction of these variable required to represent the nonlinear relationships, then the process become problematic because of the curse of dimensionality. A possible way to remedy this problem is to use non-parametric regression methods, as they require a few assumptions about the problem that are far less restricting than parametric approaches [29, 44]. Another issue about the polynomial regression analysis is that the approximated functions tend to behave erratically, i.e., they have high oscillations, at the boundaries of the input domain. This erratic behavior gets worse as the polynomial order gets higher [14]. On the other hand, oscillatory behavior at the boundaries can be avoided using piecewise polynomial functions [14].

In this part of the study, we have proposed multivariate reduced order non-parametric method to solve the inverse ECG problem using Multivariate Adaptive Regression Splines (MARS). Our goals are:

- MARS based solutions are non parametric regression methods and provides us a flexible way to represent the relationship between measurements and independent variables using smaller number of parameters compared to the original problem. That generate a large family of basis functions based on the supplied data. After that the best possible basis functions and their interactions can be selected in an algorithmic way to model the function under consideration.

- Another important goal of our study is to improve the estimation of local sharp changes in the epicardial potential distribution better than other classical regularization techniques by taking advantage of local support properties of splines. Determination of these sharp changes could be helpful to identify cardiac arrhythmias, especially in the case of PVCs, and it would expedite the planning and execution of the ablation procedure.

4.2 Multivariate Adaptive Regression Splines

Multivariate Adaptive Regression Splines is a non-parametric statistical regression procedure that makes no specific assumption about the underlying functional relationship between the dependent (response) and independent variables (predictors) to estimate general functions of high-dimensional arguments, given sparse data [32, 33]. MARS is an adaptive procedure because the selection of the basis functions (BFs) is data-based and specific to the given problem at hand [98]. It follows the divide and conquer strategy to generate a set of BFs such that the data sets are partitioned into one-dimensional piecewise linear splines of differing slopes of the form $(v - \tau)_+$ and $(\tau - v)_+$, where $(\cdot)_+$ means the positive part:

$$(v - \tau)_+ = \begin{cases} v - \tau, & \text{if } v > \tau, \\ 0, & \text{o/w,} \end{cases} \quad , \quad (\tau - v)_+ = \begin{cases} \tau - v, & \text{if } v < \tau, \\ 0, & \text{o/w.} \end{cases} \quad (4.1)$$

The relation between the input and the response in the general model is expressed as:

$$z = f(\mathbf{v}) + \varepsilon, \quad (4.2)$$

where z is a response variable, $\mathbf{v} = (v_1, v_2, \ldots, v_p)^T$ is a vector of predictors and ε is the additive stochastic error term in the observation with zero mean and finite variance. MARS builds reflected pairs for each input $\hat{\mathbf{v}}_i = (\hat{v}_{i1}, \hat{v}_{i2}, \ldots, \hat{v}_{ip})^T$ with p-dimensional knots $\tau_{\mathbf{i}} = (\tau_{i1}, \tau_{i2}, \ldots, \tau_{ip})^T$ $(i = 1, 2, \ldots, S)$. Then, the collection of 1-dimensional BFs can be defined as follows:

$$B := \{(v_j - \tau)_+, (\tau - v_j)_+ \quad | \quad \tau \in \{\tau_{j1}, \tau_{j2}, \ldots, \tau_{jS}\}, \, j \in \{1, 2, \ldots, p\}\}. \quad (4.3)$$

The fundamental idea of the MARS is to allow additive and multiplicative interactions of the linear truncated basis functions to approximate the model. Thus, the functions of MARS consist of single spline functions or the product of two or more of them to allow for the interactions, resulting in a flexible model that can handle both linear and

non-linear behavior. The MARS estimate of the unknown regression function, $\hat{f}(\mathbf{v})$, can be written as an additive function of the product-form basis functions:

$$z \approx \theta_0 + \sum_{l=1}^{L} \theta_l \psi_l(\mathbf{v}) + \epsilon, \tag{4.4}$$

$$\hat{f}(\mathbf{v}) = \theta_0 + \sum_{l=1}^{L} \theta_l \psi_l(\mathbf{v}). \tag{4.5}$$

Here, ψ_l $(l = 1, 2, \ldots, L)$ are BFs from B, or products of two or more such functions, and θ_l are the unknown coefficients for the lth basis function or for the constant 1 $(l = 0)$. Interaction BFs are created by multiplying an existing BF with a truncated linear function involving a new variable. In this case, both the existing BF and the newly created interaction BF are used in the MARS approximation. The form of the lth BF can be written as follows:

$$\psi_l(\mathbf{v}) := \prod_{j=1}^{K_l} \left(s_{K_j^l} \cdot \left(v_{K_j^l} - \tau_{K_j^l} \right) \right)_+, \tag{4.6}$$

where K_l is the number of truncated linear functions multiplied in the lth BF, $v_{K_j^l}$ is the predictor variable corresponding to the jth truncated linear function in the lth BF, $\tau_{K_j^l}$ is the knot value corresponding to the variable $v_{K_j^l}$, and $s_{K_j^l}$ is the selected sign $(+1$ or $-1)$.

MARS is motivated as a process to create a continuous model following a strategy like that utilised in recursive partitioning. As in recursive partitioning, the MARS method has a forward procedure to add terms, and a backward protocol to prune terms from the model. The MARS algorithm searches for all possible knot locations within the ranges of each predictor. The forward stepwise addition procedure can produce a large collection of basis functions, and the process is stopped when a user-specified maximum model size is reached. The forward phase starts with a constant basis function $\psi_0(\mathbf{v})$ in the model. Then, successively at each state, a pair of basis functions are added to the model that produce the largest decrease in the defined lack of criteria:

$$LOF = \|z - \hat{f}(\mathbf{v})\|_2^2, \tag{4.7}$$

by considering all possible pairs of new basis functions: $\psi_l(\mathbf{v})(v_i - \tau_{ij})$ and $\psi_l(\mathbf{v})(\tau_{ij} - v_i)$, where the variable v_i represents one of the predictors, τ_{ij} is a new knot in that predictor, and $\psi_l(\mathbf{v})$ is a basis function currently in the model that does not depend on v_i. However, here we should note that the original MARS implementation is a regression algorithm, and its lack-of-fit measure is defined as given in Eqn. (4.7), so it is not suitable to solve the ill-posed inverse ECG problem. Thus, we modified the algorithm to handle Eqn. (2.3). This modified MARS algorithm is explained in detail in Section 4.3.

Backward stepwise algorithm is employed to prevent over-fitting by decreasing the complexity of the model without degrading the fit to data, and to remove those BFs from model that contribute to the smallest increase in the lack-of-fit error at each stage, thus producing an optimally estimated model $\hat{f}_L$. The best-fitting model in the stepwise sequence is chosen to minimize the generalized cross-validation criterion, which represents the relationship between the average lack-of-fit to data and complexity of the model [32]:

$$GCV(L) = \frac{1}{N} \sum_{i=1}^{N} (z_i - \hat{f}(\mathbf{v_i}))^2 / \left[1 - \frac{C(L)}{N} \right]^2. \qquad (4.8)$$

Here, L represents the size of the model, N is the number of observations and $C(L)$ stands for the complexity cost function of the model. More detailed information about $C(L)$ can be found in [32].

4.3 Reformulation of the Inverse ECG problem

In this study, we have explored an adaptive spline-based approximation to solve the linear inverse ECG problem. The proposed method constructs a model of the potential distribution on the epicardial surface based on the MARS by benefiting the heart geometry and the body surface potentials. However since the MARS is a regression procedure, it is not possible to use it directly for solving the linear inverse problem. This part explains how the epicardial potential distribution can be defined as a continuous function, and the small modification required in the MARS algorithm to solve

the inverse ECG problem. Since the discrete linear inverse problem defined in Eqn. (2.3) is considered and solved at each time instant separately, time index k can be omitted from the equation:

$$\mathbf{y} = \mathbf{A}\mathbf{x} + \mathbf{n}, \tag{4.9}$$

where $\mathbf{y} = [y_1, y_2, \ldots, y_M]^T$, $\mathbf{x} = [x_1, x_2, \ldots, x_N]^T$, $\mathbf{n} = [n_1, n_2, \ldots, n_M]^T$, and the subscripts denote corresponding node numbers.
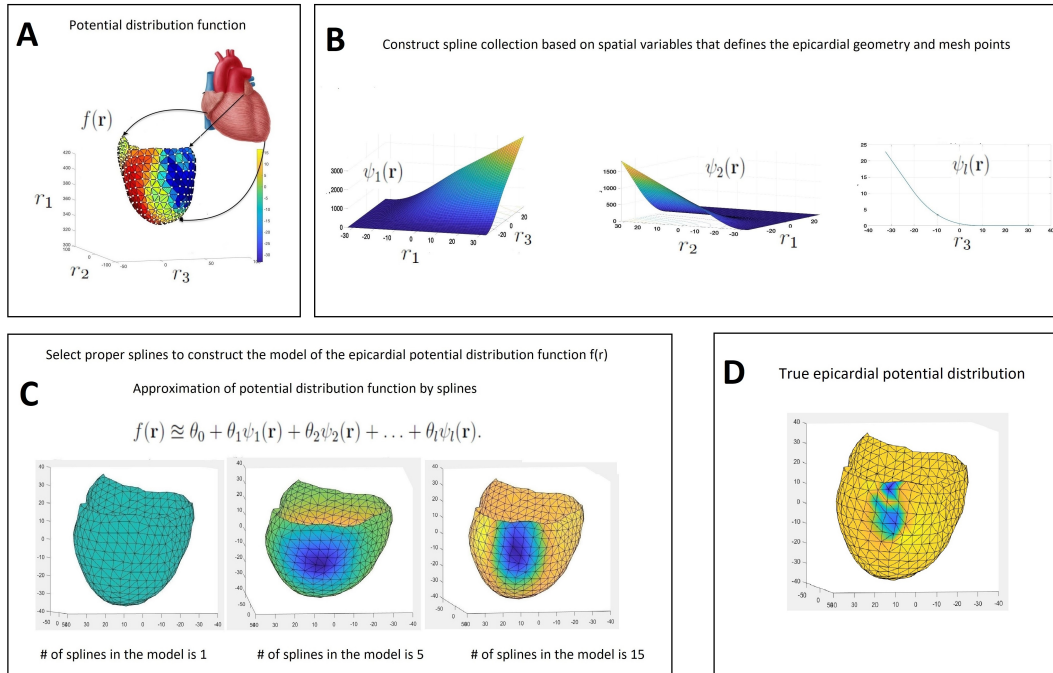
Figure 4.1: Top left (A): cardiac geometry represented in terms of triangular mesh elements and the corresponding isopotential maps. Top right (B): sample 1D and 2D splines. Left bottom corner (C): evolution of the estimated epicardial potential distribution at three MARS iterations, along with the corresponding true epicardial potentials. The potential distribution function model starts from the single constant spline and at each iteration suitable basis functions are added to the model to obtain a better approximation (approximations from left to right). Right bottom corner (D): True epicardial potential distribution.

As a first step in MARS modeling, epicardial potentials $\mathbf{x}$ should be defined as a function of some independent variables. Epicardial potential distribution is treated and modeled as a function $f(\mathbf{r})$ defined over a 3-dimensional epicardial surface, as represented in Fig. 4.1. This figure shows the cardiac geometry represented in terms

56

of triangular mesh elements and corresponding isopotential maps at the top left side, sample 1D and 2D splines at the top right side, and evolution of the estimated epicardial potential distribution at three MARS iterations, along with the corresponding true epicardial potentials at the bottom. The potential distribution function model starts from a single constant basis function, and then at each iteration suitable BFs are added to the model, step by step, a better approximation can be obtained. Consequently, $\mathbf{x}$ can be expressed as a collection of function values $f(\mathbf{r}_i)$ at predefined coordinates $\mathbf{r}_i = [r_{i1}, r_{i2}, r_{i3}]^T \in \Omega$ ($i = 1, 2, ..., N$):

$$\mathbf{x} = \left[f(\mathbf{r}_1), f(\mathbf{r}_2), \ldots, f(\mathbf{r}_N) \right]^T. \tag{4.10}$$

Here, $\Omega \in \mathbb{R}^3$ denotes the 3-dimensional epicardial surface shown in Fig. 4.1, and $\mathbf{r}$ stands for the coordinate vector of any point on this surface.

Up to here, epicardial potentials are reformulated as a function of spatial variables defined on the epicardial surface. This function now can be approximated by a spline-based approximation, as illustrated in Fig. 4.1. If we treat y_i ($i = 1, 2, \ldots, M$) as the responses, and the elements of $\mathbf{r}$ as the predictors, then MARS method can be applied to estimate the function $f(\mathbf{r})$. Thus, the MARS estimate of the unknown function $\hat{f}(\mathbf{r})$ can be written in the following form:

$$\hat{f}(\mathbf{r}) = \theta_0 + \sum_{l=1}^{L} \theta_l \psi_l(\mathbf{r}). \tag{4.11}$$

Here, L is the number of basis functions in the model. In light of the equations given above, the ith torso measurement y_i can be written as:

$$y_i = \sum_{j=1}^{N} a_{ij} \hat{f}(\mathbf{r}_j) + n_i, \tag{4.12}$$

where a_{ij} is the ith row, j^{th} column element of $\mathbf{A}$. If we substitute Eqn. (4.11) into Eqn. (4.12), we obtain:

$$y_i = \sum_{j=1}^{N} a_{ij} \left(\theta_0 + \sum_{l=1}^{L} \theta_l \psi_l(\mathbf{r}_j) \right) + n_i. \tag{4.13}$$

Then, Eqn. (4.9) can be expressed based on spline functions and corresponding coefficients as:

$$\mathbf{y} = \mathbf{A}\mathbf{\Psi}\boldsymbol{\theta} + \mathbf{n}, \tag{4.14}$$

$$\hat{\mathbf{x}} = \mathbf{\Psi}\boldsymbol{\theta}, \tag{4.15}$$

$$\boldsymbol{\theta} = \left[\theta_0, \ldots, \theta_L\right]^T, \tag{4.16}$$

$$\mathbf{\Psi} = \begin{bmatrix} 1 & \psi_1(\mathbf{r}_1) & \ldots & \psi_L(\mathbf{r}_1) \\ \vdots & \vdots & \ldots & \vdots \\ 1 & \psi_1(\mathbf{r}_N) & \ldots & \psi_L(\mathbf{r}_N) \end{bmatrix}. \tag{4.17}$$

Here, $\mathbf{\Psi}$ is a matrix composed of spline functions that are selected from the set B in Eqn. (4.3), by the MARS algorithm for each time instant separately. Thus, selected spline functions may be different at each time. The $\boldsymbol{\theta}$ represents the corresponding coefficient vector, and the $\mathbf{\Psi}\boldsymbol{\theta}$ term is the approximation of the unknown epicardial potential vector $\mathbf{x}$.

However, MARS is a regression procedure to explore the relationships between dependent and independent variables. It assumes that there exists no transformation between the measurements and the function which we wish to approximate. For this reason MARS employs the lack-of-fit function given in Eqn. (4.7). On the other hand, in the inverse ECG problem, measurements are the outputs of the transformation, obtained by applying the forward matrix $\mathbf{A}$ on the epicardial potentials that we wish to approximate. For this reason, Eqn. (4.7) is not suitable for our problem. The problem given in Eqn. (4.14) is ill-posed, thus, the solution needs to be constrained. Furthermore, epicardial potential distributions are actually correlated across time: therefore methods that only exploit spatial constraints without considering the temporal evolution of the potentials are not ideal. Consequently, the use of temporal information could improve the estimation accuracy. In this study, we have introduced the following problem formulation to estimate the spatio-temporal behavior of the epicardial potentials:

$$\underset{\boldsymbol{\theta}}{\text{minimize}} \ \|\mathbf{y} - \mathbf{A}\mathbf{\Psi}\boldsymbol{\theta}\|_2^2 + \lambda\|\mathbf{\Psi}\boldsymbol{\theta} - \hat{\mathbf{x}}_{k-1}\|_2^2. \tag{4.18}$$

Here, $\hat{\mathbf{x}}_{k-1}$ is the estimated epicardial potential vector in the previous time instant, and the initial state $\hat{\mathbf{x}}_0$ is the Tikhonov estimation at $k = 1$ and $\lambda \geq 0$ is the regularization parameter. Algorithms 1 and 2 give the simplified forms of the forward and backward steps of the modified MARS method that we have used in this study to solve the inverse ECG problem.

Algorithm 1: Simplified explanation of modified MARS forward stepwise algorithm for solving the inverse ECG problem.

Initialization;

Start from the simple model that contains constant basis function;

$$\psi_1(r) = 1, \mathbf{M} = 2, lof^* = \infty, \boldsymbol{\Psi} = \begin{bmatrix} \psi_1(\mathbf{r}_1) \\ \vdots \\ \psi_1(\mathbf{r}_N) \end{bmatrix};$$

For given λ ;

while $M < M_{max}$ **do**

    Add spline, $\psi_*(r)$, to the model from the spline collection ;

$$\boldsymbol{\Psi}^* = \begin{bmatrix} \psi_*(\mathbf{r}_1) \\ \vdots \\ \psi_*(\mathbf{r}_N) \end{bmatrix}, \boldsymbol{\Psi}_{new} = \begin{bmatrix} \boldsymbol{\Psi} & \boldsymbol{\Psi}^* \end{bmatrix};$$

    Solve the optimisation problem ;

$$lof \leftarrow \underset{\boldsymbol{\theta}}{\text{minimize}} \ \|\mathbf{y} - \mathbf{A}\boldsymbol{\Psi}_{new}\boldsymbol{\theta}\|_2^2 + \lambda\|\boldsymbol{\Psi}_{new}\boldsymbol{\theta} - \hat{\mathbf{x}}_{k-1}\|_2^2.;$$

    if $lof < lof^*$ **then**

        $\boldsymbol{\Psi} \leftarrow \boldsymbol{\Psi}_{new}$;

        $M \leftarrow M + 1$;

        $lof^* \leftarrow lof$

    end

end

The corresponding lack-of-fit criteria to replace Eqn. (4.7), PRSS, can then be written

as follows:

$$
PRSS = \sum_{i=1}^{M} \left(y_i - \sum_{j=1}^{N} a_{ij} \left(\theta_0 + \sum_{l=1}^{L} \theta_l \psi_l(\mathbf{p}_j) \right) \right)^2 +
$$
$$
\lambda \sum_{j=1}^{N} \left(\theta_0 + \sum_{l=1}^{L} \theta_l \psi_l(\mathbf{p}_j) - \hat{x}_{k-1}^{j} \right)^2, \tag{4.19}
$$

where $\hat{x}_{k-1}^{j}$ corresponds to the jth component of the vector $\hat{\mathbf{x}}_{k-1}$.

Algorithm 2: Simplified explanation of modified MARS backward stepwise algorithm to find the optimal model size.

Initialization;

$L \leftarrow$ Size of the model

$M \leftarrow$ Number of measurement points on the body surface

$PRSS = \|\mathbf{y} - \mathbf{A}\mathbf{\Psi}\boldsymbol{\theta}\|_2^2 + \lambda\|\mathbf{\Psi}\boldsymbol{\theta} - \hat{\mathbf{x}}_{k-1}\|_2^2$

$GCV^*(L) = \dfrac{PRSS}{M} \Big/ \left[1 - \dfrac{C(L)}{M} \right]^2$

for $i = M_{max}$ to 2 **do**

    Remove one of the splines from the model. ;

    Assuming that $\mathbf{\Psi}_*$ is the new matrix after removing one of the splines
    from the model,

    Calculate ;

        $PRSS = \|\mathbf{y} - \mathbf{A}\mathbf{\Psi}_*\boldsymbol{\theta}\|_2^2 + \lambda\|\mathbf{\Psi}_*\boldsymbol{\theta} - \hat{\mathbf{x}}_{k-1}\|_2^2$

    Calculate GCV ;

        $GCV(L) = \dfrac{PRSS}{M} \Big/ \left[1 - \dfrac{C(L)}{M} \right]^2$

    if $GCV(L) < GCV^*(L)$ **then**

        $\mathbf{\Psi} = \mathbf{\Psi}_*$

        $GCV^*(L) \leftarrow GCV(L)$

        $L \leftarrow L - 1$

    end

end

4.4 Results for Utah Data Collection

In this section, we evaluate the performance of proposed non-parametric MARS-based approach. Results are compared with estimates of well-known techniques such as Tikhonov and Twomey regularizations and additionally the spline-based technique introduced in [28]. In this part of the study, Spline Inverse term and SI abbreviation are used for the technique of Erem et al. [28]. Here, we should note that for Utah dataset all simulations are performed using torso potentials contaminated by 30 dB SNR Gaussian noise (except in Section 4.4.6, where noise variance varies), and all are repeated for 5 noise realizations.

The Utah data collection contains 23 ventriculary paced beats, coming from 5 different experiments. In order to comprehensively assess the performance of the proposed method from various perspective, interventions have also been applied to each dataset in the Utah data collection. These interventions are, introducing geometric errors and adding extra measurement noise.

4.4.1 Reconstruction of Electrograms

Initially, we have ran all algorithms for the 23 datasets from Utah collection during the QRS complex, and CC and RE values are computed. Tables 4.1 and 4.2 show the mean and standard deviations (std) of the CC and RE values obtained over time.

Results presented in this table can be interpreted as follows: The reconstruction which is achieved by MARS-based technique have better fidelity to the original epicardial potential distributions for almost all datasets from the perspectives of CC and RE values. However, since these average metrics do not give any detail about the change of CC and RE values during the QRS interval, sample graphs representing the change of CC and RE values with respect to time are presented in Fig. 4.2. These figures show that, MARS-based solution scheme is superior at earlier times of the wavefront propagation, but later on, when the potential distribution propagates through the epicardial surface, its accuracy is comparable to SI methods in terms of the CC and RE metrics. A similar behavior is observed for all the other datasets. High CC and low RE values at earlier times of the QRS interval obtained by MARS-based solution

61

Table 4.1: Mean ($E\{CC\}$) and standard deviation ($\sigma\{CC\}$) values of CC for the epicardial potential estimates of the Utah data collection.

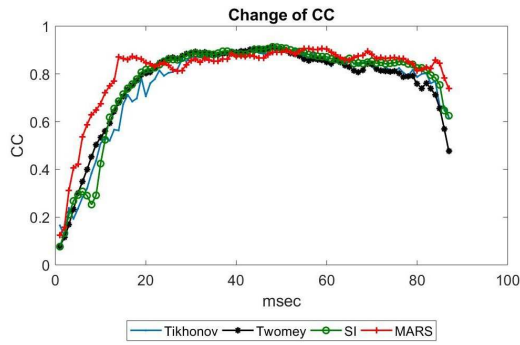| Dataset	CC			
	Tikhonov	Twomey	Spline Inverse	MARS
1	0.72 ± 0.19	0.76 ± 0.18	0.75 ± 0.19	0.84 ± 0.12
2	0.71 ± 0.19	0.74 ± 0.18	0.73 ± 0.20	0.81 ± 0.13
3	0.77 ± 0.18	0.79 ± 0.18	0.78 ± 0.18	0.82 ± 0.15
4	0.76 ± 0.20	0.77 ± 0.20	0.78 ± 0.20	0.83 ± 0.14
5	0.75 ± 0.20	0.77 ± 0.19	0.78 ± 0.20	0.81 ± 0.16
6	0.77 ± 0.17	0.80 ± 0.15	0.79 ± 0.18	0.84 ± 0.13
7	0.78 ± 0.14	0.81 ± 0.13	0.80 ± 0.15	0.86 ± 0.11
8	0.68 ± 0.29	0.72 ± 0.27	0.71 ± 0.30	0.78 ± 0.22
9	0.76 ± 0.18	0.79 ± 0.17	0.79 ± 0.18	0.85 ± 0.14
10	0.72 ± 0.17	0.74 ± 0.15	0.74 ± 0.17	0.78 ± 0.14
11	0.64 ± 0.20	0.67 ± 0.20	0.67 ± 0.21	0.73 ± 0.19
12	0.71 ± 0.16	0.73 ± 0.16	0.74 ± 0.18	0.78 ± 0.15
13	0.64 ± 0.26	0.67 ± 0.25	0.66 ± 0.27	0.73 ± 0.23
14	0.66 ± 0.19	0.70 ± 0.17	0.70 ± 0.19	0.79 ± 0.13
15	0.64 ± 0.22	0.67 ± 0.21	0.67 ± 0.23	0.75 ± 0.18
16	0.68 ± 0.24	0.70 ± 0.23	0.71 ± 0.24	0.78 ± 0.19
17	0.64 ± 0.28	0.67 ± 0.26	0.67 ± 0.28	0.76 ± 0.19
18	0.76 ± 0.19	0.77 ± 0.19	0.78 ± 0.20	0.81 ± 0.17
19	0.70 ± 0.23	0.73 ± 0.21	0.75 ± 0.22	0.76 ± 0.19
20	0.77 ± 0.17	0.79 ± 0.16	0.79 ± 0.18	0.81 ± 0.14
21	0.76 ± 0.17	0.78 ± 0.17	0.78 ± 0.19	0.82 ± 0.14
22	0.77 ± 0.18	0.80 ± 0.17	0.79 ± 0.20	0.81 ± 0.16
23	0.78 ± 0.20	0.78 ± 0.20	0.76 ± 0.26	0.84 ± 0.18
Average	0.72 ± 0.20	0.75 ± 0.19	0.74 ± 0.21	0.80 ± 0.16

Table 4.2: Mean ($E\{RE\}$) and standard deviation ($\sigma\{RE\}$) values of RE for the epicardial potential estimates of the Utah data collection.

Dataset	RE			
	Tikhonov	Twomey	Spline Inverse	MARS
1	0.64 ± 0.17	0.60 ± 0.17	0.62 ± 0.21	0.52 ± 0.17
2	0.65 ± 0.17	0.62 ± 0.15	0.67 ± 0.31	0.57 ± 0.13
3	0.59 ± 0.20	0.60 ± 0.30	0.60 ± 0.26	0.55 ± 0.18
4	0.60 ± 0.22	0.62 ± 0.30	0.60 ± 0.34	0.54 ± 0.18
5	0.63 ± 0.23	0.60 ± 0.17	0.59 ± 0.21	0.56 ± 0.16
6	0.59 ± 0.17	0.55 ± 0.17	0.59 ± 0.31	0.51 ± 0.16
7	0.59 ± 0.14	0.55 ± 0.14	0.58 ± 0.25	0.48 ± 0.14
8	0.67 ± 0.35	0.64 ± 0.30	0.63 ± 0.33	0.57 ± 0.30
9	0.61 ± 0.17	0.60 ± 0.22	0.60 ± 0.32	0.49 ± 0.13
10	0.63 ± 0.13	0.60 ± 0.11	0.61 ± 0.14	0.57 ± 0.13
11	0.69 ± 0.22	0.66 ± 0.16	0.72 ± 0.43	0.63 ± 0.24
12	0.63 ± 0.15	0.64 ± 0.22	0.70 ± 0.72	0.57 ± 0.14
13	0.72 ± 0.30	0.70 ± 0.25	0.75 ± 0.60	0.62 ± 0.20
14	0.67 ± 0.16	0.64 ± 0.16	0.63 ± 0.17	0.56 ± 0.14
15	0.69 ± 0.22	0.66 ± 0.18	0.71 ± 0.43	0.60 ± 0.18
16	0.67 ± 0.24	0.66 ± 0.23	0.72 ± 0.72	0.58 ± 0.21
17	0.71 ± 0.28	0.73 ± 0.35	0.75 ± 0.78	0.62 ± 0.23
18	0.60 ± 0.18	0.69 ± 0.19	0.64 ± 0.53	0.55 ± 0.16
19	0.66 ± 0.21	0.66 ± 0.25	0.69 ± 0.74	0.60 ± 0.22
20	0.59 ± 0.15	0.58 ± 0.16	0.60 ± 0.28	0.55 ± 0.15
21	0.60 ± 0.18	0.61 ± 0.24	0.60 ± 0.34	0.54 ± 0.16
22	0.59 ± 0.21	0.55 ± 0.16	0.59 ± 0.43	0.53 ± 0.19
23	0.56 ± 0.25	0.61 ± 0.34	0.62 ± 0.38	0.46 ± 0.21
Average	0.63 ± 0.20	0.62 ± 0.21	0.62 ± 0.26	0.56 ± 0.18

technique enhance its average metrics.

(a) CC vs time graph for dataset 5.
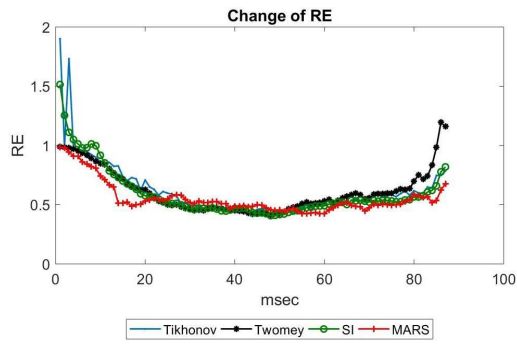
(b) RE vs time graph for dataset 5.
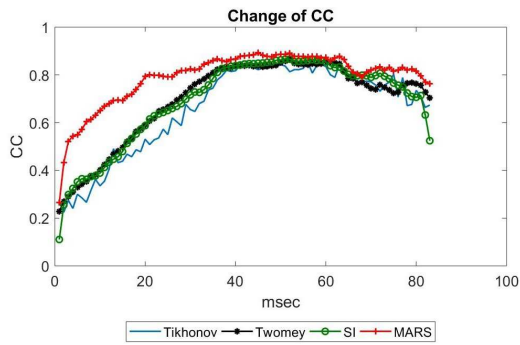
(c) CC vs time graph for dataset 14.
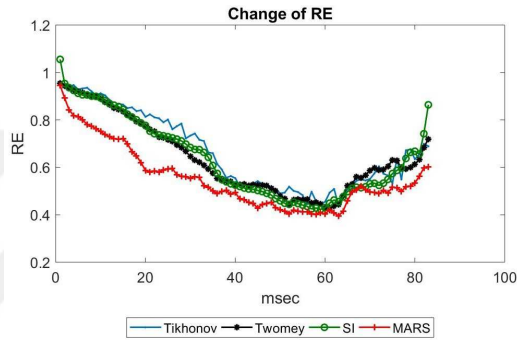
(d) RE vs time graph for dataset 14.

Figure 4.2: Evolution of CC and RE values over time for two datasets selected from the Utah data collection. These figures represents the predomination of MARS-based approach in earlier times of the wave-front propagation in terms of CC and RE metrics

4.4.2 Epicardial Potential Maps

Because CC and RE values can only give us a general idea about how these solutions vary, and in cases when CC or RE values are very close to each other, it is necessary to examine the solutions in more detail to evaluate their respective usefulness. To achieve this, the original and reconstructed epicardial potential maps are plotted at two sample times; right after pacing is applied (Fig. 4.3), and at a later time when the wave-front has propagated though the epicardial surface (Fig. 4.4).

At earlier times of the wave-front propagation in Fig. 4.3, reconstructed wave-fronts by the proposed MARS-based approach are focalized around the stimulation site better than the other three methods. Furthermore, amplitudes of the reconstructed acti-

vation wave-fronts by MARS-based method are higher and closer to the true values compared with the results of other estimation methods. On the other hand, in Fig. 4.4, although all methods reconstruct the general shape of the wave-front similar to the true maps, the wave-fronts reconstructed by the MARS-based technique are more spread than those obtained by the Tikhonov, Twomey and SI methods.
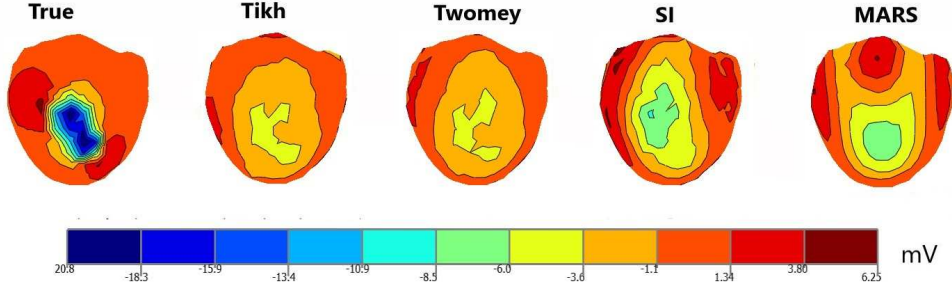
(a) Isopotential maps for dataset 5 from the Utah data collection at $t = 10$ msec.
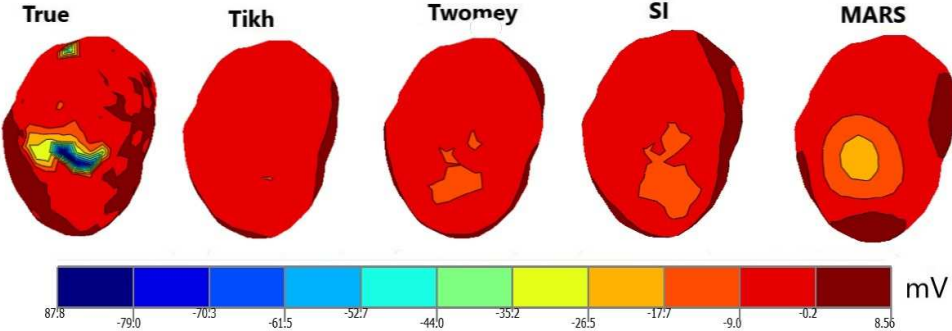
(b) Isopotentials maps for dataset 14 from the Utah data collection at $t = 10$ msec.

Figure 4.3: Sample snapshots of the original and reconstructed isopotential maps from the Utah data collection short time after the stimulation.

4.4.3 Activation Isochrone Maps

Activation isochrone maps display the propagation pattern of the reconstructed epicardial potentials, and they could be useful for calculating propagation velocity in different parts of the heart surface, and to compare success of the methods.

In order to evaluate the estimated activation times, we have plotted the CC values of activation times corresponding to each method and each dataset in Fig. 4.5, and the average CC over all datasets are calculated for each method. Estimated activation times are very close to true ones and obtained high CC values ≥ 0.90 on the average
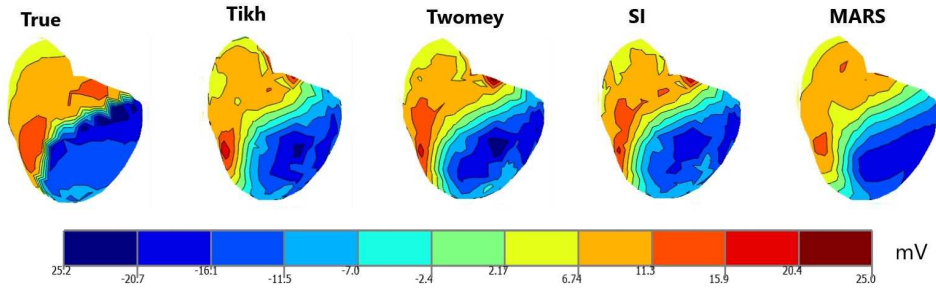
(a) Isopotentials maps for dataset 5 from the Utah data collection at $t = 50$ msec.
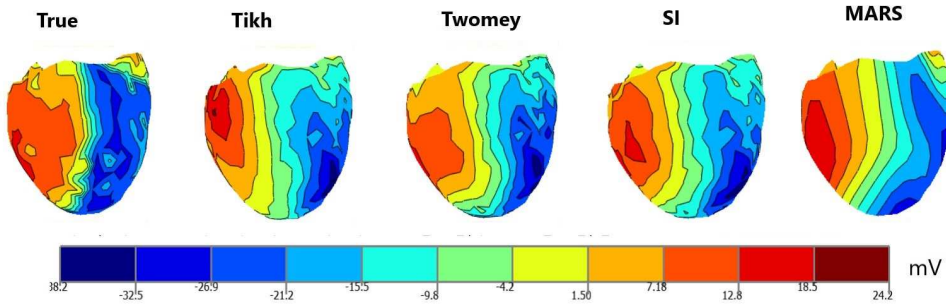
(b) Isopotentials maps for dataset 14 from the Utah data collection at $t = 50$ msec.

Figure 4.4: Sample snapshots of the original and reconstructed isopotential maps from the Utah data collection after the depolarization has spread over the heart surface.
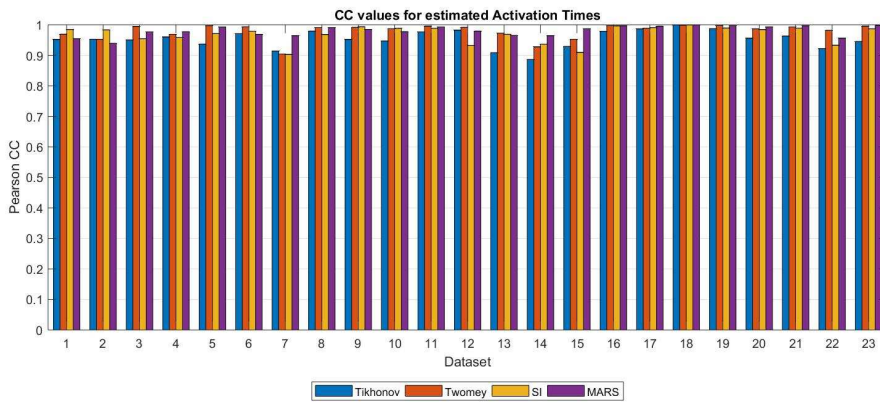
Figure 4.5: Pearson CC values for activation times for the Utah data collection.

for all methods. However depending on the dataset, success of the each method differs when compared to each other, as illustrated in Fig. 4.5. In order make visual comparisons sample isochrone maps for the Utah data collection are presented in Fig. 4.6. For dataset 5, Fig. 4.6a, except the Tikhonov regularization, all the methods

66
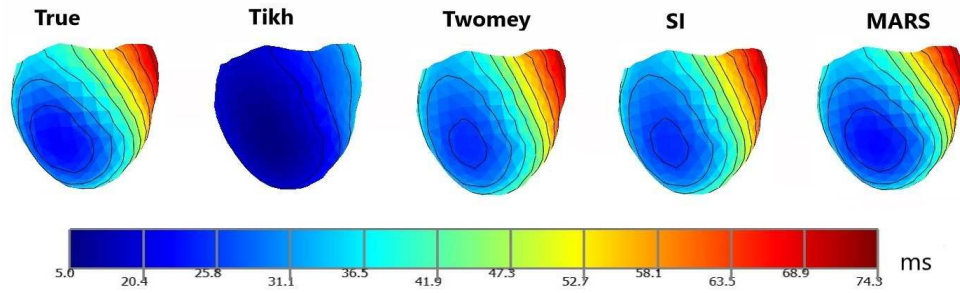
(a) Isochrone maps for dataset 5 from Utah data collection.
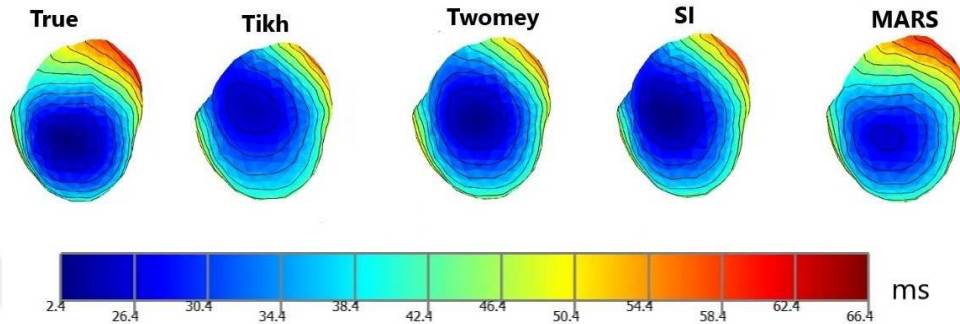
(b) Isochrone maps for dataset 14 from Utah data collection.

Figure 4.6: Sample isochrone maps for the Utah data collection.

produce similar isochrone patterns, that are close to the true activation pattern. On the other hand, for dataset 14, MARS-based approach yield an isochrone pattern with better fidelity to the true activation map. These observations are also supported by the CC values shown in Fig. 4.5.

4.4.4 Pacing Site Localization

Locating the site of earliest activation is an important issue in clinical application of ECGI and could be helpful to identify cardiac arrhythmias such as PVCs. The predomination of MARS-based solution technique at earlier times indicates that it has a potential for determining the earliest activation time and hence the stimulation location better than the other three methods. Table 4.3 presents a list of pacing site LE values. According to these values, for 12 of the 23 datasets, MARS-based technique have estimated more precise pacing locations, while Tikhonov, Twomey and Spline Inverse have succeeded in 4, 7 and 7 out of 23 datasets, respectively.

67

Table 4.3: Pacing site localization errors in mm for the Utah data collection.

Test data	Tikhonov	Twomey	Spline Inverse	MARS
1	1.28 ± 2.87	4.18 ± 3.89	7.41 ± 0.91	7.74 ± 0.74
2	10.47 ± 1.80	9.67 ± 2.20	11.28 ± 0.00	8.67 ± 2.20
3	10.91 ± 0.00	10.91 ± 0.00	11.88 ± 2.16	10.91 ± 0.00
4	7.01 ± 2.86	5.73 ± 0.00	5.73 ± 0.00	5.73 ± 0.00
5	6.57 ± 1.49	7.66 ± 0.00	7.57 ± 1.87	8.14 ± 1.08
6	14.04 ± 2.52	13.29 ± 2.72	15.80 ± 2.82	12.38 ± 2.59
7	13.23 ± 3.35	10.66 ± 0.28	12.65 ± 2.55	6.41 ± 2.49
8	21.77 ± 20.25	10.56 ± 2.75	12.24 ± 2.11	12.51 ± 0.96
9	2.11 ± 2.90	1.72 ± 2.35	0 ± 0.00	1.06 ± 2.37
10	7.21 ± 1.27	7.78 ± 0.00	7.90 ± 0.28	7.48 ± 1.69
11	7.13 ± 2.93	4.07 ± 0.00	4.07 ± 0.00	5.42 ± 1.87
12	6.42 ± 2.00	5.53 ± 0.00	5.53 ± 0.00	5.79 ± 0.36
13	11.93 ± 7.73	4.16 ± 4.12	7.55 ± 3.32	3.49 ± 3.51
14	18.81 ± 2.00	14.16 ± 4.53	16.99 ± 4.33	9.26 ± 2.39
15	16.22 ± 5.76	8.11 ± 0.62	9.74 ± 2.03	3.77 ± 2.37
16	8.53 ± 2.29	9.77 ± 0.00	7.53 ± 2.04	4.94 ± 1.00
17	10.39 ± 3.58	7.47 ± 1.64	7.85 ± 2.16	6.27 ± 0.00
18	8.31 ± 1.23	8.86 ± 0.00	7.22 ± 1.50	7.77 ± 1.50
19	11.87 ± 0.40	10.14 ± 1.41	11.69 ± 0.00	9.63 ± 1.15
20	5.48 ± 0.00	5.06 ± 0.39	4.10 ± 2.32	4.77 ± 0.00
21	6.07 ± 3.66	6.79 ± 0.00	5.43 ± 3.04	6.79 ± 0.00
22	7.88 ± 0.96	7.45 ± 0.00	7.45 ± 0.00	7.45 ± 0.00
23	9.84 ± 5.83	7.56 ± 5.42	9.36 ± 2.36	8.05 ± 2.31
Average	9.76 ± 3.38	7.88 ± 1.40	8.56 ± 1.56	7.16 ± 1.33

4.4.5   Robustness Against the Modeling Errors

Modeling inaccuracies are also important for the success of applied regularization techniques. Their influences on the inverse solutions were studied in [6, 48, 69, 100]. Modeling errors originate from several parameters or assumptions that are used in the solution of the forward problem. Variations in the conductivities of torso tissues, segmentation errors of medical images, discretization error, movement of the heart, geometry parameters such as size, location of the heart and electrode positions on the torso, are some of the important properties that cause the modeling errors. According to the outcomes of [100], heart size and location deviations have significant effect on the reconstruction performance.

Our aim in this section is to assess the robustness of our approach against the perturbations derived from modeling errors. To understand their influence, the following artificial distortions are introduced: small perturbations in the forward transfer matrix, variation in size of the heart and location inside the torso. All the tests presented here have been performed using Utah data collection with body surface potentials that are simulated using an error free model, and contaminated by 30 dB SNR zero-mean Gaussian noise. To measure the impact of model inaccuracies, average CC, RE and pacing site LE are computed over 23 datasets, for each modeling error case.

4.4.5.1   Distortions in the Transfer Matrix

In this part, the forward transfer matrix is contaminated by an additive Gaussian noise matrix of the same size, with zero mean, independent and identically distributed elements, in order to gain insight about the effects of small perturbations in the model arising possibly from many different parameters mentioned above. Two different matrix perturbation levels at 20 and 30 dB SNR are considered. Change of estimation performances in terms of average CC, RE and pacing site LE are presented in Fig. 4.7. A notable observation about the results is that when an error in the forward matrix is introduced and its SNR is changed from 30 to 20 dB, the MARS-based estimation performance remains quite robust and only a small amount of decrease is observed in all three accuracy measures. However, increasing the noise in the

forward model cause considerable degradation in estimation accuracies of the other three methods. The percentage of degradation in CC values of MARS-based method are about 2.25% and 3.75% at 30 and 20 dB SNR, respectively. On the other hand, under the same conditions other methods' CC measurements decrease approximately 7% and 14% for Tikhonov, 11% and 20% for Twomey and 6.75% and 15% for SI. Similarly, the changes in RE are approximately 3.6% and 5.4% for MARS, 8% and 23.8% for Tikhonov, 16% and 27.5% for Twomey and 11.3% and 17.7% for SI methods. When we examine the LE errors, the percentage of degradation in LE values MARS-based method are approximately 5%, 29% at 30 and 20 dB SNR respectively. However, degradation percentages become 28%, 45% for SI, 15%, 27% and 15%, 15% for Twomey and Tikhonov respectively.
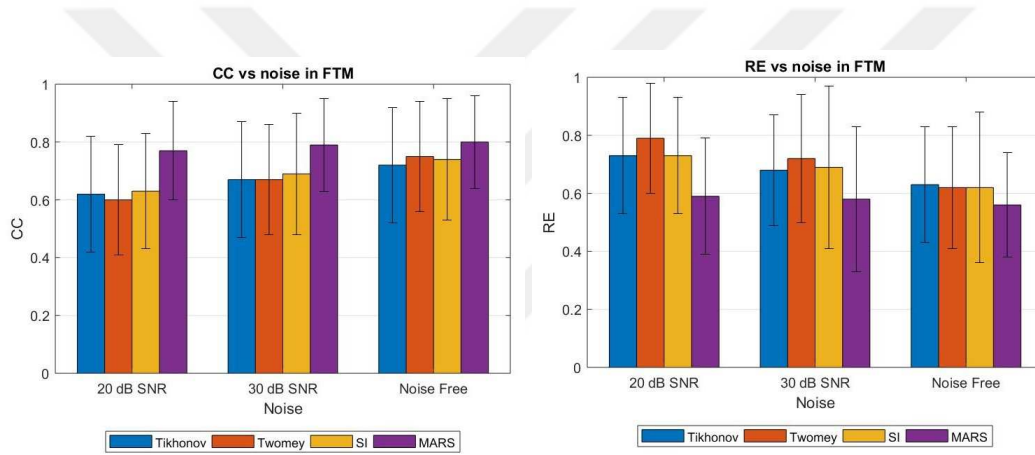
(a) Correlation coefficients.

(b) Relative errors.
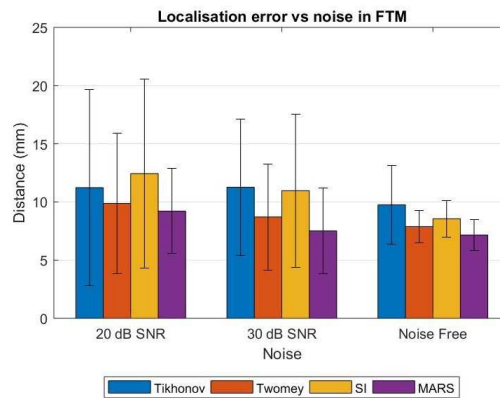
(c) Small variations in the forward transfer matrix.

Figure 4.7: Small variations in the forward transfer matrix (Utah data collection).

4.4.5.2   Errors in the Heart Location

To simulate the heart positioning errors, heart is shifted along the x-axis (i.e., right and left of the body) and y-axis (i.e., backward and onward of the body) of the original torso mesh and the forward transfer matrix corresponding to this modified mesh is employed in inverse calculations. Shift amounts are 10 mm in the $\pm x$ and $\pm y$ direction; 0 mm shift means that there is no geometric error. The average CC, RE and pacing site localization errors, corresponding to shifting to the left and right side inside the torso from its true location, are plotted in Figs. 4.8 and 4.9. Unlike the small variation in the forward transfer matrix case, the shifted heart location has degraded the estimation performances of all methods. However, MARS-based approach has showed the best performance in terms of average CC and pacing site LE metrics if shift is in the $\pm x$ direction. On the other hand, its RE evaluation seems to be sensitive against the heart position. Furthermore, if the heart position is shifted in the $\pm y$ direction, estimation performances of the MARS, SI and Twomey methods have got close to each other.

4.4.5.3   Errors in the Heart Size

The impact of the geometric errors due to the incorrect determination of heart size on the reconstruction of epicardial potentials are examined by utilizing the heart geometry of 0.8 and 1.2 times the actual heart size, and the corresponding modified forward transfer matrix for inverse solution. Scaling factor 1 means that true heart geometry is used. The average CC, RE and pacing site LE corresponding to different heart sizes are given in Fig. 4.10. Similar to the shift errors, MARS-based solution has produced the highest CC values and more precisely determined pacing site locations for all heart size errors.

4.4.6   Robustness against Measurement Noise

In order to examine the effects of measurement noise on the inverse problem solutions, body surface potentials are contaminated by a zero mean Gaussian noise of 10, 20 and 30 dB SNR. Estimation performances in terms of average CC and RE values
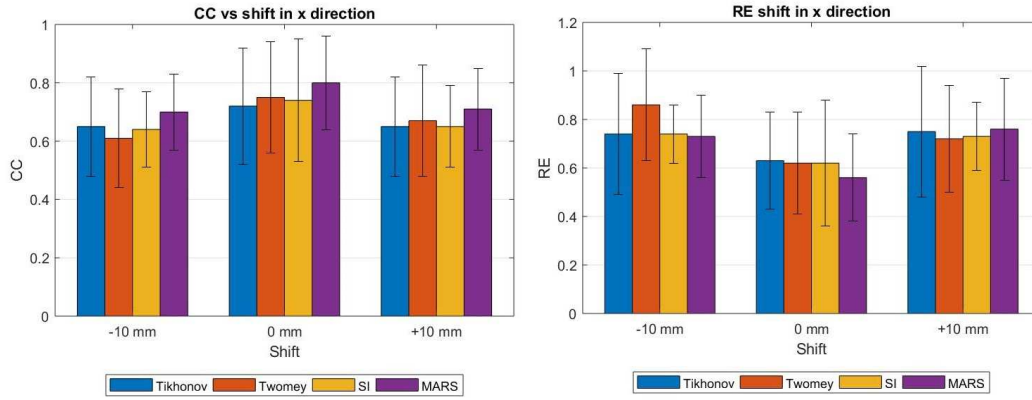
(a) Correlation coefficients.

(b) Relative errors.
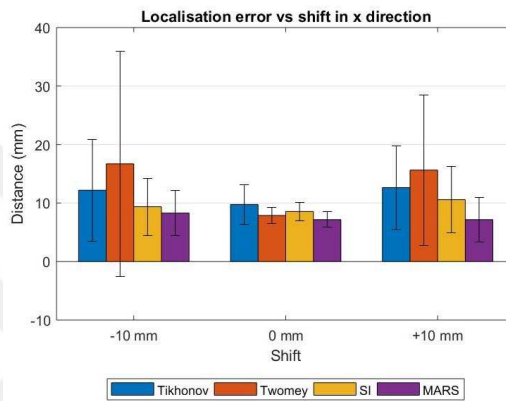
(c) Pacing site localization error.

Figure 4.8: Shifted heart location to the left and right side inside the torso from its true location (Utah data collection).

are presented in Fig. 4.11. At all noise levels, proposed method have produced higher mean CC and lower mean RE values. When noise level changed from 30 dB to 10 dB SNR, proposed method performance has degraded approximately %12 in terms of mean CC values. On the other hand, SI, Twomey and Tikhonov performances have reduced %16, %23 and %19, respectively. Similarly for relative errors, performance degradations are approximately %25 for both MARS-based approach and SI, and %32 for Twomey and Tikhonov regularizations. We have also calculated pacing site LE of all methods for each noise level. Pacing site LE for Tikhonov and Twomey methods are significantly affected due to decreasing SNR value. MARS-based method and SI have yielded similar results, which are better compared to Tikhonov and Twomey regularizations.
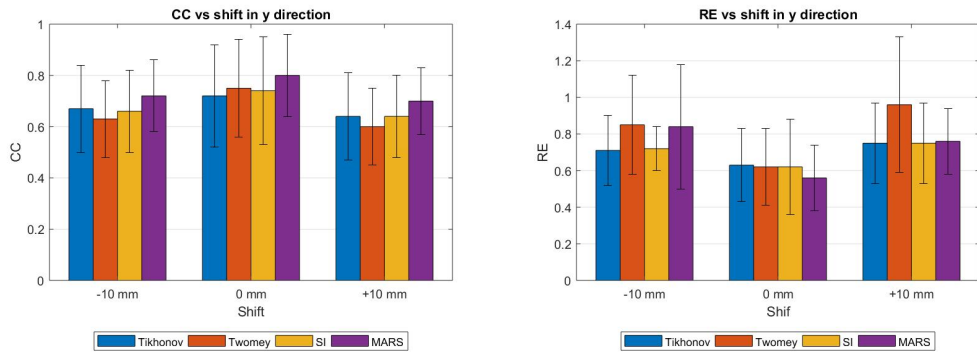
(a) Correlation coefficients.

(b) Relative errors.
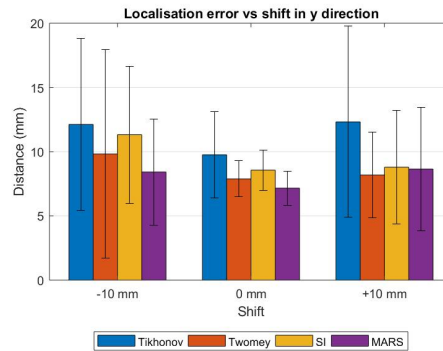
(c) Pacing site localization error.

Figure 4.9: Shifted heart location to the backward and onward inside the torso from its true location (Utah data collection).

4.5 Results for KIT Data Collection

KIT data collection contains 8 ventricularly paced beats, and pacing sites are located on the epicardium, endocardium and septum center. We have used the KIT data collection without any interventions (such as adding extra measurement noise, or introducing geometric errors) to facilitate comparison of the methods evaluated in this study with future studies. Heart surface potentials in this dataset are referred to as pericardial potentials, and although they are not the same, they are similar enough that pericardial and epicardial potential labels have been used interchangeably in literature. To be consistent with previous sections, we continue to use the term 'epicardial potentials' in this section.
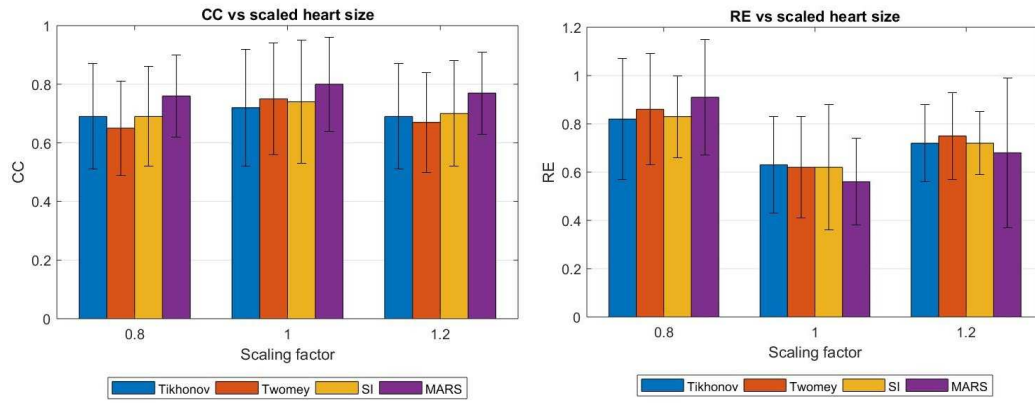
(a) Correlation coefficients.

(b) Relative errors.
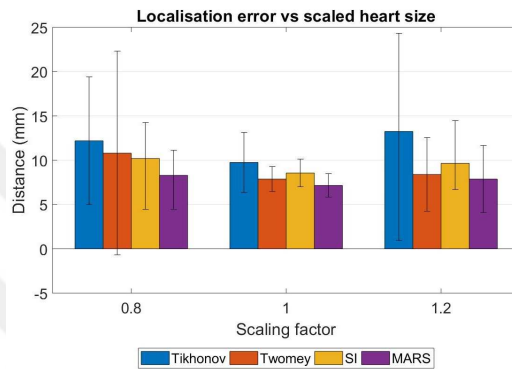
(c) Pacing site localization error.

Figure 4.10: Scaled heart size (Utah data collection).

4.5.1 Reconstruction of Electrograms

For each dataset, epicardial potential distributions have been estimated, and mean CC and RE values are computed and displayed in Tables 4.4 and 4.5. These mean and standard deviation values of the CC and RE metrics are calculated over time for each dataset. We have obtained higher mean CC values compared to other methods.

In the earlier times of the propagation, reconstructed epicardial potentials by the MARS-based approach yield higher CC values, as illustrated in Fig. 4.12. On the other hand, when we look at the RE metrics, although MARS-based technique has yielded lower RE values for the Utah data collection, for KIT data collection SI and our method have produced similar results (Tables 4.4 and 4.5). In general, CC and RE values obtained for the KIT data collection are not as good as the results of Utah data collection for all four regularization methods. The most possible reason is the

74
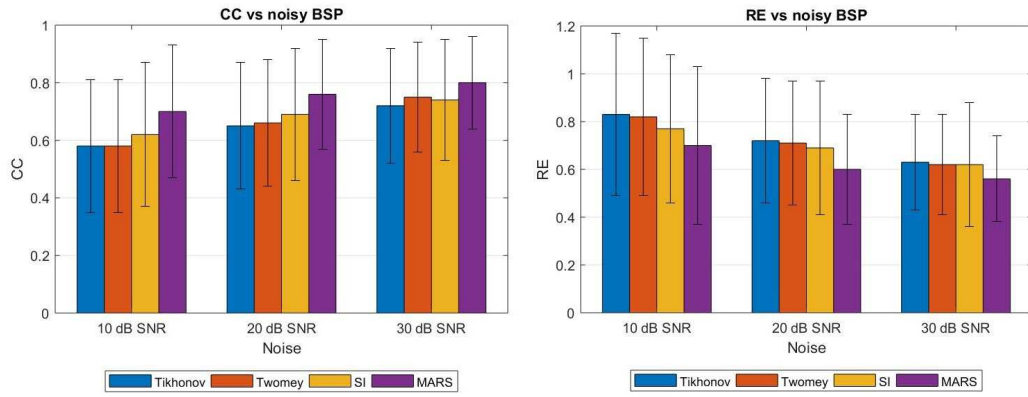
(a) Correlation coefficients.

(b) Relative errors.
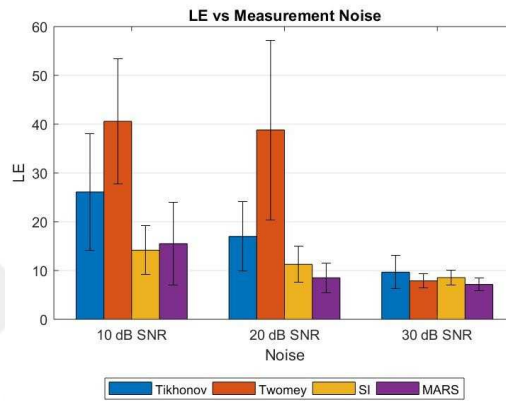
(c) Pacing site localization error.

Figure 4.11: Measurement noise at different SNR values (Utah data collection).

Table 4.4: Mean ($E\{CC\}$) and standard deviation ($\sigma\{CC\}$) values for KIT data collection.

	CC			
Dataset	Tikhonov	Twomey	Spline Inverse	MARS
SEPTUMCENTER	0.39 ± 0.11	0.34 ± 0.18	0.44 ± 0.10	0.47 ± 0.13
LVLAT	0.32 ± 0.10	0.28 ± 0.15	0.41 ± 0.11	0.45 ± 0.12
LVAPEX	0.32 ± 0.08	0.30 ± 0.15	0.39 ± 0.13	0.47 ± 0.12
LVANTERIOR	0.38 ± 0.10	0.31 ± 0.15	0.41 ± 0.08	0.46 ± 0.10
RVPOSTERIOR	0.37 ± 0.08	0.30 ± 0.13	0.38 ± 0.09	0.46 ± 0.09
RVANTERIOR	0.29 ± 0.08	0.29 ± 0.08	0.39 ± 0.06	0.42 ± 0.11
LVLATEPI	0.43 ± 0.11	0.31 ± 0.13	0.43 ± 0.10	0.47 ± 0.13
LVLATENDO	0.31 ± 0.08	0.30 ± 0.15	0.41 ± 0.12	0.47 ± 0.12
Average	0.32 ± 0.09	0.30 ± 0.14	0.41 ± 0.10	0.46 ± 0.11

difference between models used to solve the forward and inverse ECG problems.

Table 4.5: Mean ($E\{RE\}$) and standard deviation ($\sigma\{RE\}$) values for KIT data collection.

Dataset	RE			
	Tikhonov	Twomey	Spline Inverse	MARS
SEPTUMCENTER	0.94 ± 0.09	1.19 ± 1.02	0.90 ± 0.05	0.88 ± 0.09
LVLAT	1.02 ± 0.09	1.22 ± 0.72	0.92 ± 0.05	0.91 ± 0.06
LVAPEX	0.98 ± 0.06	1.60 ± 1.78	0.93 ± 0.04	1.03 ± 0.54
LVANTERIOR	0.91 ± 0.07	1.13 ± 1.10	0.89 ± 0.05	0.88 ± 0.09
RVPOSTERIOR	0.92 ± 0.03	1.12 ± 0.83	0.92 ± 0.04	0.89 ± 0.06
RVANTERIOR	1.04 ± 0.11	1.21 ± 1.25	0.91 ± 0.04	0.99 ± 0.58
LVLATEPI	0.92 ± 0.05	1.15 ± 0.53	0.92 ± 0.05	0.92 ± 0.12
LVLATENDO	1.02 ± 0.10	1.50 ± 1.70	0.92 ± 0.05	0.91 ± 0.07
Average	0.97 ± 0.08	1.27 ± 1.12	0.91 ± 0.05	0.93 ± 0.20
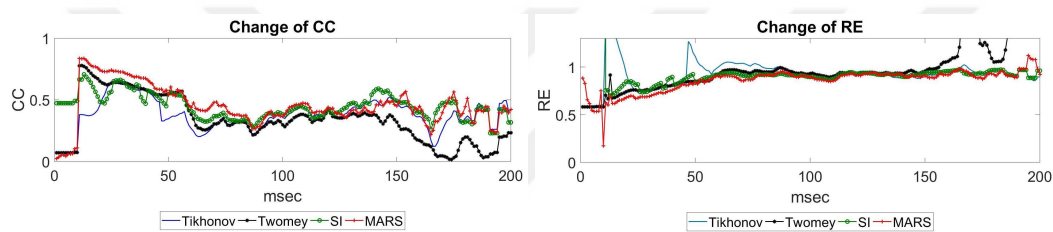
(a) Dataset SEPTUMCENTER from KIT data collection.

(b) Dataset SEPTUMCENTER from KIT data collection.
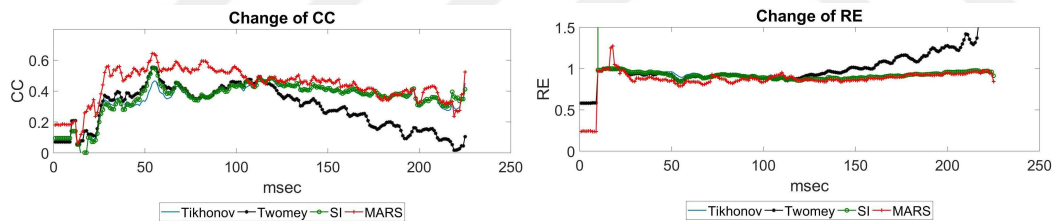
(c) Dataset RVPOSTERIOR from KIT data collection.

(d) Dataset RVPOSTERIOR from KIT data collection.

Figure 4.12: Evolution of CC and RE values over time for datasets selected from KIT data collections.

4.5.2 Epicardial Potential Maps

In order to compare the reconstruction performances of the methods, we have plotted epicardial potential distributions both in earlier times of the propagation, and at a later time for two of the datasets in Figs. 4.13 and 4.14. In general, reconstructed epicardial maps could not capture details in the true epicardial potentials, but for some

datasets such as the RVPOSTERIOR, proposed MARS-based approach has yielded focalized activity around the stimulation site better than the other three methods. For the SEPTUMCENTER dataset, none of the methods have been able to reconstruct epicardial potentials with fidelity to true distributions.
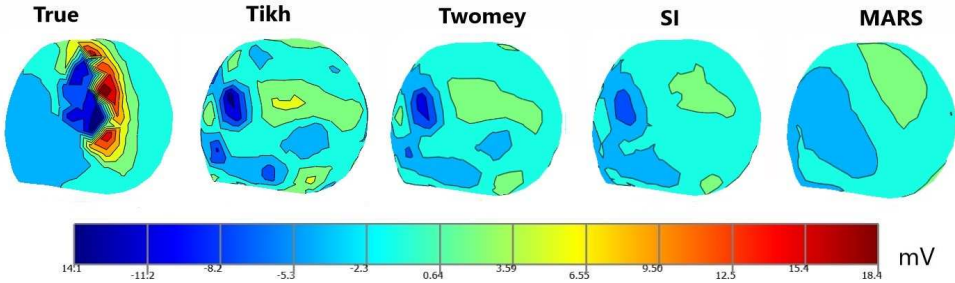
(a) KIT dataset SEPTUMCENTER at $t = 70$ msec.
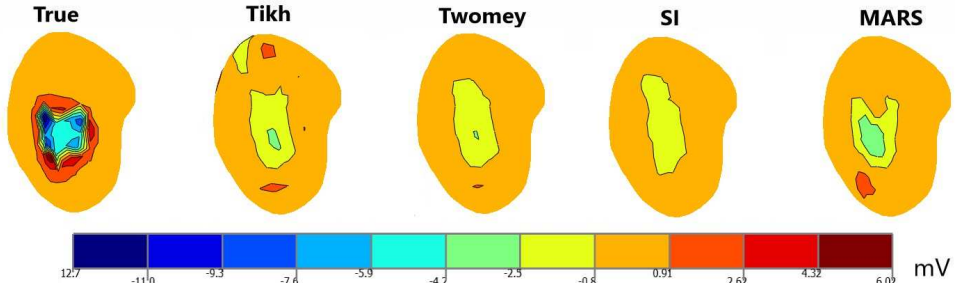
(b) KIT dataset RVPOSTERIOR at $t = 30$ msec.

Figure 4.13: Sample snapshots of the original and reconstructed isopotential maps from the KIT data collection short time after the stimulation.

4.5.3 Activation Isochrone Maps

Activation time estimate fidelity to true values for the KIT data collection given in Fig. 4.15 are poor compared to Utah data collection results. But, SI and MARS method's estimations are $\cong \%15$ better in terms of CC metrics, compared to the Tikhonov and Twomey regularizations. While MARS and SI method have yielded average CC values 0.68 and 0.66, respectively for activation times, Tikhonov and Twomey regularization have values of 0.51 and 0.50, respectively. Sample isochrone maps for the KIT data collection are given in Fig. 4.16.
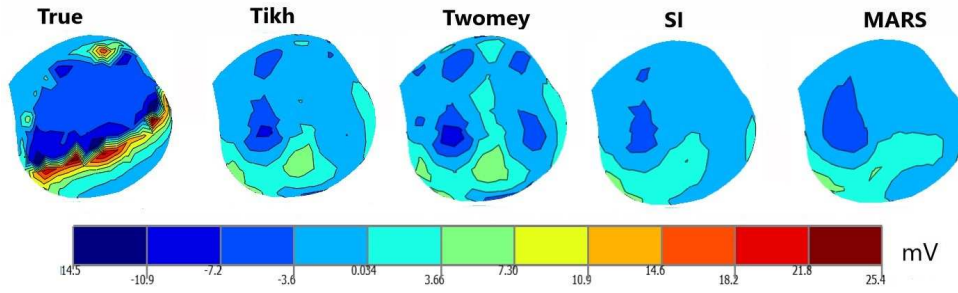
(a) KIT dataset SEPTUMCENTER at $t = 100$ msec.
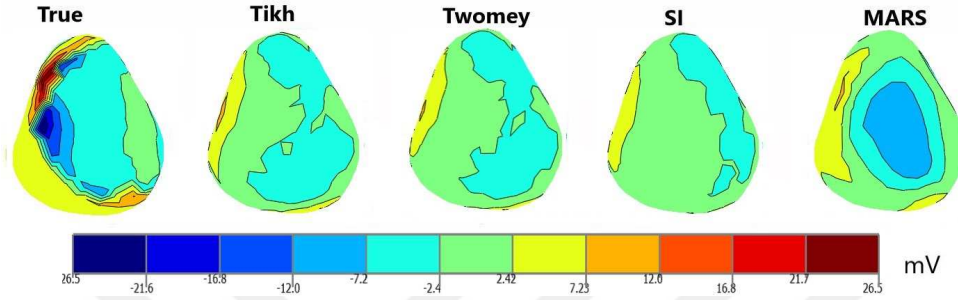
(b) KIT dataset RVPOSTERIOR at $t = 100$ msec.

Figure 4.14: Sample snapshots of the original and reconstructed isopotential maps from the KIT data collection.

4.5.4 Pacing Site Detection

Table 4.6 gives the LE values for the KIT data collection for all methods. Twomey and MARS methods have located the pacing the site better than the other methods (both have yielded best estimates for 3 datasets out of 8). On the other hand, MARS estimations are $\approx \%60$ more accurate when we check the average localization error in mm.

Table 4.6: Pacing site localization errors in mm for KIT data collection.

Test data	Tikhonov	Twomey	Spline Inverse	MARS
SEPTUMCENTEREPI	45.01	50.93	21.85	38.02
LVLAT	9.14	20.50	32.25	12.33
LVAPEX	13.79	0	14.21	8.87
LVANTERIOR	17.46	0	25.58	9.78
RVPOSTERIOR	10.95	39.39	45.02	0
RVANTERIOR	17.93	0	0	0
LVLATEPI	91.43	16.95	22.85	14.03
LVLATENDO	0	32.31	14.03	14.03
Average	25.71 ± 29.56	20 ± 19.62	21.97 ± 13.40	12.13 ± 11.88
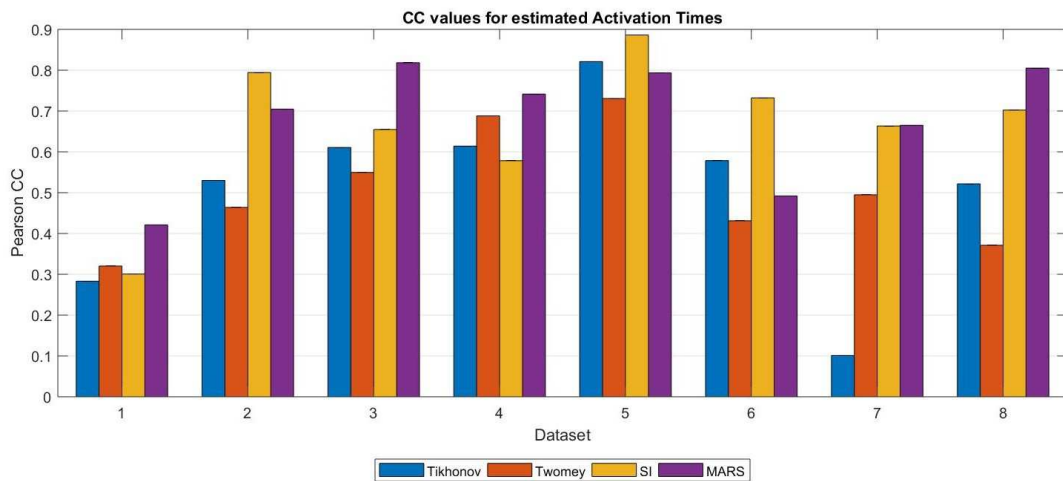
Figure 4.15: Pearson CC values for activation times for the KIT data collection. The numbers on the horizontal axis refers to the dataset number following the order given at Table 4.4.
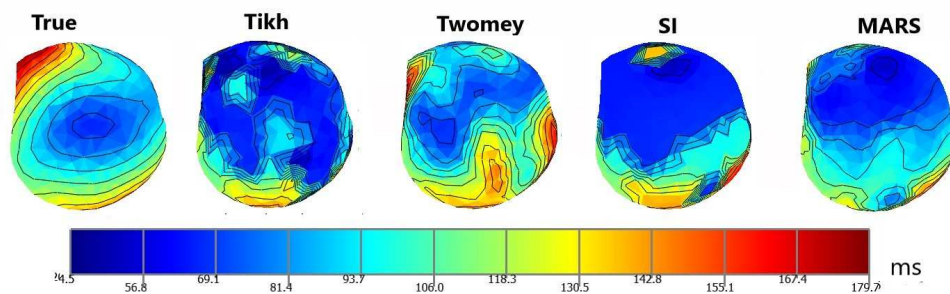
(a) Isochrone maps for dataset SEPTUMCENTER from the KIT data collection.
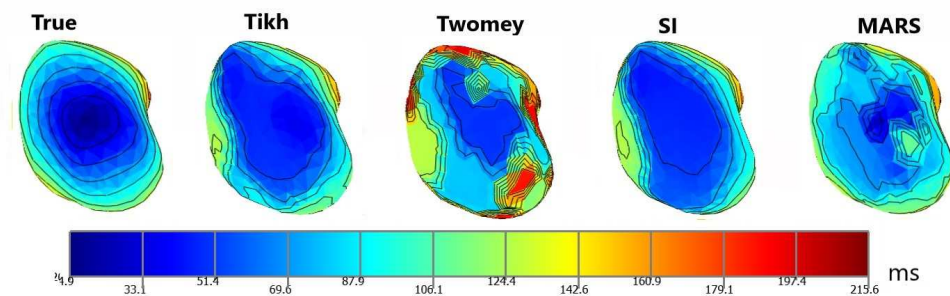
(b) Isochrone maps for dataset RVPOSTERIOR from the KIT data collection.

Figure 4.16: Sample isochrone maps for reconstructed epicardial potentials (KIT data collection).

4.6 Conclusions and Discussion

In this part of the thesis, we have presented a non-parametric MARS-based approach for reconstructing potential distributions on the epicardial surface of the heart. Our primary interest is to develop an adaptive method, which significantly reduces the problem dimension while increasing estimation accuracy. Unlike B-spline or other cubic polynomial approaches, the proposed method of this study does not require a pre-determined number of spline functions. Instead, it constructs a large collection of basis functions using possible knot locations such that both additive and interactive effects of the predictors are taken into account. From a collection of basis functions, a set of basis functions consisting of the ones which produce the largest decrease in the defined lack of fit criteria, is selected to construct the model of the unknown function.

We have tested our methods utilizing two different simulated data collections of ventricularly paced beats: Utah data collection of 23 datasets with different pacing locations, which are located on the frontal, back and side regions of the epicardium; KIT data collection of 8 beats with different pacing locations on the epicardium, endocardium and septum. Quantitative and qualitative evaluation of the results from various perspectives have been also provided to represent strong features of MARS and properties that need to be improved. Following parameter values have been used for the MARS algorithm to solve the inverse ECG problem; maximum allowed number of functions and number of allowed interactions between independent variables in the model are 40 and 3, respectively. The average number of spline functions in the estimated model turned out to be 15 ± 1 for the Utah data collection, and 21 ± 1 for the KIT data collection.

With the Utah collection, three different simulation scenarios have been carried out. In the first scenario, there are no geometric errors in the mathematical model and the measurement noise is kept at a moderate level of 30 dB SNR. Overall evaluation of our results show that, in terms of average CC and RE values, MARS has yielded better results than the other methods ($p < 0.0001$). LE values for MARS are better than Tikhonov regularization results ($p = 0.033$). Statistically, they are not significantly different from Twomey or SI results ($p = 0.16$, and $p = 0.4$, respectively), however, in terms of average LE, MARS has yielded slightly smaller values (9% and

16% lower average LE values than Twomey and SI, respectively, in mm). In the second scenario, measurement error is kept at the same level of 30 dB, but geometric error is introduced into the mathematical model in terms of random disturbance, shifting the heart position, and scaling the heart size. In case of random distortion is applied to the forward transfer matrix, MARS has produced highest CC, lowest RE and LE values. From a statistical point of view, the LE errors of MARS are not significantly different from the other methods, except the SI results obtained at 30 dB SNR ($p = 0.033866$). Similar results for CC, RE and LE values have been obtained if the heart geometry is scaled or shifted. The significant statistical differences for LE errors are between the MARS, Tikhonov and Twomey methods, but not with SI if the heart is scaled by a constant factor. For scale factors 0.8 and 1.2, the p values are computed as $p = 0.024472$ and $p < 0.000001$ for Tikhonov; $p = 0.042484$ and $p < 0.000001$ for Twomey methods. Statistically significant difference for LE errors have been observed between MARS and other 3 methods if heart is shifted in the $+x$ direction. The computed p values are $p = 0.002038$, $p < 0.000001$ and $p = 0.019618$ for Tikhonov, Twomey and SI methods, respectively. Finally, in the last scenario, the level of measurement noise are varied while excluding geometric errors. Decreasing noise SNR has significantly effected the LE errors of Tikhonov and Twomey estimations, but MARS and SI have yielded more stable outputs compared the these two methods. The p values are computed as follows; For 20 dB SNR noise p values are $p = 0.104175$, $p = 0.000242$, $p < 0.00001$. For 10 dB SNR noise p become $p = 0.369559$, $p = 0.000326$, $p = 0.996815$ for SI, Tikhonov and Twomey, respectively.

KIT data collection, on the other hand, has been used as provided by the researchers [90] to facilitate comparison in future studies. For these datasets, performances of all four methods are worse than those for the Utah data collection. This performance degradation is not surprising, since the forward model used to simulate BSPs in the KIT collection includes more inhomogeneities than the forward model that we have used for simulating BSPs in the Utah collection. In terms of average CC values, MARS has performed better than the other methods ($p < 0.001$), however, statistically comparing RE values of MARS with Tikhonov and SI have not yielded significant differences ($p = 0.14$ and $p = 0.54$, respectively). Similarly, LE values are also statistically not

significantly different from the other methods ($p = 0.25$ for Tikhonov, $p = 0.35$ for Twomey, and $p = 0.14$ for SI). Among the KIT datasets, SEPTUMCENTER has yielded the worst LE values for all methods. Septum is located between the right and left ventricles, and a wave-front initiated at the septum takes some time to reach the epicardial surface. Therefore, there is no obvious pacing site observed on the epicardium. When the LE results are evaluated excluding SEPTUMCENTER, MARS results have been found to be statistically different from the SI results ($p = 0.04$), but similar to Tikhonov and Twomey results ($p = 0.24$ and $p = 0.3$, respectively). However, we should note that, while the statistical tests for the Utah data collection have been carried out with 23 beats and 5 noise realizations for each beat, KIT data collection comparisons are for only 8 beats. It is a rather small sample set to make reliable statistical comparisons; more data are needed to come to a conclusion. When the individual results for 8 datasets are examined, MARS has yielded 40% and 45% lower average LE values than Twomey and SI, respectively, in mm.

These results show that, MARS method has potential for accurately solving the inverse ECG problem in the presence of geometric errors and measurement noise, especially for clinical applications that require pacing site localization (such as detection of PCVs). However, despite strengths of MARS, it also has some limitations that need to be addressed to accept it as a reliable approach for ECGI applications.

4.6.1 Limitations of the Study, and Future Work

- Despite good performance of the MARS method in the earlier times, its performance after the activity has spread over the heart becomes comparable to the other methods, and even yields a more spread wave-front. We believe that this is partially due to using an l_2-norm in the cost function to be minimized. l_2-norm based approaches usually produce smeared solutions. On the other hand, local support of the spline-based modeling (i.e. changing approximation in a local region without affecting the remote portion of the approximated function) has alleviated this shortcoming to some extent by adaptively selecting suitable basis functions for the model. As the wave-front progresses over the epicardial surface, sparsity of the potential distribution disappears and local support of the

spline-based approach also decreases. Using l_1-norm or l_p-norm, which have been shown to improve wave-front reconstructions could improve solutions.

- Due to its iterative nature, runtime for MARS is longer than the other methods. This is a significant disadvantage for clinical applications that require real time decision making. To increase speed and decrease overall computational cost, MARS could be employed for detecting early activation times, for localization of PVCs, but it can be replaced with a lower computational cost method as the wave-front propagates over the heart surface.

- Although we have tested the robustness of MARS to geometric errors, there are still other tests that can be done to further evaluate MARS in the presence of geometric errors. For example, to mimic actual mechanical changes during diastole and systole periods, heart geometry could be modified to reflect these changes and to study their effects on inverse solutions. Additionally, the effects of rotation of the heart within the torso has not been considered in this study, which should be included in future studies.

- Here we have only considered spatially fitted splines. Alternatively, MARS-based approach could be modified to include temporal splines as well, either alone, or combined with spatial splines.

- This study is limited to simulated data, and focuses only ventricularly paced beats. Evaluation of the MARS method should be extended to use a wider variety of data including simultaneously measured epicardial and body surface potentials, to detect different types of arrhythmia, to study its performance in the recovery region, etc.

Since MARS is a non-parametric regression procedure, it can simplify and automate the determination of the model size, construction and selection of the spline functions based on supplied data. However, these steps increase the computational complexity of the inverse solution. Parametric techniques can be preferable if sufficient information or assumptions are available about the underlying model of the function to be estimated. In addition, if the model of a function is required to be expressed by more than one variable and their interactions, then parametric methods become problematic because of the curse of dimensionality.

CHAPTER 5

CONCLUSIONS

In this dissertation, the inverse ECG problem is handled both from statistical and deterministic solution techniques perspectives. We have described adaptive approaches that expedite the solving inverse ECG problem without claiming strong assumptions and by using relatively easily obtainable prior information about the unknown epicardial potential distribution.

In Chapter 3, we have adopted statistical inversion scheme called Minimum Relative Entropy for solving the inverse ECG problem. This method treats the unknown parameters as random variables and then computes the multivariate probability density function to describe the behavior of the parameters. The solution is defined as the expected value of the parameters based on the posterior probability density function. In statistical inversion schemes, a good prior information requires knowledge about the form of the prior pdf and moments of the unknown parameters (i.e., mean, covariance, etc.) to obtain better estimates. On the other hand, it is not always possible to know the form of the pdf and to collect reliable prior information about its parameters such as, mean and covariance values, or they might be highly suspected. In such a case, MRE method provides an alternative formulation for solving the inverse problems starting from very simple prior pdf definition.

Throughout this study, we have carefully examined effects of MRE parameters to the solution. According to the results, the upper-lower bounds and expected uncertainty have no significant influence unless they are under-estimated. Compared to the Bayesian MAP estimation, MRE method does not require full covariance matrix in addition to a mean vector. However the prior mean value is the crucial parameter for

the MRE method.

In Chapter 4, we have proposed a non-parametric multivariate spline-based approach to solve the inverse ECG problem. Our aim is to reduce the number of unknowns in the model while increasing estimation accuracy by taking advantage of local support property of spline-based approaches. In contrast to the other parametric approaches, proposed technique does not make strong assumptions about the form of the function we wish to estimate, which reduces the requirement of preliminary work for modeling the inverse ECG problem. Efficiency of the proposed method is examined under various disturbances including noise and geometric errors. We have achieved better estimations compared to traditional regularization techniques, when the potential distribution activity on the heart surface is condensed in a local region (i.e. very close to stimulation time). The success in estimations close to the stimulation time also leads to determination of pacing site more accurately. In addition, we have obtained more stable outputs under disturbances measurement noise and geometric errors disturbances.

Both methods we have presented in this dissertation provide a flexible way of modeling and solving the inverse ECG problem. In addition, they can also be used to test whether parametric model is well-specified, if the problem will be modeled and solved by the parametric technique. However, within each method several developments should be implemented in the future as follows:

- MRE:

  - The prior mean value is the crucial parameter for MRE method and further studies are required to determine a proper prior mean value to increase the effectiveness of the method.

  - We have constructed the prior pdf starting from the uniform pdf. MRE method also allow us to use other pdfs such as Gaussian distribution instead of starting from simple assumption if more information is available on the underlying behavior of the parameters.

- MARS-based Scheme:

  - In this thesis we have modeled the problem only by using spatially fitted

splines. However, MARS-based approach could be modified to include temporal splines as well, either alone, or combined with spatial splines to better represent the spatio-temporal behavior of the epicardial distribution.

– Performance of the MARS-based method in the earlier times of the stimulation could be improved by using l_1 or l_p-norm based cost function definitions.

– It might be possible to improve estimations of local activities by weighting observations considering the trend changes at the estimated epicardial potential distribution.

– The adaptation of other non-parametric algorithms such as locally adaptive polynomial regression, should be investigated to increase the approximation success in local regions.

– Its efficiency should be tested for detecting multiple pacing sites.

– Performance of the MARS-based method after the activity has propagated over the heart should be improved by including additional constraints to prevent reconstructed wave-fronts from overly spreading out.

– Robustness of the method should be tested with coarse epicardial surface geometry.

• General:

– This study is limited to simulated data, and focuses only on ventricularly paced beats. Evaluation of the both methods should be extended to use a wider variety of data including simultaneously measured epicardial and body surface potentials, in order to detect different types of arrhythmia.

– Both solution approaches have higher computational complexity compared to traditional regularization methods. Any improvements in their algorithms to reduce computation time would increase the applicability of these methods in daily clinical routines.

REFERENCES

[1] G. Ahmad, D. Brooks, G. Maratos, and R. MacLeod, Joint energy and Laplacian regularization in the inverse problem of electrocardiography, in *Proceedings of 1994 20th Annual Northeast Bioengineering Conference*, pp. 59–62, IEEE, 1994.

[2] T. Amisaki and S. Eguchi, Pharmacokinetic parameter estimations by minimum relative entropy method., Journal of Pharmacokinetics and Biopharmaceutics, 23(5), pp. 479–94, 1995.

[3] Andrew Jazwinski, *Stochastic Processes and Filtering Theory, Volume 64*, Academic Press, 1970, ISBN 9780080960906.

[4] K. Aras, W. Good, J. Tate, B. Burton, D. Brooks, J. Coll-Font, O. Doessel, W. Schulze, D. Potyagaylo, L. Wang, P. van Dam, and R. MacLeod, Experimental Data and Geometric Analysis Repository—EDGAR, Journal of Electrocardiology, 48(6), pp. 975–981, 2015.

[5] R. C. Aster, , B. Borchers, , and C. H. Thurber, editors, *Parameter Estimation and Inverse Problems (Second Edition)*, Academic Press, Boston, second edition edition, 2013, ISBN 978-0-12-385048-5.

[6] U. Aydin and Y. S. Dogrusoz, A Kalman filter-based approach to reduce the effects of geometric errors and the measurement noise in the inverse ECG problem., Medical & Biological Engineering & Computing, 49(9), pp. 1003–1013, 2011.

[7] S. Babaeizadeh, D. Brooks, and D. Isaacson, A Deformable-radius B-Spline Method for Shape-based Inverse Problems, as Applied to Electrical Impedance Tomography, in *Proceedings. (ICASSP '05). IEEE International Conference on Acoustics, Speech, and Signal Processing, 2005.*, volume 2, pp. 485–488, IEEE, 2005.

[8] J. P. Barnes and P. R. Johnston, Application of robust Generalised Cross-Validation to the inverse problem of electrocardiology, Computers in Biology and Medicine, 69, pp. 213–225, 2016.

[9] A. Baussard, E. L. Miller, and D. Lesselier, Adaptive multiscale reconstruction of buried objects, Inverse Problems, 20(6), pp. S1–S15, 2004.

[10] A. Baussard, E. L. Miller, and D. Prémel, Adaptive B -spline scheme for solving an inverse scattering problem, Inverse Problems, 20(2), pp. 347–365, 2004.

[11] L. R. Bear, L. K. Cheng, I. J. LeGrice, G. B. Sands, N. A. Lever, D. J. Paterson, and B. H. Smaill, Forward Problem of Electrocardiography, Circulation: Arrhythmia and Electrophysiology, 8(3), pp. 677–684, 2015.

[12] S. M. Becker, Regularization of statistical inverse problems and the Bakushinski veto, Inverse Problems, 27(11), 2011.

[13] K. L. Berrier, D. C. Sorensen, and D. S. Khoury, Solving the Inverse Problem of Electrocardiography Using a Duncan and Horn Formulation of the Kalman Filter, IEEE Transactions on Biomedical Engineering, 51(3), pp. 507–515, 2004.

[14] C. D. Boor, *A Practical Guide to Splines (Revised Edition)*, volume 27, Springer-Verlag New York, 1 edition, 2001, ISBN 978-0-387-95366-3.

[15] M. Boulakia, E. Schenone, and J. F. Gerbeau, Reduced-order modeling for cardiac electrophysiology. Application to parameter identification, International Journal for Numerical Methods in Biomedical Engineering, 28(6-7), pp. 727–744, 2012.

[16] D. H. Brooks and G. F. Ahmad, Inverse electrocardiography by simultaneous imposition of multiple constraints, IEEE Transactions on Biomedical Engineering, 46(1), pp. 3–18, 1999.

[17] D. Calvetti, S. Morigi, L. Reichel, and F. Sgallari, Tikhonov regularization and the L-curve for large discrete ill-posed problems, Journal of Computational and Applied Mathematics, 123, pp. 423–446, 2000.

[18] H. Cardot, Spatially Adaptive Splines for Statistical Linear Inverse Problems, Journal of Multivariate Analysis, 81(1), pp. 100–119, 2002.

[19] M. Cluitmans and P. Bonizzi, Inverse reconstruction of epicardial potentials improved by vectorcardiography and realistic potentials, Computing in Cardiology Conference (CinC), pp. 369–372, 2013.

[20] M. Cluitmans, R. Peeters, R. Westra, and P. Volders, Noninvasive reconstruction of cardiac electrical activity: update on current methods, applications and challenges, Netherlands Heart Journal, 23(6), pp. 301–311, 2015.

[21] M. J. Cluitmans, P. Bonizzi, J. M. Karel, M. Das, B. L. Kietselaer, M. M. de Jong, F. W. Prinzen, R. L. Peeters, R. L. Westra, and P. G. Volders, In Vivo Validation of Electrocardiographic Imaging, JACC: Clinical Electrophysiology, 3(3), pp. 232–242, 2017.

[22] J. Coll-Font, *Model Based Approaches to Incorporate Recordings of Multiple Heartbeats into the Inverse Problem of Electrocardiography*, Ph.D. thesis, Northeastern University, 2016.

[23] J. Coll-Font, D. H. Brooks, P. M. van Dam, J. Dhamala, O. Doessel, M. d. l. S. Guillem Sanchez, R. MacLeod, D. Potyagaylo, W. Schulze, J. D. Tate, and L. Wang, The Consortium on Electrocardiographic Imaging, volume 43, pp. 1–4, 2016.

[24] C. Corrado, J.-F. Gerbeau, and P. Moireau, Identification of weakly coupled multiphysics problems. Application to the inverse problem of electrocardiography, Journal of Computational Physics, 283, pp. 271–298, 2015.

[25] Curtis R.Voge, *Computational Methods for Inverse Problems*, SIAM, ISBN 0898715075.

[26] H. Developed, T. Curran, C. N. Educator, G. Sheppard, and C. N. Specialist, Cardiology Self Learning Package, (October), pp. 1–22, 2011.

[27] EDGAR, Experimental Data and Geometric Analysis Repository, `http://edgar.sci.utah.edu/`, [Online; accessed 13.07.2018].

[28] B. Erem, J. Coll-Font, R. M. Orellana, P. St'Ovicek, and D. H. Brooks, Using transmural regularization and dynamic modeling for noninvasive cardiac potential imaging of endocardial pacing with imprecise thoracic geometry, IEEE Transactions on Medical Imaging, 33(3), pp. 726–738, 2014.

[29] J. J. Faraway, *Extending the Linear Model with R: Generalized Linear, Mixed Effects and Nonparametric Regression Models*, Chapman & Hall/CRC, Boca Raton, second edition, 1994, ISBN 9781498720960.

[30] D. Farina, *Forward and Inverse Problems of Electrocardiography: Clinical Investigations*, Ph.D. thesis, Universitat Karlsruhe, 2008.

[31] C. Figuera, V. Suárez-Gutiérrez, I. Hernández-Romero, M. Rodrigo, A. Liberos, F. Atienza, M. S. Guillem, Ó. Barquero-Pérez, A. M. Climent, and F. Alonso-Atienza, Corrigendum: Regularization techniques for ECG imaging during atrial fibrillation: A computational study [Front. Physiol., 7 (2016) 466]., Frontiers in Physiology, 7(NOV), pp. 1–17, 2016.

[32] J. H. Friedman, Multivariate Adaptive Regression Splines, The Annals of Statistics, 19(1), pp. 1–67, 1991.

[33] J. H. Friedman and C. B. Roosen, An introduction to multivariate adaptive regression splines, Statistical Methods in Medical Research, 4(3), pp. 197–217, 1995.

[34] A. M. Gavgani and Y. S. Dogrusoz, Use of genetic algorithm for selection of regularization parameters in multiple constraint inverse ECG problem, Proceedings of the Annual International Conference of the IEEE Engineering in Medicine and Biology Society, EMBS, (3), pp. 985–988, 2011.

[35] F. Gharbalchi, Y. S. Dogrusoz, and G. W. Weber, Lanczos bidiagonalization-based inverse solution methods applied to electrical imaging of the heart by using reduced lead-sets: A simulation study, Cogent Mathematics, 3(1), pp. 1–13, 2016.

[36] A. Ghodrati, A. Keely, G. Tadmor, R. MacLeod, and D. H. Brooks, A wavefront-based constraint for potential surface solutions in inverse electrocardiography, Annual International Conference of the IEEE Engineering in Medicine and Biology - Proceedings, pp. 2550–2553, 2006.

[37] S. Ghosh and Y. Rudy, Application of L1-Norm Regularization to Epicardial Potential Solution of the Inverse Electrocardiography Problem, Annals of Biomedical Engineering, 37(5), pp. 902–912, 2009.

[38] G. H. Golub, P. C. Hansen, and D. P. O'Leary, Tikhonov Regularization and Total Least Squares, SIAM Journal on Matrix Analysis and Applications, 21(1), pp. 185–194, 1999.

[39] F. Greensite, The temporal prior in bioelectromagnetic source imaging problems, IEEE Transactions on Biomedical Engineering, 50(10), pp. 1152–1159, 2003.

[40] F. Greensite and G. Huiskamp, An improved method for estimating epicardial potentials from the body surface, IEEE Transactions on Biomedical Engineering, 45(1), pp. 98–104, 1998.

[41] R. Gulrajani, The forward and inverse problems of electrocardiography, IEEE Engineering in Medicine and Biology Magazine, 17(5), pp. 84–101, 122, 1998.

[42] R. M. Gulrajani, The forward problem of electrocardiography: from heart models to body surface potentials, Proceedings of the 19th Annual International Conference of the IEEE Engineering in Medicine and Biology Society, 6(C), pp. 2604–2609, 1997.

[43] P. C. Hansen, Analysis of Discrete Ill-Posed Problems by Means of the L-Curve, SIAM Review, 34(4), pp. 561–580, 1992.

[44] W. Härdle, *Applied Nonparametric Regression*, Cambridge University Press, New York, 1994, ISBN 9780521429504.

[45] C. Harmening and H. Neuner, Choosing the Optimal Number of B-spline Control Points (Part 1: Methodology and Approximation of Curves), Journal of Applied Geodesy, 10(3), 2016.

[46] C. Harmening and H. Neuner, Choosing the Optimal Number of B-spline Control Points (Part 1: Methodology and Approximation of Curves), Journal of Applied Geodesy, 10, pp. 139–157, 2016.

[47] S. M. Hegde, Pericardial Disease, in *Essential Echocardiography*, pp. 347–353.e1, Elsevier, 2019.

[48] G. J. Huiskamp and A. van Oosterom, Tailored versus realistic geometry in the inverse problem of electrocardiography., IEEE Transactions on Biomedical Engineering, 36(8), pp. 827–35, 1989.

[49] A. Intini, R. N. Goldstein, P. Jia, C. Ramanathan, K. Ryu, B. Giannattasio, R. Gilkeson, B. S. Stambler, P. Brugada, W. G. Stevenson, Y. Rudy, and A. L. Waldo, Electrocardiographic imaging (ECGI), a novel diagnostic modality used for mapping of focal left ventricular tachycardia in a young athlete, Heart Rhythm, 2(11), pp. 1250–1252, 2005.

[50] P. Jais, Foreword Noninvasive Cardiac Mapping : A New Era in Electrophysiology, Cardiac Electrophysiology Clinics, 7(1), pp. xiii–xiv, 2015.

[51] M. Jiang, W. Huang, L. Xia, and G. Shou, The Use of Genetic Algorithms for Optimizing the Regularized Solutions of the Ill-Posed Problems, 2008 Second International Symposium on Intelligent Information Technology Application, pp. 119–123, 2008.

[52] M. Jiang, Y. Wang, L. Xia, F. Liu, S. Jiang, and W. Huang, The combination of self-organizing feature maps and support vector regression for solving the inverse ECG problem, Computers and Mathematics with Applications, 66(10), pp. 1981–1990, 2013.

[53] M. Jiang, L. Xia, G. Shou, Q. Wei, F. Liu, and S. Crozier, Effect of cardiac motion on solution of the electrocardiography inverse problem, IEEE Transactions on Biomedical Engineering, 2009.

[54] D. Joly, Y. Goussard, and P. Savard, Time-recursive solution to the inverse problem of electrocardiography: a model-based approach, Proceedings of the 15th Annual International Conference of the IEEE Engineering in Medicine and Biology Society, pp. 1–10, 1993.

[55] S. I. Kabanikhin, Definitions and examples of inverse and ill-posed problems, Journal of Inverse and Ill-Posed Problems, 16(4), 2008.

[56] J. Kaipio and E. Somersalo, Statistical inverse problems: Discretization, model reduction and inverse crimes, Journal of Computational and Applied Mathematics, 198(2), pp. 493–504, 2007.

[57] D. U. Keller, F. M. Weber, G. Seemann, and O. Dössel, Ranking the influence of tissue conductivities on forward-calculated ecgs, IEEE Transactions on Biomedical Engineering, 57(7), pp. 1568–1576, 2010.

[58] R. E. Klabunde, Cardiovascular Physiology Concepts, `http://www.cvphysiology.com/Arrhythmias/A006`, 2016, [Online; accessed 11.011.2017].

[59] R. Klepfer, C. Johnson, and R. Macleod, The effects of inhomogeneities and anisotropies on electrocardiographic fields: a 3-D finite-element study, IEEE Transactions on Biomedical Engineering, 44(8), pp. 706–719, 1997.

[60] S. Kullback, *Information Theory and Statistics*, A Wiley publication in mathematical statistics, Dover Publications, 1997, ISBN 9780486696843.

[61] P. A. Laizzo, *Handbook of Cardiac Anatomy, Physiology, and Devices*, Humana Press, Totowa, NJ, 2 nd edition, Feb 2009, ISBN 978-1-60327-371-8.

[62] R. L. Lux, Electrocardiographic mapping. Noninvasive electrophysiological cardiac imaging, Circulation, 87(3), pp. 1040–1042, 1993.

[63] R. L. Lux, C. R. Smith, R. F. Wyatt, and J. a. Abildskov, Limited lead selection for estimation of body surface potential maps in electrocardiography., IEEE Transactions on Biomedical Engineering, 25(3), pp. 270–6, 1978.

[64] D. Ma, S. Wang, and Z. Zhang, Hybrid algorithm of minimum relative entropy-particle swarm optimization with adjustment parameters for gas source term identification in atmosphere, Atmospheric Environment, 94, pp. 637–646, 2014.

[65] P. W. Macfarlane, A. van Oosterom, O. Pahlm, P. Kligfield, M. Janse, and J. Camm, editors, *Comprehensive Electrocardiology*, Springer London, London, 2010, ISBN 978-1-84882-045-6.

[66] R. MacLeod and C. Johnson, Map3d: interactive scientific visualization for bioengineering data, in *Proceedings of the 15th Annual International Conference of the IEEE Engineering in Medicine and Biology Society*, pp. 30–31, IEEE.

[67] R. MacLeod, B. Taccardi, and R. Lux, Electrocardiographic mapping in a realistic torso tank preparation, in *Proceedings of 17th International Conference of the Engineering in Medicine and Biology Society*, volume 1, pp. 245–246, IEEE, 1995.

[68] V. Mahadevan, Anatomy of the heart, Surgery (Oxford), 22(6), pp. 121–123, 2004.

[69] B. J. Messinger-Rapport and Y. Rudy, The Inverse Problem in Electrocardiography: A Model Study of the Effects of Geometry and Conductivity Parameters on the Reconstruction of Epicardial Potentials, IEEE Transactions on Biomedical Engineering, BME-33(7), pp. 667–676, 1986.

[70] B. J. Messinger-Rapport and Y. Rudy, Noninvasive recovery of epicardial potentials in a realistic heart- torso geometry. Normal sinus rhythm, Circulation Research, 66(4), pp. 1023–1039, 1990.

[71] B. Milan Horáček and J. C. Clements, The inverse problem of electrocardiography: A solution in terms of single- and double-layer sources on the epicardial surface, Mathematical Biosciences, 144(2), pp. 119–154, 1997.

[72] E. L. Miller, M. Kilmer, and C. Rappaport, A new shape-based method for object localization and characterization from scattered field data, IEEE Transactions on Geoscience and Remote Sensing, 38(4 I), pp. 1682–1696, 2000.

[73] G. C. Mohan and S. Devi, Forward problem in electrocardiogram: a review of certain approaches, IOSR Journal of Engineering, 3(8), pp. 21–24, 2013.

[74] R. M. Neupauer and B. Borchers, A MATLAB implementation of the minimum relative entropy method for linear inverse problems, Computers & Geosciences, 27(7), pp. 757–762, 2001.

[75] R. M. Neupauer, B. Borchers, and J. L. Wilson, Comparison of inverse methods for reconstructing the release history of a groundwater contamination source, Water Resources Research, 36(9), pp. 2469–2475, 2000.

[76] M. Onal and Y. Serinagaoglu, Spatio-temporal solutions in inverse electrocardiography, IFMBE Proceedings, 22, pp. 180–183, 2008.

[77] H. S. Oster and Y. Rudy, The use of temporal information in the regularization of the inverse problem of electrocardiography., IEEE Transactions on Biomedical Engineering, 39(1), pp. 65–75, 1992.

[78] J. Pinnell, S. Turner, and S. Howell, Cardiac muscle physiology, Continuing Education in Anaesthesia Critical Care & Pain, 7(3), pp. 85–88, 2007.

[79] D. Potyagaylo, E. G. Cortés, W. H. W. Schulze, and O. Dössel, Binary optimization for source localization in the inverse problem of ECG, Medical & Biological Engineering & Computing, 52(9), pp. 717–728, 2014.

[80] M. Propato, F. Sarrazy, and M. Tryby, Linear Algebra and Minimum Relative Entropy to Investigate Contamination Events in Drinking Water Systems, Journal of Water Resources Planning and Management, 136(4), pp. 483–492, 2010.

[81] A. J. Pullan, L. K. Cheng, M. P. Nash, C. P. Bradley, and D. J. Paterson, Noninvasive electrical imaging of the heart: Theory and model development, Annals of Biomedical Engineering, 29(10), pp. 817–836, 2001.

[82] A. J. Pullan, L. K. Cheng, M. P. Nash, A. Ghodrati, R. MacLeod, and D. H. Brooks, The Inverse Problem of Electrocardiography, in *Comprehensive Electrocardiology*, volume 83, pp. 299–344, Springer London, London, 2010, ISBN 0031-9333.

[83] A. Rahimi, J. Sapp, J. Xu, P. Bajorski, M. Horacek, and L. Wang, Examining the impact of prior models in transmural electrophysiological imaging: A hierarchical multiple-model Bayesian approach, IEEE Transactions on Medical Imaging, 35(1), pp. 229–243, 2016.

[84] A. Rahimi, J. Xu, and L. Wang, Lp-Norm Regularization in Volumetric Imaging of Cardiac Current Sources, Computational and Mathematical Methods in Medicine, 2013, pp. 1–10, 2013.

[85] C. Ramanathan and Y. Rudy, Electrocardiographic Imaging: I. Effect of Torso Inhomogeneities on Body Surface Electrocardiographic Potentials, Journal of Cardiovascular Electrophysiology, 12(2), pp. 229–240, 2001.

[86] R. Ramanathan, J. Ping, R. Ghanem, D. Calvetti, and Y. Rudy, Noninvasive Electrocardiographic Imaging (ECGI): Application of the Generalized Minimal Residual (GMRes) Method, Annals of Biomedical Engineering, 31(8), pp. 981–994, 2003.

[87] Y. Rudy, The Forward Problem of Electrocardiography Revisited, Circulation: Arrhythmia and Electrophysiology, 8(3), pp. 526–528, 2015.

[88] Y. Rudy, Noninvasive ECG imaging (ECGI): Mapping the arrhythmic substrate of the human heart, International Journal of Cardiology, 237, pp. 13–14, 2017.

[89] S. Schuler, D. Potyagaylo, and O. Doessel, ECG Imaging of Simulated Atrial Fibrillation: Imposing Epi-Endocardial Similarity Facilitates the Reconstruction of Transmembrane Voltages, in *Computing in Cardiology*, volume 44, pp. 1–4, 2017.

[90] W. H. W. Schulze, D. Potyagaylo, R. Schimpf, T. Papavassiliu, E. Tulumen, B. Rudic, V. Liebe, C. Doesch, J. Trachtler, M. Borggrefe, and O. Dössel, A simulation dataset for ECG imaging of paced beats with models for transmural, endo- and epicardial and pericardial source imaging, in *ECG Imaging 2015*, November, pp. 1–6, 2015.

[91] Y. Serinagaoglu, D. H. Brooks, and R. S. MacLeod, Improved performance of bayesian solutions for inverse electrocardiography using multiple information sources., IEEE Transactions on Biomedical Engineering, 53(10), pp. 2024–34, 2006.

[92] S. Shah, G. Gnanasegaran, J. Sundberg-Cohon, and J. R. Buscombe, The heart: Anatomy, physiology and exercise physiology, Integrating Cardiology for Nu-

clear Medicine Physicians: A Guide to Nuclear Medicine Physicians, pp. 3–22, 2009.

[93] J. Shore, On a relation between maximum likelihood classification and minimum relative-entropy classification (Corresp.), IEEE Transactions on Information Theory, 30(6), pp. 851–854, 1984.

[94] J. Shore and R. Johnson, Properties of cross-entropy minimization, IEEE Transactions on Information Theory, 27(4), pp. 472–482, 1981.

[95] G. Shou, L. Xia, M. Jiang, Q. Wei, F. Liu, and S. Crozier, Truncated total least squares: a new regularization method for the solution of ECG inverse problems., IEEE Transactions on Biomedical Engineering, 55(4), pp. 1327–35, 2008.

[96] A. Y. Sun and J.-P. Nicot, Inversion of pressure anomaly data for detecting leakage at geologic carbon sequestration sites, Advances in Water Resources, 44, pp. 20–29, 2012.

[97] A. Tarantola, *Inverse Problem Theory*, SIAM, ISBN 0-89871-572-5.

[98] P. Taylan, G.-W. Weber, and F. Yerlikaya Özkurt, A new approach to multivariate adaptive regression splines by using Tikhonov regularization and continuous optimization, TOP, 18(2), pp. 377–395, 2010.

[99] R. D. Throne and L. G. Olson, A generalized eigensystem approach to the inverse problem of electrocardiography., IEEE Transactions on Biomedical Engineering, 41(6), pp. 592–600, 1994.

[100] R. D. Throne and L. G. Olson, The Effects of Errors in Assumed Conductivities and Geometry on Numerical Solutions to the Inverse Problem of Electrocardiography, IEEE Transactions on Biomedical Engineering, 42(12), pp. 1192–1200, 1995.

[101] G. J. Tortora, J. Wiley, B. Roesch, L. Wojcik, B. Salisbury, K. Gerdes, and H. Grossman, *Principles of Anatomy and Physiology*, John Wiley & Sons, 12th edition, 2010, ISBN 9780470084717.

[102] S. Twomey, On the Numerical Solution of Fredholm Integral Equations of the First Kind by the Inversion of the Linear System Produced by Quadrature, Journal of the ACM, 10(1), pp. 97–101, 1963.

[103] P. M. Van Dam, R. Tung, K. Shivkumar, and M. Laks, Quantitative localization of premature ventricular contractions using myocardial activation ECGI from the standard 12-lead electrocardiogram, Journal of Electrocardiology, 46(6), pp. 574–579, 2013.

[104] A. Van Oosterom, The use of the spatial covariance in computing pericardial potentials, IEEE Transactions on Biomedical Engineering, 46(7), pp. 778–787, 1999.

[105] A. van Oosterom, A comparison of electrocardiographic imaging based on two source types, Europace, 16(suppl 4), pp. iv120–iv128, 2014.

[106] J. C. A. Vinay Kumar, Abul K. Abbas, *Robbins & Cotran Pathologic Basis of Disease*, Elsevier Health Sciences, 9th edition, 2014, ISBN 9781455726134.

[107] D. Wang, R. M. Kirby, R. S. MacLeod, and C. R. Johnson, Inverse electrocardiographic source localization of ischemia: An optimization framework and finite element solution, Journal of Computational Physics, 250(9), pp. 403–424, 2013.

[108] L. Wang, X. Li, Y. Chen, and J. Qin, Application of L0-Norm Regularization to Epicardial Potential Reconstruction, in *MICCAI 2015, Part I, Lecture Notes in Computer Science*, volume 9349, pp. 493–500, 2015, ISBN 978-3-319-24552-2.

[109] R. H. Whitaker, Anatomy of the heart, Medicine, 38(7), pp. 333–335, 2010.

[110] WHO, Cardiovascular diseases (CVDs), `http://www.who.int/mediacentre/factsheets/fs317/en/`, September 2016, [Online; accessed 11.07.2017].

[111] A. D. Woodbury, Minimum Relative Entropy, Bayes and Kapur, Geophysical Journal International, 185(1), pp. 181–189, 2011.

[112] A. D. Woodbury and T. J. Ulrych, Minimum relative entropy: Forward probabilistic modeling, Water Resources Research, 29(8), pp. 2847–2860, 1993.

[113] A. D. Woodbury and T. J. Ulrych, Minimum Relative Entropy Inversion: Theory and Application to Recovering the Release History of a Groundwater Contaminant, Water Resources Research, 32(9), pp. 2671–2681, 1996.

[114] A. D. Woodbury and T. J. Ulrych, Minimum relative entropy and probabilistic inversion in groundwater hydrology, Stochastic Hydrology and Hydraulics, 12(5), pp. 317–358, 1998.

[115] J. Xu, A. R. Dehaghani, F. Gao, and L. Wang, Noninvasive transmural electrophysiological imaging based on minimization of total-variation functional, IEEE Transactions on Medical Imaging, 33(9), pp. 1860–1874, 2014.

[116] B. Yao and H. Yang, Physics-driven Spatiotemporal Regularization for High-dimensional Predictive Modeling: A Novel Approach to Solve the Inverse ECG Problem., Scientific Reports, 6, p. 39012, 2016.

[117] N. Zemzemi, C. Dobrzynski, L. Bear, M. Potse, C. Dallet, Y. Coudiere, R. Dubois, and J. Duchateau, Effect of the torso conductivity heterogeneities on the ECGI inverse problem solution, in *2015 Computing in Cardiology Conference (CinC)*, volume 42, pp. 233–236, IEEE, sep 2015.

[118] O. Zettinig, T. Mansi, B. Georgescu, E. Kayvanpour, F. Sedaghat-Hamedani, A. Amr, J. Haas, H. Steen, B. Meder, H. Katus, N. Navab, A. Kamen, and D. Comaniciu, Fast data-driven calibration of a cardiac electrophysiology model from images and ECG, Lecture Notes in Computer Science (including subseries Lecture Notes in Artificial Intelligence and Lecture Notes in Bioinformatics), 8149 LNCS(PART 1), pp. 1–8, 2013.

[119] O. Zettinig, T. Mansi, D. Neumann, B. Georgescu, S. Rapaka, P. Seegerer, E. Kayvanpour, F. Sedaghat-Hamedani, A. Amr, J. Haas, H. Steen, H. Katus, B. Meder, N. Navab, A. Kamen, and D. Comaniciu, Data-driven estimation of cardiac electrical diffusivity from 12-lead ECG signals, Medical Image Analysis, 18(8), pp. 1361–1376, 2014.

[120] M. Zorzi, F. Ticozzi, and A. Ferrante, Minimum Relative Entropy for Quantum Estimation: Feasibility and General Solution, IEEE Transactions on Information Theory, 60(1), pp. 357–367, 2014.

APPENDIX A

MRE ESTIMATION RESULTS

Table A.1: Mean ($E\{CC\}$) and standard deviation ($\sigma\{CC\}$) values for CC obtained for various upper and lower bounds. Results are presented for the true prior mean vector, and noisy prior mean vectors at 15 and 5 dB SNR values.

α	True prior mean $E\{CC\} \pm \sigma\{CC\}$	Prior mean at 15 dB SNR $E\{CC\} \pm \sigma\{CC\}$	Prior mean at 5 dB SNR $E\{CC\} \pm \sigma\{CC\}$
0.4	0.7976 ± 0.1130	0.7766 ± 0.1128	0.5278 ± 0.3163
0.5	0.8761 ± 0.1371	0.8490 ± 0.1298	0.6644 ± 0.1417
0.6	0.8944 ± 0.1944	0.8787 ± 0.1864	0.6918 ± 0.1404
0.7	0.8911 ± 0.2270	0.8681 ± 0.2337	0.7125 ± 0.1221
0.8	0.9237 ± 0.1915	0.8852 ± 0.2323	0.6904 ± 0.0955
0.9	0.9922 ± 0.0281	0.9540 ± 0.0674	0.7109 ± 0.0877
1.0	0.9993 ± 0.0035	0.9819 ± 0.0064	0.7367 ± 0.0894
1.5	0.9999 ± 0.0003	0.9823 ± 0.0057	0.8295 ± 0.0479
2.0	0.9996 ± 0.0016	0.9820 ± 0.0065	0.8536 ± 0.0313

Table A.2: Mean ($E\{CC\}$) and standard deviation ($\sigma\{CC\}$) values for CC obtained for various prior mean vectors. Upper and lower bounds, and expected uncertainty in the error are fixed, the true prior mean vector is disturbed by Gaussian white noise at different SNR values.

SNR	$E\{CC\} \pm \sigma\{CC\}$
1	0.7331 ± 0.0328
5	0.8595 ± 0.0270
10	0.9476 ± 0.0158
15	0.9819 ± 0.0073
20	0.9939 ± 0.0037
True	0.9996 ± 0.0016

Table A.3: Mean ($E\{CC\}$) and standard deviation ($\sigma\{CC\}$) values for CC obtained for various expected uncertainty values. Results are presented for the true prior mean vector, and noisy prior mean vectors at 15 and 5 dB SNR values.

β	True prior mean $E\{CC\} \pm \sigma\{CC\}$	Prior mean at 15 dB SNR $E\{CC\} \pm \sigma\{CC\}$	Prior mean at 5 dB SNR $E\{CC\} \pm \sigma\{CC\}$
0.4	0.6593 ± 0.2673	0.8013 ± 0.1923	0.7225 ± 0.1638
0.6	0.9945 ± 0.0105	0.9400 ± 0.1230	0.8283 ± 0.1021
0.8	0.9972 ± 0.0136	0.9821 ± 0.0060	0.8557 ± 0.0315
1.0	0.9996 ± 0.0016	0.9817 ± 0.0062	0.8531 ± 0.0298
1.2	0.9997 ± 0.0009	0.9819 ± 0.0063	0.8541 ± 0.0331
1.4	0.9988 ± 0.0048	0.9819 ± 0.0061	0.8555 ± 0.0340
1.6	0.9997 ± 0.0009	0.9808 ± 0.0070	0.8503 ± 0.0405

Table A.4: Mean ($E\{CC\}$) and standard deviation ($\sigma\{CC\}$) values for CC obtained for previous time instant solution multiplied by a constant.

	MRE $\mu = 0.9$ from prev. sol.	MRE $\mu = 1.0$ from prev. sol.	MRE $\mu = 1.1$ from prev. sol.
$E\{CC\}$	0.7496	0.7251	0.6798
$\sigma\{CC\}$	0.2005	0.2014	0.2038

APPENDIX B

MARS ESTIMATION RESULTS

Table B.1: Pearson CC values for activation times for the Utah data collection.

Dataset	CC			
	Tikhonov	Twomey	Spline Inverse	MARS
1	0.95	0.97	0.98	0.95
2	0.95	0.95	0.98	0.94
3	0.95	0.99	0.95	0.98
4	0.96	0.97	0.96	0.98
5	0.94	0.99	0.97	0.99
6	0.97	0.99	0.98	0.97
7	0.91	0.90	0.90	0.96
8	0.98	0.99	0.97	0.99
9	0.95	0.99	0.99	0.98
10	0.95	0.99	0.99	0.99
11	0.98	0.99	0.99	0.99
12	0.98	0.99	0.93	0.99
13	0.91	0.97	0.97	0.97
14	0.89	0.94	0.94	0.97
15	0.93	0.95	0.91	0.99
16	0.98	0.99	0.99	0.99
17	0.99	0.99	0.99	0.99
18	0.99	0.99	0.99	0.99
19	0.99	0.99	0.99	0.99
20	0.96	0.99	0.98	0.99
21	0.96	0.99	0.99	0.99
22	0.92	0.99	0.93	0.96
23	0.95	0.99	0.99	0.99

Table B.2: Mean CC values for small variations in the forward transfer matrix.

Noise SNR	CC			
	Tikhonov	Twomey	Spline Inverse	MARS
Noise Free	0.72 ± 0.20	0.75 ± 0.19	0.74 ± 0.21	0.80 ± 0.16
30 dB	0.67 ± 0.20	0.67 ± 0.19	0.69 ± 0.21	0.79 ± 0.16
20 dB	0.62 ± 0.20	0.60 ± 0.19	0.63 ± 0.20	0.77 ± 0.17

Table B.3: Mean RE values for small variations in the forward transfer matrix.

Noise SNR	RE			
	Tikhonov	Twomey	Spline Inverse	MARS
Noise Free	0.63 ± 0.20	0.62 ± 0.21	0.62 ± 0.26	0.56 ± 0.18
30 dB	0.68 ± 0.19	0.72 ± 0.22	0.69 ± 0.28	0.58 ± 0.25
20 dB	0.73 ± 0.20	0.79 ± 0.19	0.73 ± 0.20	0.59 ± 0.20

Table B.4: Mean LE values for small variations in the forward transfer matrix.

Noise SNR	LE in mm			
	Tikhonov	Twomey	Spline Inverse	MARS
Noise Free	9.76 ± 3.38	7.88 ± 1.40	8.56 ± 1.56	7.16 ± 1.33
30 dB	11.27 ± 5.87	8.71 ± 4.56	10.97 ± 6.59	7.52 ± 3.58
20 dB	11.23 ± 8.42	9.87 ± 6.06	12.44 ± 8.11	9.22 ± 3.66

Table B.5: Mean CC values for shifted heart location to the left and right side inside the torso from its true location.

Shift (in mm)	CC			
	Tikhonov	Twomey	Spline Inverse	MARS
10	0.65 ± 0.17	0.67 ± 0.19	0.65 ± 0.14	0.71 ± 0.14
0	0.72 ± 0.20	0.75 ± 0.19	0.74 ± 0.21	0.80 ± 0.16
-10	0.65 ± 0.17	0.61 ± 0.17	0.64 ± 0.13	0.70 ± 0.13

Table B.6: Mean RE values for shifted heart location to the left and right side inside the torso from its true location.

Shift (in mm)	RE			
	Tikhonov	Twomey	Spline Inverse	MARS
10	0.75 ± 0.27	0.72 ± 0.22	0.73 ± 0.14	0.76 ± 0.21
0	0.63 ± 0.20	0.62 ± 0.21	0.62 ± 0.26	0.56 ± 0.18
-10	0.74 ± 0.25	0.86 ± 0.23	0.74 ± 0.12	0.73 ± 0.17

Table B.7: Mean LE values for shifted heart location to the left and right side inside the torso from its true location.

Shift (in mm)	LE			
	Tikhonov	Twomey	Spline Inverse	MARS
10	12.65 ± 7.09	15.64 ± 12.86	10.58 ± 5.63	7.16 ± 3.78
0	9.76 ± 3.38	7.88 ± 1.40	8.56 ± 1.56	7.16 ± 1.33
-10	12.19 ± 8.72	16.7 ± 19.26	9.37 ± 4.9	8.3 ± 3.86

Table B.8: Mean CC values for shifted heart location to the backward and onward inside the torso from its true location.

Shift (in mm)	CC			
	Tikhonov	Twomey	Spline Inverse	MARS
10	0.64 ± 0.17	0.60 ± 0.15	0.64 ± 0.16	0.70 ± 0.14
0	0.72 ± 0.20	0.75 ± 0.19	0.74 ± 0.21	0.80 ± 0.16
-10	0.67 ± 0.17	0.63 ± 0.15	0.66 ± 0.16	0.72 ± 0.14

Table B.9: Mean RE values for shifted heart location to the backward and onward inside the torso from its true location.

Shift (in mm)	RE			
	Tikhonov	Twomey	Spline Inverse	MARS
10	0.75 ± 0.22	0.96 ± 0.37	0.75 ± 0.22	0.76 ± 0.18
0	0.63 ± 0.20	0.62 ± 0.21	0.62 ± 0.26	0.56 ± 0.18
-10	0.71 ± 0.19	0.85 ± 0.27	0.72 ± 0.12	0.84 ± 0.34

Table B.10: Mean LE values for shifted heart location to the backward and onward inside the torso from its true location.

Shift (in mm)	LE			
	Tikhonov	Twomey	Spline Inverse	MARS
10	12.32 ± 7.44	8.18 ± 3.32	8.79 ± 4.4	8.65 ± 4.8
0	9.76 ± 3.38	7.88 ± 1.40	8.56 ± 1.56	7.16 ± 1.33
-10	12.12 ± 6.7	9.82 ± 8.12	11.32 ± 5.33	8.42 ± 4.13

Table B.11: Mean CC values for scaled heart size.

Scale factor	CC			
	Tikhonov	Twomey	Spline Inverse	MARS
1.2	0.69 ± 0.18	0.67 ± 0.17	0.70 ± 0.18	0.77 ± 0.14
1	0.72 ± 0.20	0.75 ± 0.19	0.74 ± 0.21	0.80 ± 0.16
0.8	0.69 ± 0.18	0.65 ± 0.16	0.69 ± 0.17	0.76 ± 0.14

Table B.12: Mean RE values for scaled heart size.

Scale factor	RE			
	Tikhonov	Twomey	Spline Inverse	MARS
1.2	0.72 ± 0.16	0.75 ± 0.18	0.72 ± 0.13	0.68 ± 0.31
1	0.63 ± 0.20	0.62 ± 0.21	0.62 ± 0.26	0.56 ± 0.18
0.8	0.82 ± 0.25	0.86 ± 0.23	0.83 ± 0.17	0.91 ± 0.24

Table B.13: Mean LE values for scaled heart size.

Scale factor	LE			
	Tikhonov	Twomey	Spline Inverse	MARS
1.2	2.73 ± 7.09	15.64 ± 12.86	10.58 ± 5.63	7.16 ± 3.78
1	9.76 ± 3.38	7.88 ± 1.40	8.56 ± 1.56	7.16 ± 1.33
0.8	12.19 ± 8.72	16.7 ± 19.26	9.37 ± 4.9	8.3 ± 3.86

Table B.14: Mean CC values for measurement noise at different SNR levels.

Noise SNR	CC			
	Tikhonov	Twomey	Spline Inverse	MARS
30 dB	0.72 ± 0.20	0.75 ± 0.19	0.74 ± 0.21	0.80 ± 0.16
20 dB	0.65 ± 0.22	0.66 ± 0.22	0.69 ± 0.23	0.76 ± 0.19
10 dB	0.58 ± 0.23	0.58 ± 0.23	0.62 ± 0.25	0.70 ± 0.23

Table B.15: Mean RE values for measurement noise at different SNR levels.

Noise SNR	RE			
	Tikhonov	Twomey	Spline Inverse	MARS
30 dB	0.63 ± 0.20	0.62 ± 0.21	0.62 ± 0.26	0.56 ± 0.18
20 dB	0.72 ± 0.26	0.71 ± 0.26	0.69 ± 0.28	0.60 ± 0.23
10 dB	0.83 ± 0.34	0.82 ± 0.33	0.77 ± 0.31	0.70 ± 0.33

Table B.16: Mean LE values for measurement noise at different SNR levels.

Noise SNR	LE in mm			
	Tikhonov	Twomey	Spline Inverse	MARS
30 dB	9.76 ± 3.38	7.88 ± 1.40	8.56 ± 1.56	7.16 ± 1.33
20 dB	17 ± 7.1	38.83 ± 18.4	11.27 ± 3.7	8.51 ± 3.05
10 dB	26.11 ± 12	40.58 ± 12.8	14.17 ± 5.03	15.51 ± 8.53

Table B.17: Mean activation times Pearson CC values for KIT data collection.

Dataset	CC			
	Tikhonov	Twomey	Spline Inverse	MARS
SEPTUMCENTER	0.53	0.32	0.30	0.42
LVLAT	0.53	0.46	0.79	0.70
LVAPEX	0.61	0.55	0.66	0.82
LVANTERIOR	0.61	0.69	0.58	0.74
RVPOSTERIOR	0.82	0.73	0.89	0.79
RVANTERIOR	0.58	0.43	0.73	0.49
LVLATEPI	0.10	0.50	0.66	0.67
LVLATENDO	0.52	0.37	0.70	0.81
Average	0.51	0.51	0.66	0.68

CURRICULUM VITAE

PERSONAL INFORMATION

Surname, Name: Onak, Önder Nazım

Nationality: Turkish

Date and Place of Birth: 1974, Aksaray

Marital Status: Single

Phone: +90 312 5921488

Fax: NA

EDUCATION

Degree	Institution	Year of Graduation
M.S.	Scientific Computing, IAM, METU	2011
B.S.	Electrical and Electronics Eng., Hacettepe Un.	1997
High School	Antalya Çağlayan Lisesi	1992

COMPUTER SKILLS

Programming languages C, C++, C#, Matlab, Octave.

Markup and Interface description languages XML, XSLT, ASN.1.

Communication protocols TCP/IP, UDP, X.25.

PROFESSIONAL EXPERIENCE

Year	Place	Enrollment
1997-1999	Hacettepe University	Research Assistant
1999-2007	Aselsan Inc.	Senior Software Engineer
2007-2008	Military Service	Project Officer
2008-Present	Aselsan Inc.	Lead Software Engineer

PUBLICATIONS

International Peer-reviewed Journals

- Onak, O. N., Serinagaoglu Dogrusoz, Y., and Weber, G.-W., *Evaluation of multivariate adaptive non-parametric reduced-order model for solving the inverse electrocardiography problem: A simulation study.* In review, Medical and Biological Eng and Computing (SCI).

- Onak, O. N., Serinagaoglu Dogrusoz, Y., and Weber, G.-W., *Effects of a priori parameter selection in minimum relative entropy method on inverse electrocardiography problem.* Inverse Problems in Science and Engineering, 26(6), 877–897, 2018 (SCI).

- Onak, O. N., Serinagaoglu Dogrusoz, Y., and Weber, G.-W., *Minimum relative entropy method for inverse electrocardiography problem*, Problems of Nonlinear Analysis in Engineering Systems No.1(41), vol. 20, 64-70, 2014.

International Conference Publications

- Onak, O. N., Serinagaoglu Dogrusoz, Y., and Weber, G.-W., *Robustness of Reduced Order Non-Parametric Model for Inverse ECG Solution Against Modelling and Measurement Noise*, Computing in Cardiology, Maastricht, Nederland, Sep. 23-26, 2018.

- Onak, O. N., Serinagaoglu Dogrusoz, Y., and Weber, G.-W., *Effect of the Geometric Inaccuracy in MARS-based Inverse ECG Solution Approach*, Computing

in Cardiology, Rennes, France, Sep. 24-27, 2017.

National Conference Publications

- Onak, O. N., Serinagaoglu Dogrusoz, Y., and Weber, G.-W., *Effects of Measurement Noise in MARS-based Inverse ECG Solution Approach*, 26th IEEE Signal Processing and Communications Applications Conference, Çesme, Izmir, 2-5 May. 2018.

- Onak, O. N., Serinagaoglu Dogrusoz, Y., and Weber, G.-W., *Application of Multivariate Adaptive Regression Splines for Inverse ECG Problem*, 20th National Biomedical Engineering Meeting, Seferihisar, Izmir, 3-5 Nov. 2016.